Generation and characterization of angiogenin mutants as improved effector domains for H22(scFv)-based cytolytic fusion proteins

Von der Fakultät für Mathematik, Informatik und Naturwissenschaften der RWTH Aachen University zur Erlangung des akademischen Grades eines Doktors der Naturwissenschaften genehmigte Dissertation
vorgelegt von

Diplom-Biologe

Christian Cremer

aus Düren-Birkesdorf

Berichter: Universitätsprofessor Dr. Rainer Fischer
Universitätsprofessor Dr. Paolo Carloni

Tag der mündlichen Prüfung: 13.01.2017

Diese Dissertation ist auf den Internetseiten der Hochschulbibliothek online verfügbar.

Summary

Human cytolytic fusion proteins (hCFPs) are a new class of anti-cancer drugs that are usually less cytotoxic than former generations of immunotoxins (ITs) but feature a strongly reduced immunogenic potential due to their human or humanized components. Thus, the directed modification of CFPs to increase their efficacy represents a promising strategy.

The goal of this doctoral thesis was to investigate if the cytotoxicity of the human ribonuclease angiogenin (Ang) can be increased by modifying adverse enzymatic properties by site-directed mutagenesis. Characteristics that limit the pro-apoptotic potency of Ang as effector domain are its weak enzymatic activity, its strong cytosolic inhibition by the ribonuclease inhibitor RNH1 and its rapid accumulation in the nucleus under certain cellular conditions. By literature research, we identified promising mutations referring to the Ang wild type protein. They were either characterized by *in vitro* assays or revealed from crystallographic and neovascularization studies. Since these mutations abolish the above-mentioned limitations, they might be suitable to increase the cytotoxic potential of Ang as effector domain in cytolytic fusion proteins.

As a *proof-of-concept*, the mutations were introduced into the Ang wild type sequence by site-directed mutagenesis and the different variants were fused to the CD64-specific antibody fragment H22(scFv) for subsequent evaluation. The CFPs were tested for an increased *in vitro* cytotoxicity compared to H22-Ang wild type and favorable mutants underwent detailed characterizations to reveal the contribution of individual enzymatic properties. Promising mutations were combined to test if cooperative or synergistic effects may be achieved whereas molecular dynamic simulations revealed detailed insights into the individual interactions of Ang variants and RNH1. Based on this knowledge, the generation of a variant with increased substrate cleavage activity and decreased inhibition susceptibility compared to the wild type was aimed as the overall objective.

In this work, two Ang variants were generated that outperformed the *in vitro* cytotoxicity of Ang wild type on IFNγ-stimulated HL-60 cells and pro-inflammatory macrophages substantially in fusion to H22. They either combined an improved substrate cleavage activity with a reduced RNH1 affinity or were almost resistant towards the inhibitor. One variant even demonstrated a cytotoxicity similar to a *Pseudomonas aeruginosa* exotoxin A-based IT on leukemia cells *ex vivo*. The incorporation of a synthetic translocation sequence into a CFP did not further improve the cytotoxicity.

Zusammenfassung

Humane zytolytische Fusionsproteine (hZFP) weisen aufgrund ihrer humanen oder humanisierten Komponenten eine verringerte Immunogenität als herkömmliche Immuntoxine (IT) auf, zeichnen sich in der Regel jedoch auch durch eine geringere Wirksamkeit aus. Mittels gerichteter Modifizierung in ihrer Wirksamkeit verbesserte ZFPs stellen deshalb eine vielversprechende Alternative zu konventionellen Immuntoxinen dar.

Im Rahmen dieser Arbeit wurde untersucht, ob das zytotoxische Potential der humanen Ribonuklease Angiogenin (Ang) durch zielgerichtete Mutagenese verbessert werden kann. Ang wird zytoplasmatisch durch das Protein RNH1 inhibiert, verfügt über eine geringe Enzymaktivität und kann im Nukleus von Zellen akkumulieren. In der Literatur konnten wir verschiedene Ang-Mutationen identifizieren, welche auf die genannten Limitierungen abzielen und die im Zuge von Kristallisierungs- und Neovaskularisierungsstudien sowie *in vitro*-Experimenten charakterisiert wurden. Verglichen mit dem Wildtyp-Protein könnten entsprechende Mutanten ein erhöhtes zytotoxisches Potential aufweisen, sofern die beschriebenen Effekte durch die Fusion mit einer Bindekomponente erhalten bleiben.

Entsprechende Mutanten wurden auf Basis der Ang-Wildtyp-Sequenz generiert und mit dem CD64-spezifischen Antikörperfragment H22 fusioniert, um deren Zytotoxizität zu ermitteln. ZFPs, welche die Effizienz des Wildtyp-basierten Fusionsproteins übertrafen, wurden detailliert charakterisiert, um die individuellen Beiträge einzelner Eigenschaften zu bestimmen. Darüber hinaus wurden vorteilhafte Mutationen kombiniert und auf kooperative Effekte hin untersucht. Molekulardynamik-Simulationen halfen dabei, individuelle Interaktionen zwischen Ang-Mutanten und RNH1 auf atomarer Ebene darzustellen. Abschließend wurde auf Basis der gewonnenen Erkenntnisse die Generierung einer Variante angestrebt, welche über eine Kombination verschiedener vorteilhafter Charakteristika verfügt.

In Fusion mit H22 konnten zwei der hier generierten Ang-Varianten die Zytotoxizität des Wildtyp-Proteins gegenüber HL-60 Zellen und entzündlichen Makrophagen signifikant übertreffen. Die Varianten verfügen über eine stark verringerte Affinität gegenüber RNH1 oder kombinieren eine reduzierte Affinität mit einer verbesserten Enzymaktivität. Darüber hinaus konnte eine der Mutanten leukämische Zellen mit einer vergleichbaren Effizienz wie ein *Pseudomonas aeruginosa* Exotoxin A-basiertes IT eliminieren. Die Kombination einer artifiziellen Translokationsdomäne und einer Ang Mutante erwies sich nicht als vorteilhaft.

Output of the thesis

Publications

[1] Cremer C, Vierbuchen T, Hein L, Fischer R, Barth S, Nachreiner T: Angiogenin mutants as novel effector molecules for the generation of fusion proteins with increased cytotoxic potential. *J Immunother* 2015, 38:85-95.

[2] Cremer C, Braun H, Mladenov R, Schenke L, Cong X, Jost E, Brummendorf TH, Fischer R, Carloni P, Barth S, Nachreiner T: Novel angiogenin mutants with increased cytotoxicity enhance the depletion of pro-inflammatory macrophages and leukemia cells *ex vivo*. *Cancer Immunol Immunother* 2015, 64:1575-86.

[3] Cremer C, Hehmann-Titt G, Schiffer S, Melmer G, Carloni P, Barth S, Nachreiner T: Engineered versions of granzyme B and angiogenin overcome intrinsic resistance to apoptosis mediated by human cytolytic fusion proteins. In: Verma RS, Bonavida B (eds.) Resistance to immunotoxins in cancer therapy. *Springer International Publishing Switzerland* 2015, pp. 185-219.

[4] Cong X, Cremer C, Nachreiner T, Barth S, Carloni P: Engineered human angiogenin mutations in the placental ribonuclease inhibitor complex for anticancer therapy: Insights from enhanced sampling simulations. *Protein Sci* 2016, 25:1451-60.

[5] Mladenov R, Hristodorov D, Cremer C, Hein L, Kreutzer F, Stroisch T, Niesen J, Brehm H, Blume T, Brummendorf TH, Jost E, Thepen T, Fischer R, Stockmeyer B, Barth S, Stein C: The Fc-alpha receptor is a new target antigen for immunotherapy of myeloid leukemia. *Int J Cancer* 2015, 137:2729-38.

[6] Mladenov R, Hristodorov D, Cremer C, Gresch G, Grieger E, Schenke L, Klose D, Amoury M, Woitok M, Jost E, Brummendorf TH, Fendel R, Fischer R, Stein C, Thepen T, Barth S: CD64-directed microtubule associated protein tau kills leukemic blasts *ex vivo*. *Oncotarget* 2016, 7:67166-74.

International poster presentation

Cremer C, Fischer R, Barth S, Nachreiner T: Human angiogenin mutants as improved effector domains for the generation of cytolytic fusion proteins with increased cytotoxic potential. Poster session presented at: 25th Annual Antibody Engineering & Therapeutics Conference, 2014, Los Angeles, CA, USA.

Technically supervised master's theses (unpublished)

[7] Neß M: Evaluierung von ABT-737 als Additiv zur Verbesserung der Effizienz zytolytischer Fusionsproteine. (Master's thesis) RWTH Aachen University, Germany 2013.

[8] Vierbuchen T: *In vitro* characterization of novel cytolytic fusion proteins and evaluation of a synergistic treatment strategy. (Master's thesis) RWTH Aachen University, Germany 2014.

The supervision of Tim Vierbuchen was carried out in close cooperation with Lea Schenke (Institute of Applied Medical Engineering, Department of Experimental Medicine and Immunotherapy, University Hospital Aachen).

[9] Braun H: Generation and characterization of novel recombinant angiogenin mutants with improved cytotoxic potential. (Master's thesis) RWTH Aachen University, Germany 2015.

Table of Contents

I Introduction 1
I.1 Therapeutic fusion proteins 1
I.1.1 Immunotoxins 1
I.1.2 Human cytolytic fusion proteins 2
I.2 The Fc gamma receptor I as a therapeutic target 3
I.2.1 Appearance, function and targeting of the Fc gamma receptor I 3
I.2.2 CD64 and its role in pathogenesis 5
I.3 Human angiogenin and its usability as effector domain for CFPs 6
I.3.1 Angiogenin - a ribonuclease with double-edged properties 6
I.3.2 Inhibition of angiogenin by the eukaryotic ribonuclease inhibitor RNH1 9
I.4 Objectives 9
II Material and Methods 12
II.1 Material 12
II.1.1 Chemicals and consumables 12
II.1.2 Equipment & supplies 12
II.1.3 Restriction endonucleases and kits 13
II.1.4 Standard buffer and media compositions 13
II.1.5 Bacterial strains 15
II.1.6 Eukaryotic cell lines 15
II.1.7 Vector system 16
II.1.8 Antibodies 17
II.1.9 Synthetic oligonucleotides 17
II.2 Methods 18
II.2.1 Mutagenesis and splicing by overlap extension PCR 18
II.2.2 Preparation and transformation of heat-shock competent *E.coli* cells 19
II.2.3 Storage and culturing of bacteria 20
II.2.4 Preparation of DNA and determination of concentration 20
II.2.5 Restriction of DNA 20
II.2.6 Analytical and preparative agarose gel electrophoresis 20
II.2.7 Ligation of restricted DNA 21
II.2.8 DNA sequencing 21
II.3 Cell culture 21

II.3.1 Cultivation, cryopreservation and thawing of eukaryotic cells 21
II.3.2 Transfection of eukaryotic cells 22
II.3.3 Preparation of mononuclear cells and polarization of M1 macrophages 22
II.3.4 Light and fluorescence microscopy 23
II.4 Immunological methods and protein characterization 23
II.4.1 Protein purification from cell culture supernatant using IMAC 23
II.4.2 SDS-PAGE and western blot analysis 24
II.4.3 Protein enrichment, buffer exchange and sample storage 25
II.4.4 Determination of protein concentration 25
II.5 Flow cytometry analyses 25
II.6 Yeast tRNA cleavage assays 26
II.7 Demonstration of enzymatic activity and inhibition susceptibility 27
II.8 Electrophoretic mobility shift assays 27
II.9 XTT viability assays 28
II.10 Apoptosis assays 28
II.11 Determination of serum stability 28
II.12 Preparation of cell lysates and quantification of inhibitor amounts 29
II.13 Oxidative regulation of the ribonuclease inhibitor activity 29
II.14 Statistical analysis 30
II.15 Safety levels 30
III Results 31
III.1 1st mutagenesis and evaluation round 31
III.1.1 Mutagenesis of H22-Ang wild type, CFP expression & purification 31
III.1.2 Binding analysis of CFPs by flow cytometry 33
III.1.3 CFP-mediated reduction of HL-60 cell viability 34
III.2 2nd mutagenesis and evaluation round 36
III.2.1 Generation, expression & purification of H22-Ang GGRR/QG$_{mut}$ 36
III.2.2 Ribonucleolytic activity and inhibition susceptibility of CFPs 37
III.2.3 The binding of CFPs to genomic DNA 40
III.2.4 Preparation of M1 macrophages and binding analysis of CFPs 42
III.2.5 *In vitro* cytotoxicity of CFPs 43
III.2.6 Molecular dynamic simulation of RNH1-Ang interactions 45
III.3 3rd mutagenesis and evaluation round 50
III.3.1 Generation, expression and purification of novel H22-Ang variants 51

III.3.2 Enzymatic activity and inhibition resistance of the generated CFPs 52
III.3.3 *In vitro* binding activity of the CFPs 54
III.3.4 CFP-mediated cytotoxic effects on different cell types *in vitro* 56
III.4 Stability of CFPs in human and mouse serum 58
III.5 Targeted *ex vivo* depletion of leukemia cells with H22-Ang variants 60
III.5.1 Preparation of leukemia cells and flow cytometry analyses 61
III.5.2 Pro-apoptotic effects of CFPs on leukemia cells *ex vivo* 63
III.6 The effect of CatAd on the cytotoxicity of H22-Ang $GGRR_{mut}$ 65
III.7 Summarized performance of H22-Ang variants 66
III.8 IFNγ sensitizes target cells for the depletion with H22-Ang 67
IV Discussion 74
IV.1 Expression and purification of H22-Ang variants 74
IV.2 *In vitro* characteristics and pro-apoptotic potencies of CFPs 76
IV.2.1 CD64-specific binding activity of H22-Ang variants 76
IV.2.2 Preventing the nuclear translocation of H22-Ang has no favorable effect 77
IV.2.3 The impact of enzymatic activity and inhibition susceptibility 78
IV.2.4 Endowing H22-Ang $GGRR_{mut}$ with CatAd does not increase its potency 81
IV.3 IFNγ modulates the target cell sensitivity towards H22-Ang variants 82
IV.4 Therapeutic applications and the heterogeneity of target cells 84
IV.5 Additional strategies to increase the cytotoxicity of angiogenin 87
V Outlook 90
VI List of references 92
VII Appendix 113
VII.1 Single-letter code of amino acids 113
VII.2 List of abbreviations 113
VII.3 Index of tables 116
VII.4 Index of figures 116
VII.5 DNA sequence of H22-Ang wild type and primer binding sites 117
VII.6 Acknowledgements 122
VII.7 Curriculum Vitae 123

I Introduction

I.1 Therapeutic fusion proteins

I.1.1 Immunotoxins

Immunotoxins (ITs) are recombinant therapeutic fusion proteins that comprise a toxic effector domain genetically linked to a tumor cell-specific binding component. Initial binding moieties like antibodies or derivatives thereof usually originate from mice whereas popular toxins are typically of bacterial or plant origin [10]. The most common toxins used for the generation of ITs are *Pseudomonas aeruginosa* exotoxin A (ETA), diphtheria toxin or ricin A. The natural binding domains of these toxins are generally deleted to ensure target cell specificity mediated by the antibody moiety, resulting in truncated variants such as ETA' [11, 12]. ITs were initially developed for the treatment of different cancer entities as their target cell specificity overcomes the major drawbacks of traditional chemotherapy [13]. However, the treatment of solid tumors still remains difficult due to a poor tumor penetration efficiency of the ITs [11]. The use of smaller antibody formats like single chain variable fragments (scFvs) addressed this challenge. Although the plasma stability was reduced, an improved tumor penetration with decreased retention time in non-target tissue could be achieved [14, 15]. The cytotoxic potential of ITs has been demonstrated in several *in vitro* and *in vivo* studies so far [16-25]. However, their application is limited by several drawbacks mainly caused by the potential immunogenicity [26]. The occurrence of the vascular or capillary leak syndrome (VLS, CLS) [27, 28] has led to the development of recombinant toxins with a decreased ability for CLS induction and reduced antigenicity [29, 30]. Still, neutralizing antibodies against non-human parts of ITs prohibit repeated applications as they promote an accelerated blood clearance [31-33]. Therefore, latest efforts aimed to eliminate immunodominant B and T cell epitopes of the respective toxins [34-36]. Also the humanization of target cell-specific binding moieties markedly reduced the immunogenicity [37]. In addition to cancer-specific therapies, the targeting of malignant B cells and autoreactive plasma cells could be demonstrated by using immunodominant B cell epitopes as binding moieties [38, 39]. So far, ricin A- and ETA'-based ITs have passed phase I/II clinical trials for the treatment of Hodgkin's lymphoma and hematologic malignancies [40, 41]. However, improvements are still necessary to achieve a better tolerance by patients and the reduction of unwanted immunologic responses. Therefore, an alternative strategy is pursued that focuses on the use of human or humanized components.

I.1.2 Human cytolytic fusion proteins

Humanized ITs, also known as cytolytic fusion proteins (CFPs), have been developed to overcome the immunogenicity of ITs while maintaining target cell specificity [42]. CFPs are equipped with human pro-apoptotic enzymes as effector domains. In fusion to a humanized scFv, the immunogenic potential can be markedly reduced or even abolished. Human enzymes with pro-apoptotic activities are represented in several protein classes. The most common ones are granzyme B (Gb), granzyme M (Gm), angiogenin (Ang), pancreatic ribonuclease (HPR), eosinophil-derived neurotoxin (EDN, a member of the ribonuclease A superfamily) and death-associated protein kinase family members. Intracellular activities that promote apoptosis induction include the direct or indirect activation of pro-apoptotic effector caspases, inhibition of translation, cleavage of nuclear RNAs, induction of pro-apoptotic signaling pathways and autophagy [43-47]. The specific pro-apoptotic potency of respective human enzymes fused to a binding moiety could be demonstrated *in vitro*, *in vivo* and *ex vivo* accordingly [48-60]. However, the efficacy of CFPs is rather moderate compared to conventional ITs. This could be linked to several limitations that hamper the impact of human enzymes while toxins circumvent these drawbacks, *e.g.* an inefficient cytosolic delivery. Bacterial toxins usually contain a natural translocation domain which facilitates the endosomal escape upon internalization [61]. Since human enzymes lack such domains, it strongly reduces their pro-apoptotic potency [62, 63]. For cytotoxic variants of RNase A, approximately 95% of the internalized ribonuclease was found to be degraded in lysosomal compartments before the cytosol can be reached [64]. Several strategies have been described to address this drawback. Cell-penetrating peptides (CPPs) derived from natural proteins or were even rationally designed [65]. The translocation domain of ETA was incorporated into CFPs, either alone or in combination with additional CPPs [48, 66-68]. A synthetic adapter sequence containing an endosomal-cleavable peptide, a membrane transfer peptide and a cytosolic-cleavable peptide was recently described to enhance the pro-apoptotic potency of H22(scFv)-Ang by 20-fold [69]. However, the benefit of increased pro-apoptotic potency has to compensate the enhanced immunogenicity of CPP-equipped CFPs for being considerable as promising for therapeutic approaches. Furthermore, some human enzymes require certain intracellular conditions that facilitate their pro-apoptotic activity. Also intracellular inhibitor proteins that mitigate the activity of human effector domains and the accumulation in non-target cell compartments markedly reduce the CFP potency. These drawbacks can be targeted by protein engineering to modify unfavorable

enzymatic properties. Promising strategies to increase the cytotoxic potential of human pro-apoptotic enzymes are 1) controlling or modifying the intracellular routing and localization, 2) improving the endosomal release into the cytosol, 3) enhancing the substrate cleavage activity necessary for apoptosis induction and 4) decreasing the intracellular inhibition susceptibility to prevent inactivation of the enzyme. Additionally, well-regulated human enzymes, such as the microtubule-associated protein tau, can be endowed with cytotoxic activity by enforcing a constitutively active state following mutagenesis [58]. According to the above-mentioned strategies, several mutants of human enzymes have been generated that markedly outperform the efficacy of the wild-type variants [46, 58, 70-75].

I.2 The Fc gamma receptor I as a therapeutic target

I.2.1 Appearance, function and targeting of the Fc gamma receptor I

Fc receptors (FcRs) are expressed on all hematopoietic cells and are essential for immune defense. They represent the connection between antibody-antigen complexes and cellular effector functions [76]. FcRs mediate phagocytosis, antibody-dependent cellular cytotoxicity, the recruitment and activation of inflammatory cells and they regulate the maturation of dendritic cells [77]. The Fc gamma receptor I (FcγRI), also known as CD64, is the high affinity receptor for monomeric human immunoglobulin G (IgG) and is predominantly expressed by monocytes, macrophages and dendritic cells (Figure 1). CD64 binds the IgG subclasses 1, 3 and 4 but not 2 whereas the highest affinity was found for IgG1 ($K_A \approx 6.5 \times 10^7\ M^{-1}$) [78]. However, also IgG3 and IgG4 are efficiently bound (K_As $\approx 6.1 \times 10^7\ M^{-1}$ and $3.4 \times 10^7\ M^{-1}$, respectively) suggesting its saturation *in vivo*. During host defense, IgG-opsonized pathogens and particles are efficiently bound and internalized by phagocytes, *e.g.* macrophages (MΦ cells). Cross-linking of CD64 directs the opsonized complex to the lysosomal pathway via fusion of the phagosome with intracellular lysosomes [79]. Toxic reactive oxygen species (ROS) are usually generated from cellular oxygen and contribute to the rapid destruction of pathogens [80]. CD64 also internalizes monomeric IgG whereas the lack of cross-linking directs the antibody to route along a recycling pathway [79, 81]. The internalization of CD64 was found to occur rapidly since 25-50% of labeled immune complexes were found inside FcγRIa-positive IIA1.6 cells within the first 30 min after addition [82]. A murine monoclonal antibody (M22) was developed by Guyre *et al.* recognizing an epitope

of CD64 distinct from the natural ligand-binding site of IgG [83]. Antibody humanization was carried out to reduce its immunogenicity and resulted in the full-length antibody H22 with maintained binding specificity and affinity [84]. It was later converted into a scFv format by de Kruif *et al.* [85]. H22(scFv) retains the target specificity of the initial full size antibody and internalizes within 30 min after binding to CD64 as demonstrated with H22(scFv)-SNAP 647 on HL-60 cells [86]. The functionality of H22(scFv)-based fusion proteins could be demonstrated *in vitro, in vivo* and *ex vivo* [17, 18, 20, 49-51, 69, 86].

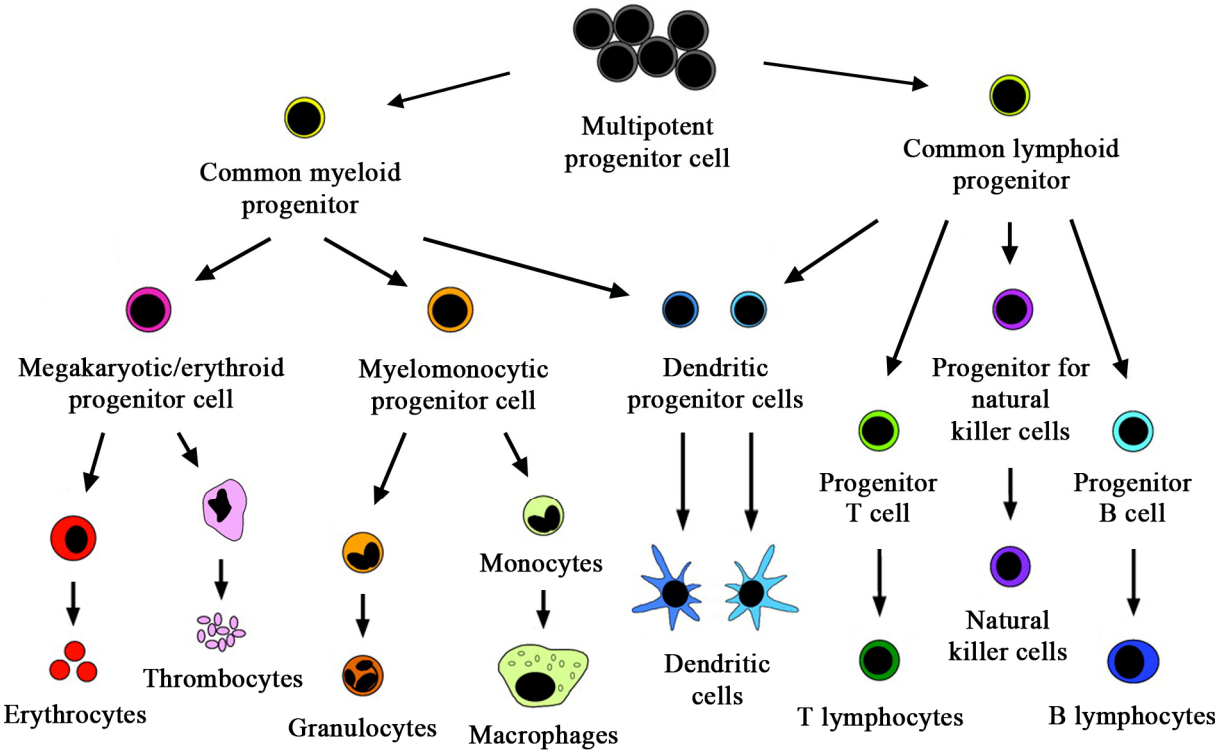


Figure 1: The development and diversity of hematopoietic immune cells.
A multipotent hematopoietic progenitor cell bears progenitor cells for the myeloid or the lymphoid pathway, respectively. Natural killer cells and all other lymphocytes develop from the lymphoid progenitor cell whereas erythrocytes, thrombocytes, granulocytes and monocytes differentiate from the myelomonocytic progenitor cell. During host defense, monocytes are recruited to damaged or injured tissue where they differentiate into macrophages. The present microenvironment defines the distinct macrophage subtype. Common myeloid progenitor cells and common lymphoid progenitor cells can both give rise to dendritic cells. The illustration was modified from [87].

I.2.2 CD64 and its role in pathogenesis

During immune response, monocytes are efficiently recruited to damaged or infected tissue where they differentiate into macrophages and dendritic cells [88]. Especially MΦ cells are highly heterogeneous and essential for inflammation and host defense among other functions [89]. Pro-inflammatory macrophages (M1Φ cells) are termed as 'classically activated' and efficiently destroy invading pathogens. They express genes encoding for various cytokines, inflammatory molecules and proteases [90]. Furthermore, they are associated with several inflammatory human disorders such as neurodegenerative and autoimmune diseases, chronic wounds and arthritis [91]. M1Φ cells trigger inflammatory responses during type 1 diabetes initiating insulitis and pancreatic β cell death [92]. The persistence of M1 macrophages in chronic skin diseases or wounds prevents the resolution of inflammation and is mediated by sustained local inflammatory conditions [93]. Compared to other MΦ subtypes, M1 macrophages are characterized by an increased expression of CD64 suggesting it as a suitable cellular marker for inflammation [94]. Interferon gamma (IFNγ) and lipopolysaccharide (LPS) are well-described inducers for the M1 polarization *in vitro* [90]. In contrast, 'alternatively activated' macrophages (M2Φ cells) are involved in wound healing and restoration of damaged tissue after initial injury and inflammatory responses. The local tissue microenvironment determines the specialization and function of the present macrophages whereas the subtype differentiation is reversible and allows the cells to adapt to changing environmental conditions [95]. CD64 can also be expressed by neutrophils depending on their previous activation [96]. Similar to M1Φ cells, activated neutrophils potentially damage tissue, bone and cartilage by secreting proteases, toxic oxygen metabolites and pro-inflammatory cytokines thereby facilitating diseases like rheumatoid arthritis or skin fibrosis [97]. Additionally, CD64 represents an interesting target receptor for some clonal hematopoietic disorders. Acute myeloid leukemia (AML) is characterized by misdirected signal transduction pathways causing uncontrolled proliferation of myeloid precursors in the bone marrow, impaired cell differentiation capacity and increased cell survival [98, 99]. A strong genetic heterogeneity and the accumulation of acquired somatic mutations in hematopoietic progenitor cells are common. Balanced chromosomal translocations, inversions or deletions are at least detectable in more than 50% of adult patients [100]. Distinct AML subtypes are classified either according to their morphological and cytochemical characteristics (French-American-British (FAB) cooperative group classification) or their genetic, immunophenotypic, biological,

and clinical features (World Health Organization (WHO) classification) [101]. Following the FAB classification, seven subtypes are distinguished (AML-M0-M7). Acute basophilic leukemia appears rarely and has not been included into the FAB classification so far [102]. Common chemotherapeutics such as anthracyclines, cytarabines, flavopiridol or voreloxin are used to treat AML. These substances target the DNA replication, the DNA repair and the cell cycle control [98]. Also antisense oligonucleotides and agents that target anti-apoptotic cascades have been evaluated in clinical trials. However, there is a strong need to develop treatment strategies with a higher target cell specificity. Regarding the application of H22-based CFPs, varying CD64 expression levels are reported for the distinct subtypes whereas the highest is shown by AML-M5 cells [103]. Similarly, the expression of CD64 differs markedly between cells of chronic myelomonocytic leukemia (CMML) patients [104, 105]. The disease is characterized by extraordinary numbers of monocytes, blasts, dysplasia and the ability to progress into AML [106]. Acquired somatic mutations with varying frequency indicate a great clinical, morphological and genetic heterogeneity [104]. Thus, a potential application of H22-based CFPs to support the chemotherapeutic treatment of leukemia would require individual marker analyses of patients.

Nevertheless, CD64 represents a promising target for antibody-based therapeutics due to its unique or upregulated expression on inflammatory cell populations as well as its absence on pluripotent stem cells and CD34-positive hematopoietic progenitor cells [107]. The depletion of M1Φ cells with H22-ETA' has been shown to allow remission of chronic wounds *in vivo* and *ex vivo* supporting the therapeutic potential of our approach [93]. Leukemia patients with CD64-positive blasts might benefit from an H22-based CFP treatment strategy by reducing the total blast number with higher specificity than standard chemotherapy.

I.3 Human angiogenin and its usability as effector domain for CFPs

I.3.1 Angiogenin - a ribonuclease with double-edged properties

Human angiogenin, also known as RNase 5, is a 14-kDa stress-activated ribonuclease sharing 35% sequence homology with HPR [108]. It strongly induces neovascularization (angiogenesis) and was found to facilitate the growth and metastasis of several tumor entities [109, 110]. Loss-of-function mutants have been associated with the persistence of amyotrophic lateral sclerosis (ALS) indicating certain neuroprotective activities of the

enzyme [111]. The ribonucleolytic activity of Ang is 10^5-10^6-fold lower compared to RNase A caused by an active center obstruction by glutamine at position 117 [112]. However, the low activity is necessary for its biological function. Ang is expressed by mast cells and fibroblasts, which secrete the enzyme into the blood stream via an N-terminal signal peptide [108, 113, 114]. It can bind to smooth muscle cells, endothelial cells and motor neurons to stimulate their proliferation, cell migration and tubular development in response to environmental conditions [112, 115]. Surface actin and a 170-kDa putative receptor are both recognized and required for endocytosis. Their prevalence strongly depends on the cellular and environmental conditions of the target cells, thereby regulating the specific uptake of the ribonuclease [116]. After receptor-mediated endocytosis, Ang is expected to translocate into the cytosol from early endosomes but this has still to be verified [117]. A nuclear localization signal (NLS) spanning amino acids 55-59 facilitates its rapid accumulation in the nucleus under physiological conditions [118]. It promotes the transcription of ribosomal RNA (rRNA) in the nucleoli by enhancing the formation of the RNA polymerase I pre-initiation complex at the ribosomal DNA promoter [119]. This stimulates the protein biosynthesis necessary for blood vessel growth, primary tumor development and metastasis. Under physiological conditions, the uptake and nuclear translocation of Ang is a well-regulated process depending on the cell density and environmental conditions. However, some cancer cells were found to continuously take up the ribonuclease, most probably to accomplish the extraordinary metabolic requirements [120, 121]. In contrast to these anti-apoptotic functions, Ang can also inhibit cell-free protein synthesis by cleaving 5S, 18S and 28S rRNA as well as transfer RNA (tRNA) at the 3'-CCA termini and certain anticodon loops [112, 122]. The cleavage was found to be species-dependent [51] and mediates the rapid inactivation of ribosomes and tRNAs. It further leads to the emergence of tRNA-derived stress-induced RNAs (tiRNAs). The 5'-tiRNA fragments have multiple functions including 1) the formation of stress granules, 2) the RNA-induced silencing complex-mediated degradation or silencing of messenger RNA (mRNA), 3) the displacement of eukaryotic initiation factors eIF4A and eIF4G from capped and uncapped mRNAs and finally 4) the displacement of eIF4F from the m7G-cap [45, 123, 124]. These events ultimately cause a translational shutdown and reflect an active cellular stress response that rapidly blocks energy-intensive processes during unfavorable environmental conditions [125]. During translational arrest, the internal ribosome entry site (IRES)-mediated translation of repair enzymes is described to enable the eradication

of cellular damage [126, 127]. How Ang induces apoptosis has not been clarified so far but it is known to be cytotoxic when injected into *Xenopus* oocytes [128]. It further reduced the growth and DNA replication of bovine smooth muscle cells *in vitro* [129]. According to these findings, the targeted cell depletion using Ang as human effector domain in CFPs could be demonstrated in several studies [53, 130-135]. The assumed mode of action is illustrated in Figure 2.

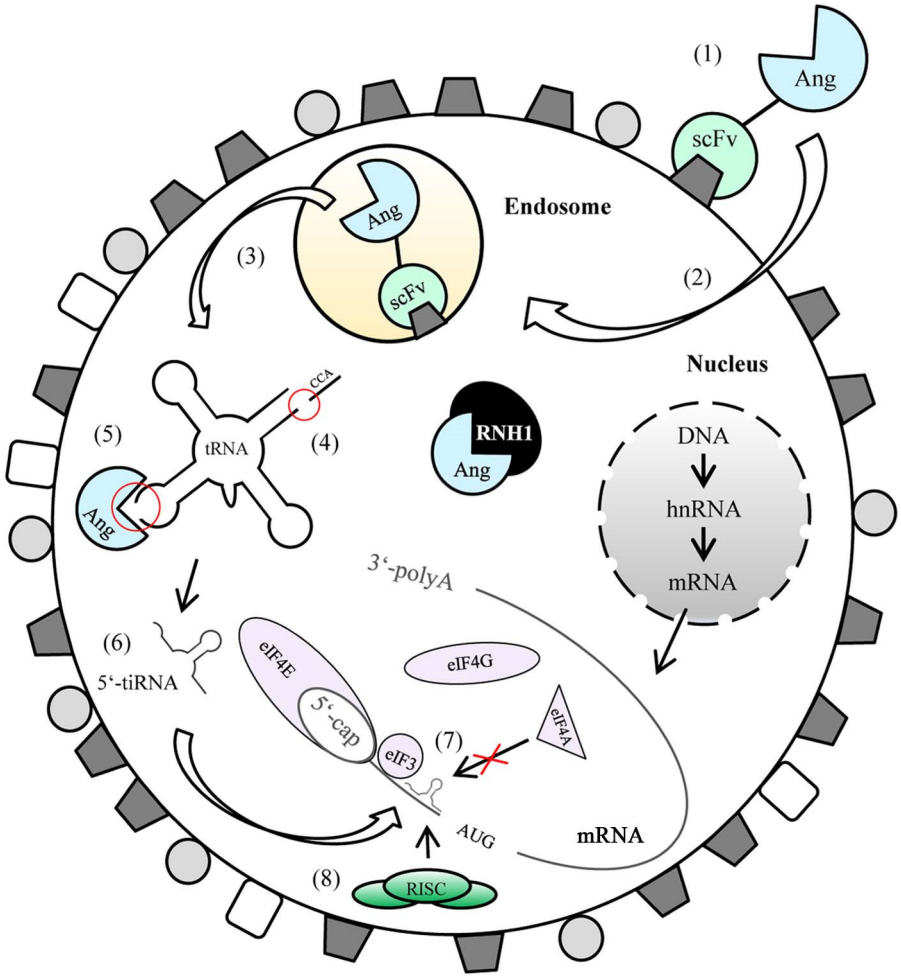


Figure 2: Assumed cytotoxic activity of an angiogenin-based cytolytic fusion protein.
The angiogenin-based cytolytic fusion protein specifically targets an overexpressed receptor on the surface of malignant cells (1). After receptor-mediated internalization (2), the early endosome acidifies and Ang escapes into the cytosol (3). There it cleaves the 3'-CCA termini of tRNAs (4) and particular anticodon-loops (5) to generate tiRNAs (6). 5'-tiRNA fragments efficiently induce translational arrest by masking binding sites for eIF4A and eIF4G on mRNA (7). 5'-tiRNAs are further incorporated into RISC (8) to mediate mRNA degradation and silencing. All events synergistically promote a translational arrest and apoptosis induction. Abbreviations: Ang, Angiogenin; scFv, Single chain variable fragment; tRNA, Transfer RNA; hnRNA, Heterogeneous nuclear RNA; mRNA, Messenger RNA; tiRNA, tRNA-derived stress-induced RNAs; eIF, Eukaryotic initiation factor; RISC, RNA-induced silencing complex. The illustration was modified from [3].

I.3.2 Inhibition of angiogenin by the eukaryotic ribonuclease inhibitor RNH1

The eukaryotic ribonuclease inhibitor RNH1 (also known as RI, RNH or PRI) binds all monomeric members of the pancreatic RNase family with high affinity [55] whereas the strongest interaction is described with human Ang ($K_i \approx 7.1 \times 10^{-16}$ M) [136]. Accordingly, the complex stability of RNH1-Ang is almost 60-fold higher than with RNase A. The protein interaction occurs in 1:1 stoichiometry, has an extraordinary half-life and completely abolishes the ribonucleolytic and angiogenic activity of Ang [137-139]. RNH1 is continuously expressed in all human cell types explaining its abundance being ≥ 0.01% of the total intracellular protein content [140-142]. The inhibitor is predominantly located in the cytosol but it can also be found in mitochondria and the nucleus [143]. It has a horseshoe-shaped structure with a molecular weight of approximately 50 kDa, composes of entirely leucine-rich repeats and supports the maintenance of intracellular redox homeostasis [144, 145]. Under physiological conditions, cytoplasmic Ang is strongly inhibited by RNH1 to prevent the induction of translational arrest but it remains active in the nucleus to stimulate rRNA transcription and protein biosynthesis [146]. In the presence of stress, cytoplasmic Ang is no longer inhibited and thus able to execute the cellular stress response by tRNA cleavage [147]. Some non-human ribonucleases, such as ranpirnase (onconase) or bovine seminal RNase (BS-RNase), demonstrate a remarkable cytotoxic potency because they are less sensitive or even resistant towards the inhibitor [142, 148]. Thus, the evasion of RNH1 is considered as essential for the cytotoxicity of human ribonucleases [11]. Apoptosis induction with Ang or similar RNH1-sensitive ribonucleases consequently requires the delivery of sufficient amounts to overcome the intracellular inhibition by RNH1 [55].

I.4 Objectives

The pro-apoptotic activity of Ang is believed to depend on cytoplasmic tRNA cleavage in the cytosol of target cells in the presence of the inhibitor. According to the considered requirements for cytotoxic ribonucleases, the potency of human Ang as effector domain is hampered by four adverse properties being 1) the lack of a natural translocation domain, 2) a weak ribonucleolytic activity, 3) the cytoplasmic inhibition by RNH1 and 4) the potential translocation into the nucleus as non-target cell compartment. The aim of this work was to investigate if the cytotoxic potential of Ang wild type can be improved by modifying these

limiting properties. To reach this goal, the literature was screened for angiogenin mutations that abolish the above-mentioned limitations (points 2-4) and thus may increase the cytotoxicity of the ribonuclease as CFP effector domain. Several promising mutations were identified referring to the wild type enzyme. Corresponding variants have been characterized by neovascularization studies, protein crystallizations and immunofluorescence experiments. Selected amino acid exchanges were incorporated into wild type Ang using site-directed mutagenesis and the variants were fused to the scFv H22 (declared as H22 hereafter) to allow the evaluation of cytotoxicity. Figure 3 illustrates the underlying working strategy based on successive rounds of mutagenesis and evaluations.

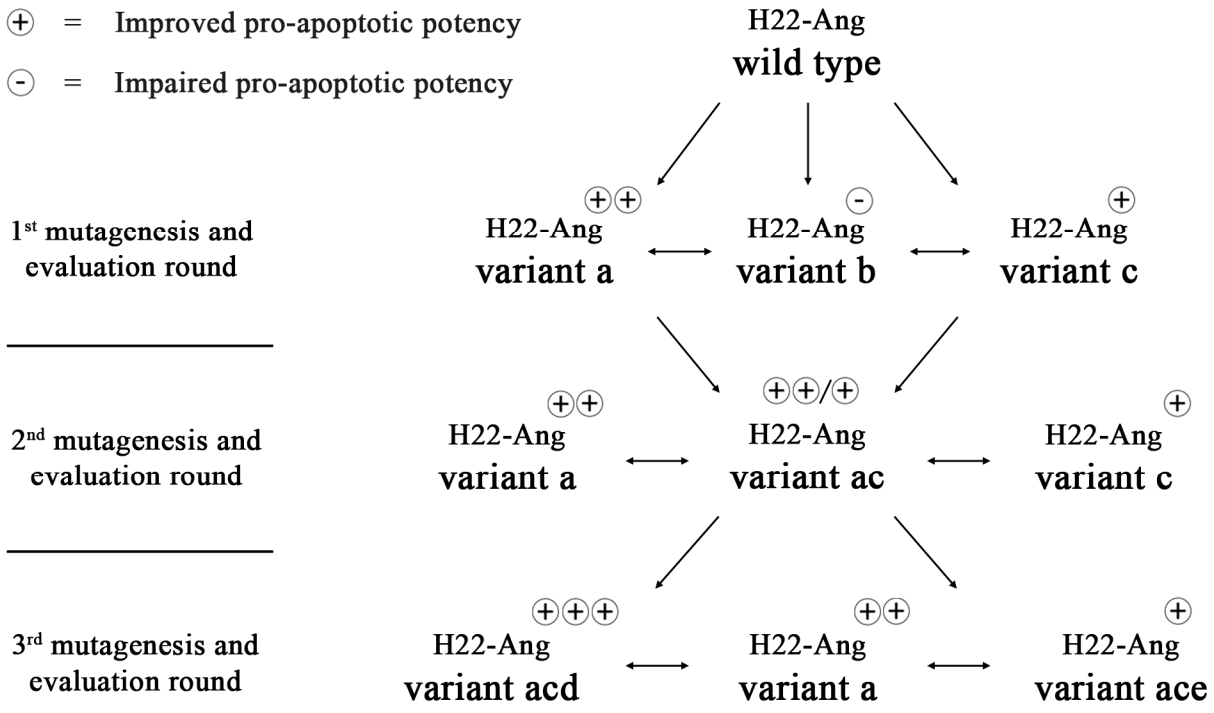


Figure 3: Theoretical workflow of mutant generation and evaluation.
Individual letters behind the variants indicate single introduced mutations whereas subsequent letters represent a combination of these mutations. The H22-Ang wild type DNA was used as template to introduce amino acid exchanges into the Ang-encoding sequence using site-directed mutagenesis. After fusion protein production, the mutant CFPs were tested for an increased pro-apoptotic activity compared to H22-Ang wild type *in vitro*. In the second round, promising CFPs underwent detailed characterization studies and mutations that increased the efficacy were joined to investigate if synergistic or cooperative effects can be achieved upon combination. The superior aim of the third round was to use the revealed knowledge for the development of an Ang variant that combines multiple improved properties that cooperatively or synergistically increase the cytotoxicity. Abbreviation: Ang, Angiogenin; CFP, Cytolytic fusion protein.

The first round was carried out as *proof-of-concept* to investigate if the following strategies increase the potency of H22-Ang wild type: 1) increasing the enzymatic activity of Ang, 2) abolishing the ability for nuclear translocation and 3) decreasing the inhibition susceptibility. Fusion proteins that did not outperform the potency of H22-Ang wild type were excluded from further experiments. In the second round, H22-Ang wild type and favorable CFPs underwent detailed *in vitro* characterization to reveal if the described modified properties of the mutants retained in fusion to H22 and contributed to the increased potency, respectively. Furthermore, favorable mutations were joined in a single variant to test if the mediated effects act in a cooperative or even synergistic manner upon combination. Molecular dynamic (MD) simulations were carried out to demonstrate the individual interactions of Ang mutants and RNH1 at an atomistic level. They further supported the selection of mutations in the third round aiming to generate a variant with increased enzymatic activity and decreased inhibition susceptibility compared to the wild type enzyme.

All fusion proteins were transiently expressed in HEK293T cells and purified from the cell culture supernatant via immobilized metal ion affinity chromatography (IMAC). The characterization of CFPs included the demonstration of 1) cellular binding activity, 2) enzymatic activity, 3) inhibition susceptibility, 4) binding activity towards genomic DNA (gDNA), 5) *in vitro* cytotoxicity towards CD64-positive HL-60 cells and M1 macrophages, 6) protein stability in human and mouse serum and 7) pro-apoptotic activity towards mononuclear cells of leukemia patients *ex vivo*. Additionally, the most efficient H22-Ang variant was equipped with a translocation peptide to reveal a potentially beneficial effect.

II Material and Methods

II.1 Material

II.1.1 Chemicals and consumables

Unless otherwise noted, chemicals and consumables were purchased from Becton Dickinson Bioscience (Heidelberg), Bio-Rad (Munich), Biozym (Oldendorf), Carl Roth (Karlsruhe), Eppendorf (Hamburg), Fluka (Neu-Ulm), GE Healthcare (Freiburg), Gibco BRL (Eggstein), Greiner (Solingen), ICN (Eschwege), Invitrogen (Leek, Netherlands), Millipore (Eschborn), New England Biolabs (NEB, Frankfurt am Main), Nunc (Wiesbaden), Promega (Mannheim), Roche Molecular Biochemicals (Mannheim), Serva (Heidelberg), Sigma Aldrich (Deisenhofen), Starlab (Ahrensburg) and VWR (Darmstadt).

II.1.2 Equipment & supplies

Table 1: Used equipment

Equipment	Supplier
Mini Protean III gel chamber, Bio-Rad Power Supply	Bio-Rad, Munich
Molecular Imager Gel Doc XR System, Quantity One 4.6 software	Bio-Rad, Munich
Mini Trans-Blot Cell	Bio-Rad, Munich
Biowizard Silver Line BW-130	Kojair, Villpula, Finland
Laminar flow hood, Hera Safe HS12	Kendro, Hanau
Retina 420R centrifuge	Hettich Centrifuges, Tuttlingen
Eppendorf 5415 D & 5415 R centrifuges	Eppendorf, Hamburg
Microcentrifuge AL-220 Vac	Carl Roth, Karlsruhe
Biofuge primo R	Heraeus Instruments, Hanau
Thermomixer compact, Thermomixer comfort	Eppendorf, Hamburg
Rotator SB3	Stuart, Staffordshire, UK
Stella Reader 3200, XStella Camera Control software	Raytest GmbH, Straubenhardt
DISCOVERY Comfort Variable Volume Multichannel Pipette	HTL LAB SOLUTIONS, Warsaw, PL
Hera Cell Incubator	Kendro Laboratory Products, Hanau
FACSVerse™, FACSuite™ software	Becton Dickinson, Heidelberg
FACSCalibur™, CellQuest™ Pro v6.0 and Cyflogic v.1.2.1 software	Becton Dickinson, Heidelberg and CyFlo Ltd, Turku, Finland
2720 Thermal Cycler	Applied Biosystems, Carlsbad, CA, USA
DMIL Fluoreszenz Microscope with L5 filter cube,	Leica, Wetzlar
ProgRes® CapturePro v.2.8.8 software	Jenoptik, Jena
DMIL LED Microscope, Leica Application Suite v3.7.0 software	Leica, Wetzlar
ÄKTApurifier, Unicorn 5.10 software	GE Healthcare, Freiburg
Casy 1 TT Cell Counter	Schärfe System, Reutlingen
Heraeus HeraFreeze	Thermo Fisher Scientific, Schwerte
Tecan Genios Pro microplate reader, Magellan v7.1 SPI software	Tecan, Mainz
Epoch Micro-Volume Spectrophotometer System	BioTek, Bad Friedrichshall

II.1.3 Restriction endonucleases and kits

Restriction endonucleases and appropriate buffers were obtained from NEB and applied according to the manufacturer's instructions. Used reaction kits are listed in Table 2.

Table 2: Used reaction kits

Kit	Manufacturer
NucleoSpin® Plasmid	Macherey-Nagel, Düren
NucleoSpin® Gel and PCR Clean-up	Macherey-Nagel, Düren
QuikChange II XL Site-Directed Mutagenesis	Agilent Technologies, Böblingen
QIAamp® DNA Mini and Blood Mini	Qiagen, Hilden

II.1.4 Standard buffer and media compositions

All pH values were adjusted with 32% (v/v) HCl, 1 M NaOH or 5 M NaOH, respectively. Sterilization of media was carried out by autoclaving for 20 min at 121°C and 1 bar. Agar plates for short-term cultivation of bacteria (II.2.3) were prepared by adding 1.5% (w/v) bacto agar to LB medium (Table 3) prior to autoclaving. If required, 0.1% (v/v) ampicillin (50 mg/mL) was added after cooling to ~50°C (LB-amp). Approximately 20 mL of the medium was transferred into sterile petri dishes and allowed to cool down. After solidification, the plates were stored at 4°C for up to one month.

Table 3: Media compositions
Abbreviations: FCS, Fetal calf serum; DMSO, Dimethyl sulfoxide.

Medium	Component	Concentration
LB medium	Bacto tryptone	1% (w/v)
	Yeast extract	0.5% (w/v)
	NaCl	1% (w/v)
SOC medium	Peptone	2% (w/v)
	Yeast extract	0.5% (w/v)
	NaCl	10 mM
	KCl	25 mM
	$MgCl_2$	10 mM
	$MgSO_4$	10 mM
	Glucose	20 mM
RPMI 1640 medium (R10)	FCS	10% (v/v)
	Penicillin	5% (w/v)
	Streptomycin	5% (w/v)
	L-glutamine	2 mM
R20 medium	FCS	10% (v/v)
	R10 medium	
Cryopreservation medium	R20 medium	
	DMSO	10% (v/v)

Table 4: Buffer compositions

Buffer	Component	Concentration
TAE buffer	Tris-base	40 mM
	Acetic acid	19 mM
	EDTA x $2H_2O$	10 mM
5x Orange G loading buffer, pH 7.6	TAE buffer	
	Orange G	0.1% (w/v)
	Glycerol	30% (v/v)
TfBI buffer, pH 5.8	RbCl	50 mM
(sterile-filtered, stored at 4°C)	$MnCl_2$	20 mM
	Potassium acetate	15 mM
	$CaCl_2$	7 mM
	Glycerol	15% (v/v)
TfBII buffer, pH 6.8	RbCl	5 mM
(sterile-filtered, stored at 4°C)	MOPS	5 mM
	$CaCl_2$	50 mM
	Glycerol	15% (v/v)
4x Incubation buffer, pH 8.0	NaH_2PO_4	200 mM
	NaCl	1.2 M
	Imidazole	40 mM
Elution buffer, pH 8.0	NaH_2PO_4	50 mM
	NaCl	300 mM
	Imidazole	500 mM
10x PBS buffer	NaCl	1.37 M
	KCl	27 mM
	Na_2HPO_4 x $2H_2O$	100 mM
	KH_2PO_4	17.6 mM
PBST buffer	PBS buffer	
	Tween 20	0.05% (v/v)
RNase cleavage buffer, pH 7.5	Tris-base	30 mM
	NaCl	30 mM
	RNase-free H_2O	30 mM
Triton X-100 lysis buffer	PBS buffer	
	Triton X-100	1% (v/v)
	Protease inhibitor tablet with EDTA	1x per 50 mL
10x Annexin V binding buffer, pH 7.4	HEPES	100 mM
	NaCl	1.4 M
	$CaCl_2$	25 mM
5x Protein loading buffer (reducing)	Tris-HCl (pH 6.8)	62.5 mM
	Glycerol	30% (v/v)
	SDS	4% (v/v)
	β-mercaptoethanol	10% (v/v)
	Bromophenol blue	0.05% (v/v)
5x Loading buffer, RNase-free	Formaldehyde	48% (v/v)
	Glycerol	48% (v/v)
	Na_3PO_4	20 mM
	Bromophenol blue	0.25% (v/v)
5x TGS buffer	Tris-base	125 mM
	Glycerol	9.6 mM
	SDS	8.7 mM
Transfer buffer	TGS buffer	
	Methanol	20% (v/v)

Table 5: Other solutions

Solution	Component	Concentration
Coomassie staining solution	Coomassie Brilliant Blue G-250	0.25% (w/v)
	Methanol	50% (v/v)
	Acetic acid	9% (v/v)
	Trichloroacetic acid	2% (v/v)
XTT solution	RPMI 1640	
	XTT substrate	100% (w/v)
	PMS	0.1% (w/v)
RNase-free H_2O	H_2O	
	DEPC *	0.1% (v/v)
Membrane blocking solution	PBST buffer	
	Milk powder	5% (w/v)

* DEPC was incubated overnight and inactivated by autoclaving for 20 min at 121°C and 1 bar.

II.1.5 Bacterial strains

The following *Escherichia coli* strain was used for amplification and cloning of recombinant plasmids:

DH5α: genotype: F^-, endA1, hsdR17(r_K^-, m_K^+), supE44, thi-1, recA1, gyrA96, relA1 (Thermo Fisher Scientific, Schwerte) [149].

II.1.6 Eukaryotic cell lines

Eukaryotic cell lines used in this work are listed in Table 6 and were cultivated under standard conditions (II.3.1). HL-60 cells were kindly provided by Dr. Theophilus Thepen (Fraunhofer Institute for Molecular Biology and Applied Ecology IME (IME), Department of Pharmaceutical Product Development (PPD), Aachen). L-540cy cells were kindly provided by Prof. Dr. Andreas Engert (University Hospital of Cologne).

Table 6: Used eukaryotic cell lines

Cell type	Supplier	Description	Reference
HEK293T	ATCC-No.: CRL-11268	Adherent embryonic kidney cells, human	[150]
HL-60	ATCC-No.: CCL-240 *	Promyeloblastic suspension cells, human	[151]
L-540cy	**	Hodgkin's-derived suspension cells, human	[152]
A431	DSMZ-No.: ACC 91	Adherent epidermoid carcinoma cells, human	[153]

* Kindly provided by Dr. Theophilus Thepen, Fraunhofer IME, PPD, Aachen.

** Kindly provided by Prof. Dr. med. Andreas Engert, University Hospital of Cologne.

II.1.7 Vector system

The eukaryotic pMS expression vector was used for the production of CFPs (Figure 4). It represents a derivative of the pSecTag2 vector (Invitrogen, Carlsbad, CA, USA) and the pIRES-eGFP vector (Clontech Laboratories, Mountain View, CA, USA) [132]. The CFP expression is mediated by a cytomegalovirus (CMV)-derived promotor whereas the N-terminal encoded Ig-kappa leader mediates the secretion of the expressed proteins into the cell culture supernatant. The C-terminal polyhistidine tag (His-tag) allows the purification of CFPs via IMAC (II.4.1) and the Myc-tag can be used for immunodetection. The tags are followed by a synthetic intron sequence (IVS) to stabilize the mRNA whereas an internal ribosomal entry site (IRES) enables the co-translation of the enhanced green fluorescent protein (eGFP). Resistance genes for ampicillin (ampR) and zeocin™ (zeoR) allow for selection during cloning and transient expression (II.2.3, II.3.1).

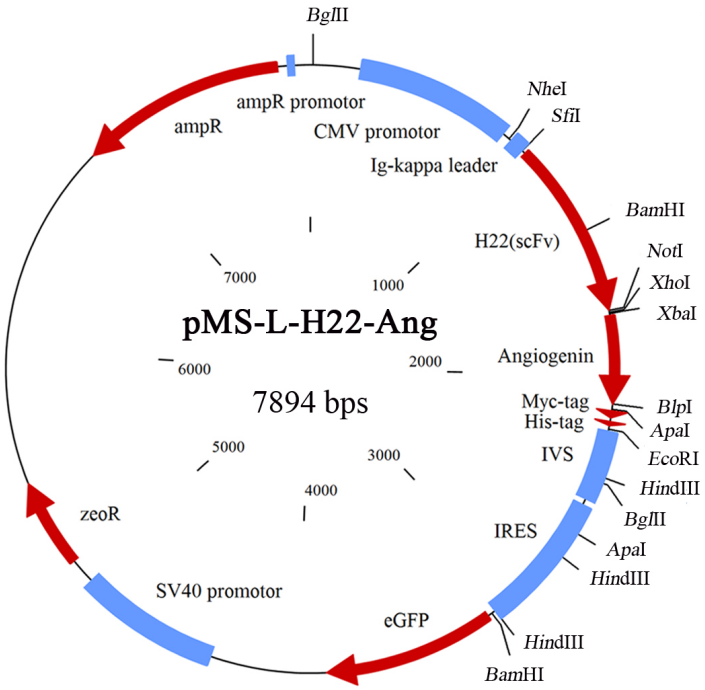


Figure 4: Schematic overview of the pMS expression vector.
The CFP expression is mediated by a CMV-derived promotor whereas the N-terminal encoded Ig-kappa leader induces the secretion into the cell culture supernatant. The C-terminal His-tag allows the purification of fusion proteins by affinity chromatography and the Myc-tag can be used for immunodetection. The tags are followed by an IVS sequence to stabilize the mRNA. An IRES sequence enables the co-translation of eGFP as reporter protein [132]. Resistance genes for ampicillin (ampR) and zeocin™ (zeoR) are for selection purposes. Abbreviations: CFP, Cytolytic fusion protein; CMV, Cytomegalovirus; His-tag, Polyhistidine tag; IVS, Synthetic intron sequence; IRES, Internal ribosomal entry site; eGFP, Enhanced green fluorescent protein.

Theoretical cloning was carried out using the Clone Manager 9 Professional Edition software (Scientific & Educational Software, Morrisville, NC, USA). The annotated DNA sequence encoding for H22-Ang wild type is shown in VII.5.

II.1.8 Antibodies

The following antibodies (Table 7) were used for immunodetection of proteins (II.4.2) and flow cytometry analyses (II.5) according to the manufacturer's instructions.

Table 7: Antibodies and their application
Abbreviations: WB, Immunodetection after western blotting; FC, Flow cytometry; HRPO, Horseradish peroxidase; FITC, Fluorescein isothiocyanate; APC, Allophycocyanin.

Antibody	Manufacturer	Application
Mouse-anti-penta-his	Qiagen, Hilden	WB
Mouse-anti-hexa-his (HIS.H8)	Thermo Fisher Scientific, Schwerte	WB
Goat-anti-mouse, Fc-specific, HRPO labelled	Sigma Aldrich, Taufkirchen	WB
Mouse-anti-β-actin, HRPO labelled	Sigma Aldrich, Taufkirchen	WB
Mouse-anti-RNH1 (F-5)	Santa Cruz Biotechnology, Heidelberg	WB
Mouse-anti-penta-his, ALEXA Fluor® 488 Conjugate	Qiagen, Hilden	FC
Mouse-anti-human CD14, FITC labelled	BioLegend, San Diego, CA, USA	FC
Mouse-anti-human CD33, APC labelled	BioLegend, San Diego, CA, USA	FC
Mouse-anti-human CD64, FITC labelled	BioLegend, San Diego, CA, USA	FC
Mouse-anti-human CD64, APC labelled	eBioscience, Frankfurt	FC
Mouse-anti-human CD206, FITC labelled	BioLegend, San Diego, CA, USA	FC
Mouse-anti-human CD301, APC labelled	BioLegend, San Diego, CA, USA	FC

II.1.9 Synthetic oligonucleotides

All oligonucleotides (Table 8) were designed with Clone Manager 9 software, synthesized by Eurofins (Ebersberg) and used for DNA sequencing (II.2.8) or site-directed mutagenesis (II.2.1) as indicated. The oligonucleotides 5'-*Sfi*_for and hinterhis_rev were kindly provided by the Fraunhofer IME, Aachen. Complementary binding sites are indicated in the annotated DNA sequence of H22-Ang wild type, respectively (VII.5).

Table 8: Oligonucleotide primer and their application
Abbreviations: SQ, DNA sequencing; MC, Molecular cloning; NE, Nucleotide exchange.

Primer	Sequence (5'-3')	Application
Ang-5'-Seq_for	GGATAACTCCAGGTACACACACTTCC	SQ
Ang-3'-Seq_rev	CCGGACGACGGAAAATTGACTGATCC	SQ
5'-*Sfi*_for	CGGCCCAGCCGGCC	MC
hinterhis_rev	CCAACAGCTGGCCCTCGCAGACAG	MC
GGRR_for	CCACTTGCAAGCTACATCGGCGCTCCCCCTGGCCTCCATGCC	NE
GGRR_rev	GGCATGGAGGCCAGGGGGAGCGCCGATGTAGCTTGCAAGTGG	NE
NLS_RA_for	GCATCATGAGGAGAGCGGGCCTGACCTCACCC	NE
NLS_RA_rev	GGGTGAGGTCAGGCCCGCTCTCCTCATGATGC	NE
QG_for	CCTGTCCACTTGGATGGATCAATTTTCCGTCG	NE
QG_rev	CGACGGAAAATTGATCCATCCAAGTGGACAGG	NE
R55A_for	GTGAAAGCATCATGGCGAGACGGGGCCTGACC	NE
R55A_rev	GGTCAGGCCCCGTCTCGCCATGATGCTTTCAC	NE
WA_for	GGAGGTTCCCCCGCGCCTCCATGCCAG	NE
WA_rev	CTGGCATGGAGGCGCGGGGGAACCTCC	NE
HA_for	GGATAACTCCAGGTACACAGCCTTCCTGACCCAGCACTATGAT	NE
HA_rev	GCATCATAGTGCTGGGTCAGGAAGGCTGTGTACCTGGAGTTAT	NE
R5A_for	CGAGTCTAGACAGGATAACTCCGCGTACACACACTTCCTGACC	NE
R5A_rev	GGGTCAGGAAGTGTGTGTACGCGGAGTTATCCTGTCTAGACTC	NE
DH_for	GGCTTACCTGTCCACTTGCATGGATCAATTTTCCGTCGTCCGG	NE
DH_rev	CCGGACGACGGAAAATTGATCCATGCAAGTGGACAGGTAAGC	NE
KQ_for	GCCTGACCTCACCCTGCCAAGACATCAACACATTTATTCATGG	NE
KQ_rev	GCCATGAATAAATGTGTTGATGTCTTGGCAGGGTGAGGTCAGG	NE

II.2 Methods

II.2.1 Mutagenesis and splicing by overlap extension PCR

The Ang-encoding sequence (VII.5) comprised amino acids 25-147 of the native ribonuclease since the first 24 amino acids encode for a signal peptide [108]. Amino acid exchanges were introduced into the pMS-L-H22-Ang wild type sequence (II.1.7) using the QuikChange II XL Site-Directed Mutagenesis Kit (II.1.3) according to the manufacturer's instructions. Primer combinations, annealing temperatures and primer-specific data are summarized in Table 9. The expression vector pMS-L-H22-Ang GGRR/QG$_{mut}$ was generated by using the pMS-L-H22-Ang GGRR$_{mut}$ DNA as template and the primer QG_for and QG_rev (Table 8) to introduce the additional mutation. Splicing by overlap extension (SOE) PCR was carried out to introduce the R5A, H8A, K40Q and D116H mutations into the pMS-L-H22-Ang GGRR/QG$_{mut}$ DNA, respectively [2]. Corresponding oligonucleotide exchange primer are listed in Table 8. All plasmids were used to transform heat-shock competent *E.coli* DH5α cells (II.2.2, II.1.5) that were spread on selective LB agar plates (II.2.3). Overnight (o/n) suspension cultures were

inoculated using a single bacteria colony and plasmid DNA was prepared the next day (II.2.4). Successful base exchanges were verified by DNA sequencing (II.2.8).

Table 9: Primer combinations and annealing temperatures for mutagenesis PCR
Abbreviations: $T_{m,}$ Melting temperature; T_a, Annealing temperature.

Primer combination	Ang variant	GC content (%)	Mismatch (%)	T_m (°C)	T_a (°C)
GGRR_for, GGRR_rev	$GGRR_{mut}$	66.7	9.52	83	75
NLS_RA_for, NLS_RA_rev	NLS RA_{mut}	65.6	9.38	81	71
QG_for, QG_rev	QG_{mut}, GGRR/QG_{mut}	50	9.38	71	57
R55A_for, R55A_rev	RA_{mut}	62.5	6.25	79.8	73
WA_for, WA_rev	WA_{mut}	74.1	7.41	79.5	73

II.2.2 Preparation and transformation of heat-shock competent *E.coli* cells

Cells from a glycerol stock of *E.coli* DH5α cells (II.2.3, II.1.5) were spread on a LB agar plate (II.1.4) and cultivated o/n under standard conditions without antibiotics (II.2.3). A single grown bacteria colony was used to inoculate 100 mL LB medium (II.1.4, Table 3) as pre-culture and incubation was carried out o/n at 37°C and 225 rpm. Then a 100 mL main-culture was inoculated 1:100 with the pre-culture and shaken with 225 rpm at 37°C until an OD_{600} of 0.5 was reached. Bacteria were centrifuged (3,500 *g*, 5 min, 4°C) and the supernatant was removed. The cell pellet was carefully resuspended in cold TfBI buffer (II.1.4, Table 4) following centrifugation (3,500 *g*, 5 min, 4°C). After supernatant removal, 4 mL cold TfBII buffer (II.1.4, Table 4) was used to resuspend the bacteria. Aliquots of 200 µl volume were shock-frozen in liquid nitrogen and stored at -80°C. For the transformation of *E.coli*, one aliquot of prepared heat-shock competent bacteria was mixed with DNA on ice. The latter was either a ligation reaction (II.2.7) or 100 pg of purified plasmid DNA for retransformations (II.2.4). After 10 min incubation, the suspension was heated to 42°C for 90 s and rapidly cooled down for 2 min on ice. Then 800 µl SOC medium (II.1.4, Table 3) was added for 1 h at 37°C on a rotator allowing the regeneration of bacteria and expression of the ampicillin resistance gene (II.1.7, Figure 4). The cells were settled by centrifugation (2,000 *g*, 2 min), dissolved in 100 µl SOC medium and plated on selective LB agar plates (II.1.4, II.2.3). In case of retransformations, 100 µl of the transformed bacteria were plated without a preceding centrifugation step. Incubation was carried out o/n at 37°C to allow colony forming.

II.2.3 Storage and culturing of bacteria

Bacterial suspension cultures grew in LB medium (II.1.4, Table 3) on an orbital shaker (37°C, 225 rpm). Transformed bacteria were cultivated in the presence of 0.1% (v/v) ampicillin (50 mg/mL) for selection and to ensure plasmid preservation. The short-term storage of bacteria was carried out on LB-amp agar plates at 4°C (II.1.4). For long-term storage, glycerol stocks were prepared by mixing 125 µl sterile 70% (v/v) glycerol with 375 µl transformed bacteria in LB medium. The glycerol stocks were shock-frozen in liquid nitrogen and stored at -80°C.

II.2.4 Preparation of DNA and determination of concentration

Plasmid DNA was prepared from overnight cultures of transformed *E.coli* cells (II.1.5, II.2.3) using the NucleoSpin® Plasmid kit (II.1.3) and gDNA was isolated from A431 cells (II.1.6) using the QIAamp® DNA Mini and Blood Mini kit (II.1.3) according to the manufacturer's instructions. The DNA concentration was determined using the Epoch Micro-Volume Spectrophotometer (Biotek, Bad Friedrichshall). The $A_{260/280}$ ratio allowed estimating the purity of the preparation. DNA samples were stored at -20°C.

II.2.5 Restriction of DNA

Restriction digests were performed using one (single digest) or two (double digest) restriction endonucleases according to the manufacturer's instructions in the most appropriate buffer system (II.1.3). The digest of plasmid DNA with *Sfi*I was carried out o/n at 50°C.

II.2.6 Analytical and preparative agarose gel electrophoresis

DNA fragments were separated according to their size by using analytical agarose gel electrophoresis [154]. The separation was carried out in 0.8-2% (w/v) agarose gels with a field intensity of 4-5 V/cm depending on the expected fragment sizes. Gels were prepared using 1x TAE buffer (II.1.4, Table 4) and 0.1 µg/mL ethidium bromide to allow fragment visualization at 302 nm. DNA samples were supplemented with 5x Orange G loading buffer (II.1.4, Table 4) whereas 3 µl of 2-log DNA ladder (NEB) was co-separated to allow size

estimation. Gel images were captured using the Molecular Imager Gel Doc XR System and Quantity One 4.6 software (Bio-Rad, Munich) (II.1.2). Following preparative gel electrophoresis, the desired DNA fragments were excised from the gel using a clean scalpel and extraction was carried out using the NucleoSpin® Gel and PCR Clean-up kit (II.1.3) according to the manufacturer's instructions. The concentration and purity of DNA samples was determined as described in II.2.4.

II.2.7 Ligation of restricted DNA

Purified DNA fragments (II.2.6) with compatible ends (II.2.5) were ligated using the T4 DNA Ligase (NEB) in a reaction volume of 10-20 µl following the manufacturer's instructions. Insert DNA was applied in a 3-fold molar excess relative to the vector amount. After 1 h incubation at room temperature (RT), the ligation reaction was mixed with one aliquot of heat-shock competent *E.coli* DH5α cells for transformation (II.2.2).

II.2.8 DNA sequencing

DNA samples (plasmid DNA, 500 ng; PCR fragments, 60 ng) were supplemented with 20 pmol sequencing primer (Table 8) and analyzed by the sequencing facility of the Fraunhofer IME (Aachen) on an ABI Prism 3700 DNA Analyzer using BigDye™ cycle sequencing terminator chemistry (Applied Biosystems). The method bases on the incorporation of chain-terminating dideoxynucleotides during strand replication in a PCR reaction [155]. Data evaluation was carried out using Lasergene SeqMan v7.0 software (DNASTAR software, Madison, WI, USA).

II.3 Cell culture

II.3.1 Cultivation, cryopreservation and thawing of eukaryotic cells

All used cell lines (II.1.6) were cultured under standard conditions (37°C, 100% humidity and 5% CO_2) in R10 medium (II.1.4, Table 3). Depending on the growth rate, cell passaging was carried out to maintain the density below 1 x 10^6 cells/mL for suspension cells. Adherent cells were detached from the culture flask using a cell scraper before reaching confluency and diluted 1:20 with R10 medium. Transfected HEK293T cells (II.3.2) were cultivated under

standard conditions and in the presence of 100 ng/mL zeocin™ (Invitrogen) for selection and to ensure plasmid preservation (II.1.7). The CFP expression was carried out in cell culture flasks with a surface area of 25-500 cm^2. Prior to cryopreservation, HEK293T cells were collected in an exponential growth phase with at least 90% cell viability. Suspension cells were grown to a cell density of 10^7 cells/mL. The cells were centrifuged (10 min, 300 *g*) and resuspended in 2 mL sterile cryopreservation medium (II.1.4, Table 3) per cell culture flask. One mL aliquots were prepared in sterile cryogenic vials and incubation was carried out in Mr. Frosty™ Freezing Containers (Thermo Fisher Scientific) at -80°C for 24 h. After the freezing process, the vials were transferred into liquid nitrogen. For re-cultivation of cells, the aliquots were rapidly thawed and 30 mL cold RPMI 1640 medium was gently added to dilute DMSO and to avoid a cellular heat-shock. After centrifugation (10 min, 300 *g*), the supernatant was discarded and the cells were resuspended in 10 mL R20 medium (II.1.4, Table 3) following transfer into T25 cell culture flasks. Transfected cells were cultivated under standard conditions and in the presence of zeocin™ as described above.

II.3.2 Transfection of eukaryotic cells

The transfection of HEK293T cells (II.1.6) was carried out using Roti®-Fect (Carl Roth) according to the manufacturer's instructions. Briefly, 2 µg of plasmid DNA (II.2.4) and 10 µl transfection reagent were mixed and incubated for 30 min at RT. The mixture was then added to the cells for 4 h at 37°C. Afterwards, the transfection medium was replaced by R10 medium without antibiotics (II.1.4, Table 3). The eGFP-mediated green fluorescence of the cells (II.1.7) was analyzed after 24-72 h under UV light exposure (II.3.4) and zeocin™ was added to the culture medium for selection (II.3.1).

II.3.3 Preparation of mononuclear cells and polarization of M1 macrophages

Human buffy coats were obtained from the Department of Transfusion Medicine, University Hospital Aachen. The isolation and cultivation of peripheral blood mononuclear cells as well as the polarization of M1Φ cells was carried out as previously described [51]. The differentiation process was visually confirmed by investigating morphological changes using light microscopy (II.3.4). Peripheral blood or bone marrow specimens of leukemia patients

were kindly provided by the Department of Hematology and Oncology (University Hospital Aachen, Internal Medicine IV) after prescreening for CD64 availability and subtype determination. Samples were donated after informed consent and with the approval of the clinical research ethics board of the RWTH Aachen University. Mononuclear leukemia cells were prepared as described previously [2].

II.3.4 Light and fluorescence microscopy

The morphological changes of macrophages following M1 polarization (II.3.3) were visualized using the DMIL microscope (Leica, Wetzlar) with ProgRes® CapturePro v.2.8.8 software (Jenoptik, Jena). Additionally, the DMIL LED microscope (Leica) with Leica Application Suite v3.7.0 software was used to analyze the eGFP expression in HEK293T cells (II.1.6) 72 h after transfection (II.3.2) with pMS expression vectors (II.1.7). Images were captured with 400-fold magnitude, respectively. Processing was carried out using Adobe Photoshop CS5.1 software.

II.4 Immunological methods and protein characterization

II.4.1 Protein purification from cell culture supernatant using IMAC

Prior to purification, the culture supernatant was cleared by filtration using glass fiber pre-filters (Sartorius, Göttingen). The cell-free supernatant was supplemented with 4x incubation buffer (II.1.4, Table 4) and cleared from remaining solids by filtration using 0.44 µm cellulose acetate membrane filters (Sartorius). CFP purification was carried out by IMAC using prepacked 5-mL Ni^{2+}-NTA Superflow cartridges (Qiagen, Hilden) on an ÄKTApurifier system (GE Healthcare, Freiburg) with Unicorn 5.10 software. Prior to sample loading, the column was equilibrated with 1x incubation buffer (II.1.4, Table 4). The supernatant was passed through the column o/n with an average flow rate of 1.5-2.5 mL/min at RT to avoid degassing effects. Afterwards, the Ni^{2+}-NTA matrix was washed with imidazole concentrations from 20-40 mM. The release of recombinant proteins was achieved by rinsing the columns with elution buffer (II.1.4, Table 4) until a base line at A_{280} established. Elution fractions were collected and analyzed by sodium dodecyl sulfate (SDS) polyacrylamide gel electrophoresis (PAGE) (II.4.2).

II.4.2 SDS-PAGE and western blot analysis

Protein samples were analyzed by discontinuous SDS-PAGE as described previously [156]. The samples were mixed with 5x reducing protein loading buffer (II.1.4, Table 4) and denatured at 100°C for 5 min. Sample separation was carried out for 60 min in 1x TGS buffer (II.1.4, Table 4) at 160 V and RT using the Mini-Protean III gel electrophoresis equipment. Seven µl of the Prestained Protein Marker or the Color Protein Standard (both NEB) were co-separated as internal size standard as indicated. Protein bands were stained for 30 min at RT using Coomassie staining solution (II.1.4, Table 5) and destained o/n in water. For immunodetection, the separated proteins were transferred from SDS gels onto nitrocellulose membranes (GE Healthcare) by an electro-tank blotting method described earlier [157]. The transfer was carried out at 4°C and 270 mA for 70 min following by the addition of membrane blocking solution (II.1.4, Table 5). A general workflow for the detection of proteins on western blot membranes is given in Table 10. All steps were carried out at RT or at 4°C when incubated o/n. Antibodies (II.1.8) were diluted in PBST buffer (II.1.4, Table 4) as indicted. SIGMA*FAST*™ 3,3'-Diaminobenzidine tablets (Sigma-Aldrich) and Pierce™ ECL Western Blotting Substrate (Thermo Fisher Scientific) were used according to the manufacturer's instructions, respectively. Chemiluminescence imaging was carried out using the Stella Reader 3200 (Raytest GmbH, Straubenhardt) and XStella Camera Control software.

Table 10: Workflow for immunodetection of proteins on western blot membranes
Abbreviations: HRPO, Horseradish peroxidase; o/n, Overnight.

Step	Description	Components and conditions	Duration
1	Membrane blocking	Membrane blocking solution	1 h or o/n
2	Primary antibody	Mouse-anti-penta-his (1:5,000)	1 h or o/n
		Mouse-anti-hexa-his (1:3,000)	1 h or o/n
		Mouse-anti-β-actin-HRPO (1:10,000)	1 h or o/n
		Mouse-anti-RNH1 (1:500)	1 h or o/n
3	Washing	3 x with PBST buffer	
4	Secondary antibody (if required)	Goat-anti-mouse-HRPO (1:5,000)	30 min
5	Washing	3 x with PBST buffer	
6	Detection	SIGMA*FAST*™ 3,3'-Diaminobenzidine tablets	
		Pierce™ ECL Western Blotting Substrate	

II.4.3 Protein enrichment, buffer exchange and sample storage

Fusion proteins were concentrated by centrifugation (3,500 *g*, 4°C) using Vivaspin® 6 columns (Sartorius) with a 10-kDa cut off according to the manufacturer's instructions. Imidazole was removed by dialysis against 5 L cold 1x PBS buffer (II.1.4, Table 4) at 4°C o/n using Spectra/Por® dialysis membranes with a 6-8-kDa cut off (SPECTRUMLABS, Rancho Dominguez, CA, USA). Sterilization of the samples was achieved by either passing the proteins through a 0.22 µm sterile filter (Nalgene, Roskilde, Denmark) or using Corning® Costar® Spin-X® centrifuge tube filters with 0.22 µm pore size (Costar, Corning Incorporated, MA, USA). Short-term storage of fusion proteins was carried out at 4°C whereas long-term storage took place at -80°C.

II.4.4 Determination of protein concentration

Protein concentrations were densitometrically determined in comparison to bovine serum albumin (BSA) standards of known quantity (0.25-2 µg) in a Coomassie Brilliant Blue-stained SDS gel (II.1.4, II.4.2). The visualized protein bands were analyzed using the "Advanced Image Data Analyzer" (AIDA) software (Raytest GmbH) and band intensities for standards were correlated with the respective quantities by linear regression. The standard equation was used to calculate the CFP concentrations, respectively.

II.5 Flow cytometry analyses

The binding activity of recombinant fusion proteins towards cells was investigated by flow cytometry either on a BD FACSVerse™ (Becton Dickinson, Heidelberg) with the BD FACSuite™ software or on a BD FACSCalibur™ with BD CellQuest™ Pro v.6 software. Each sample was prepared with 5 x 10^5 cells. HL-60 cells (II.1.6) were stimulated with 300 U/mL human IFNγ (Sigma Aldrich) the day prior to use and macrophages were polarized into M1 (II.3.3). L-540cy cells (II.1.6) served as a negative control. Briefly, the cells were incubated with 1 µg purified CFPs (II.4.1, II.4.3, II.4.4) or 500 µl cell culture supernatant of transfected cells for 20 min on ice. One µg/mL anti-penta-his ALEXA Fluor® 488 antibody (II.1.8) was applied for 15 min on ice in the dark whereas intermediate washing with 1 mL cold 1x PBS buffer (II.1.4, Table 4) removed unbound proteins. Target cell

populations were gated in the dot plot representing the FSC-H and SSC-H channels and 10^4 cells were counted, respectively. No gating was carried out for isolated leukemia cells (II.3.3). Here, the CFPs were incubated with 1% (v/v) heat-inactivated human serum to increase the binding specificity. The presence of CD64 on these cells was confirmed by staining with anti-CD64-FITC and anti-CD33-APC antibodies (II.1.8) for 20 min on ice according to the manufacturer's instructions. After washing with cold 1x PBS buffer, the fluorescence signals were measured in the FL1-H and FL4-H channels. To verify the M1 subtype of polarized macrophages (II.3.3), the expression levels of CD14, CD64, CD206 and CD301 were analyzed against undifferentiated hMΦ cells as reference [158]. Combinations of anti-CD14-FITC and anti-CD64-APC or anti-CD206-FITC and anti-CD301-APC antibodies (II.1.8) were incubated with the cells for 20 min on ice according to the manufacturer's instructions. Fluorescence signals were detected as described above. Apoptosis induction following CFP exposure (II.10) was demonstrated by staining the cells with propidium iodide (PI) and cell-free annexin V-eGFP cell culture supernatant as described previously [2].

II.6 Yeast tRNA cleavage assays

Decreasing amounts of fusion proteins (as indicated) were incubated with 600 ng yeast tRNA (Sigma-Aldrich) in 20 µl RNase cleavage buffer (II.1.4, Table 4) for 1.5 h at 37°C using RNAse-free equipment. The addition of 100 ng RNase A (Thermo Fisher Scientific) served as positive control whereas tRNA dissolved in RNase cleavage buffer represented the negative control. Following incubation, the mixtures were supplemented with 5x RNase-free loading buffer (II.1.4, Table 4) and separated on a 1% (w/v) RNase-free agarose gel (90 V, 7 min). Ethidium bromide was added to the gel as described previously (II.2.6). TAE buffer and agarose gels were prepared with RNase-free water (II.1.4, Table 5) to avoid ribonuclease contaminations. To induce inhibiting conditions, either 40 U or 5 U RiboLock™ (Thermo Fisher Scientific) was applied to 1 µg CFPs in the cleavage reactions as indicated. Substrate bands were quantified using AIDA software and control bands were correlated with 0% and 100% substrate cleavage, respectively.

II.7 Demonstration of enzymatic activity and inhibition susceptibility

The cleavage activities and inhibition susceptibilities of CFPs were demonstrated using the fluorophore- and quencher-coupled RNaseAlert® substrate (Integrated DNA Technologies, Leuven, Belgium) as described previously [2]. Briefly, 50 nM substrate was cleaved by 100 nM CFPs o/n at RT in RNase cleavage buffer (II.1.4, Table 4). The fusion protein H22(scFv)-SNAP was applied as negative control under equal conditions [159]. Sample excitation was carried out at 485 nm whereas the emission was detected at 520 nm using the Tecan Genios Pro microplate reader (Tecan, Mainz) with Magellan 7.1 SP1 software. Determined signals were normalized against the fluorescence background of dissolved substrate (0% activity) and the averaged emission of the H22-Ang wild type-mediated cleavage reaction (100% enzymatic activity). Evaluation was carried out using GraphPad Prism 5 software. The substrate cleavage was monitored by measuring the increasing fluorescence signal in 3-min intervals. The addition of decreasing RiboLock™ amounts (200-0.2 nM) to the reactions revealed the enzymatic activity of CFPs in the presence of certain inhibitor concentrations. After overnight incubation, the remaining relative cleavage activities were calculated by signal normalization against the fluorescence background of dissolved substrate (0% activity) and the individual maximal fluorescence intensities of the respective cleavage reactions without inhibition (100% relative cleavage activity, respectively). The relative cleavage activities were plotted against the logarithmic RiboLock™ quantity and individual inhibition responses were fitted using GraphPad Prism 5 software and a log (inhibitor) vs. response algorithm with variable slope.

II.8 Electrophoretic mobility shift assays

Genomic DNA of A431 cells (II.1.6) was isolated using the QIAamp® DNA Mini and Blood Mini kit (Qiagen, Hilden) according to the manufacturer's instructions (II.1.3). The DNA concentration was determined (II.2.4) and electrophoretic mobility shift assays (EMSA) were carried out. Briefly, 170 ng gDNA was incubated with 15 pmol CFPs for 30 min at 37°C. Decreasing RiboLock™ amounts (6, 2, 1 and 0.6 pmol) were added to prevent the binding in an affinity-dependent manner. The samples were supplemented with 5x loading buffer (II.1.4, Table 4) and separated on a 0.5% (w/v) agarose gel for 65 min at 70 V in the presence of 0.1 µg/mL ethidium bromide (II.2.6). Three µl of the 2-log DNA ladder (NEB) was co-separated and fragments were visualized under UV light.

II.9 XTT viability assays

XTT viability assays were carried out as described earlier [51]. Briefly, HL-60 cells were stimulated with 300 U/mL IFNγ the day prior to use and 1 x 10^5 cells/mL were seeded into 96-well cell culture plates. Macrophages were seeded in a density of 5 x 10^5 cells/mL and polarized into the M1 subtype before adding CFPs (II.3.3). All samples were prepared as triplicate. Viable cells were colorimetrically visualized after 72 h exposure to serial CFP dilutions using XTT tetrazolium salt (II.1.4, Table 5). EC_{50} values were calculated from sigmoidal dose-response fits with variable slope using GraphPad Prism 5 software.

II.10 Apoptosis assays

After isolation of leukemia cells (II.3.3), 8 x 10^5 cells per mL were seeded into 24-well cell culture plates as described previously [2]. Cultivation was carried out in RPMI 1640 medium supplemented with 10% (v/v) heat-inactivated human serum, 100 U/mL IFNγ (both Sigma Aldrich) and 200 nM CFPs for 12 h. Untreated control cells were not supplemented with CFPs. Cells exposed to 30 µl camptothecin (1 mg/mL, dissolved in DMSO) served as internal positive control. Fusion proteins with irrelevant binding moieties, such as 2112(scFv), anti-Her2(scFv), anti-EpCAM(scFv) and a myelin oligodendrocyte glycoprotein (MOG)-based binding component, were applied under equal conditions [7, 25, 160] [Bialon *et al*., unpublished data]. H22-ETA' served as reference IT to estimate the treatment efficacy [20]. Apoptotic cells were detected using flow cytometry analysis (II.5) and data evaluation was carried out using GraphPad Prism 5 software.

II.11 Determination of serum stability

The CFP stability in human and mouse serum was demonstrated by determination of the remaining binding activity on target cells after serum incubation. Solely the binding of intact CFPs could be recognized by flow cytometry (II.5) as the N-terminal scFv and the C-terminal his-tag are both required for detection. One µg CFPs were dissolved in 10 µl of 1x PBS buffer (II.1.4, Table 4) and 10 µl human or mouse serum (Sigma-Aldrich; Invitrogen) were added, respectively. After incubation for 0, 0.5, 1, 2, 4 and 6 h at 37°C, cold 1x PBS buffer (80 µl) was added and the samples were frozen at -20°C for later analysis. The remaining binding activities

were demonstrated on 10^4 gated HL-60 cells (II.1.6) that have been stimulated with 300 U/mL IFNγ the day prior to use. Individual mean fluorescence intensities (MFIs) were determined whereas the MFI for anti-penta-his ALEXA Fluor® 488 (II.1.8) alone indicated no binding (0% CFP integrity) and the MFI values obtained for 0 h serum incubation indicated 100% CFP integrity, respectively. Data evaluation was carried out using GraphPad Prism 5 software.

II.12 Preparation of cell lysates and quantification of inhibitor amounts

HL-60 cells (II.1.6) were seeded into 6-well cell culture plates (2.5 x 10^6 cells/well, 3 mL end volume) and cultivated under standard conditions (II.3.1) in the presence of either 0, 300 or 600 U/mL IFNγ as indicated (III.8). Cell harvesting was carried out after 15, 18, 21 and 24 h, respectively. Otherwise HL-60 cells were stimulated with 300 U/mL IFNγ and harvested after 24 h. M1 macrophages were prepared as described in II.3.3. For lysis, 1 x 10^7 cells/sample were washed with 1x PBS buffer (II.1.4, Table 4), frozen at -20°C for at least 1 h and incubated in Triton X-100 lysis buffer (II.1.4, Table 4) for 1 h on ice. Centrifugation was carried out to remove cell debris (16,000 *g*, 4°C, 10 min) and 6-10 µl of the protein content was separated by SDS-PAGE (II.4.2). After western blotting (II.4.2), RNH1 and β-actin were specifically detected according to the workflow in Table 10. Band intensities for both proteins were quantified by AIDA software and the inhibitor content was normalized to 100 a.u. β-actin, respectively. Data evaluation was carried out using GraphPad Prism 5 software.

II.13 Oxidative regulation of the ribonuclease inhibitor activity

The cleavage of 50 nM RNaseAlert® substrate was mediated by 3.65 nM RNase A as described in II.7 whereas fluorescence intensities were measured after 1 h at RT. Relative cleavage activities were calculated by signal correlation against the fluorescence background of dissolved substrate (0% activity) and the emission obtained for the RNase A-mediated substrate digestion (100% relative cleavage activity). Dose-dependent inhibition of RNase A was achieved by the addition of 18, 109, 218 and 327 nM RiboLock™. The effect of inhibitor oxidation was demonstrated by applying a serial 1:5 dilution of 30% hydrogen peroxide (Carl Roth), corresponding to 1-0.0016% (v/v), to the cleavage reaction containing 327 nM RiboLock™. Incubation times for H_2O_2 and inhibitor as well as inhibitor and RNase A

were 10 min at RT, respectively. Prepared controls contained substrate dissolved in RNase cleavage buffer (II.1.4, Table 4) with or without RNase A and both with and without 1% (v/v) H_2O_2 (30%). All samples were prepared as duplicates whereas fluorescence signals were measured 18-times in 3 min intervals to consider ongoing cleavage during measurement as standard deviation. Data evaluation was carried out using GraphPad Prism 5 software.

II.14 Statistical analysis

Shown values express means ± standard deviation (SD) or standard error mean (SEM) indicating the number of experiments. Statistical analyses were carried out using GraphPad Prism 5 software and either Kruskal-Wallis tests following Dunn's multiple comparison analyses or nonparametric Mann-Whitney tests, respectively. *$p \leq 0.05$, **$p \leq 0.01$, ***$p \leq 0.001$.

II.15 Safety levels

The work was carried out according to the S1 (file number: 64-K-1.51/05) and S2 safety levels (file number: 64-K-1.50/05) at the Fraunhofer IME, Aachen, Germany.

III Results

III.1 1st mutagenesis and evaluation round

The aim of the first mutagenesis and evaluation round was to reveal if 1) a disrupted NLS sequence, 2) an increased enzymatic activity and 3) a reduced inhibitor affinity can improve the pro-apoptotic potential of human Ang as CFP effector domain. The literature was screened for promising amino acid exchanges described to mediate these effects and selected ones are summarized in Table 11. The R55A and W113A mutations were identified by Dr. Adriana Pietropaolo (University of Catanzaro, Italy) using Baker's Alanine Scanning of the X-ray structure of RNH1-Ang wild type and were supposed to decrease the affinity of Ang for RNH1.

Table 11: Selected amino acid exchanges for *proof-of-concept* mutagenesis
Abbreviations: Ang, Angiogenin; RNH1, Ribonuclease inhibitor.

Mutation	Ang variant	Described effect on wild type Ang	Reference
R33A	NLS RA_{mut}	Disruption of the nuclear localization signal, loss of nuclear translocation activity	[161]
G85R/G86R	$GGRR_{mut}$	Increased angiogenic activity due to a 10^6-fold reduced RNH1 affinity	[162]
Q117G	QG_{mut}	Up to 30-fold increased enzymatic activity due to removal of the active center obstruction	[163]
R55A	RA_{mut}	Expected to decrease the RNH1 affinity, identified by Baker's Alanine Scanning of the X-ray structure of RNH1-Ang wild type	*
W113A	WA_{mut}	Expected to decrease the RNH1 affinity, identified by Baker's Alanine Scanning of the the X-ray structure of RNH1-Ang wild type	*

* Carried out by Dr. Adriana Pietropaolo, University of Catanzaro, Italy.

III.1.1 Mutagenesis of H22-Ang wild type, CFP expression & purification

The selected mutations (Table 11) were introduced into the H22-Ang wild type DNA sequence (II.1.7) by site-directed mutagenesis (II.2.1, Table 8). After sequencing (II.2.8), HEK293T cells (II.1.6) were transfected (II.3.2) and analyzed for the expression of eGFP (II.1.7, II.3.4) as representatively shown in Figure 5. Transient CFP expression was carried out in the presence of zeocin™ for selection and to ensure plasmid preservation (II.3.1).

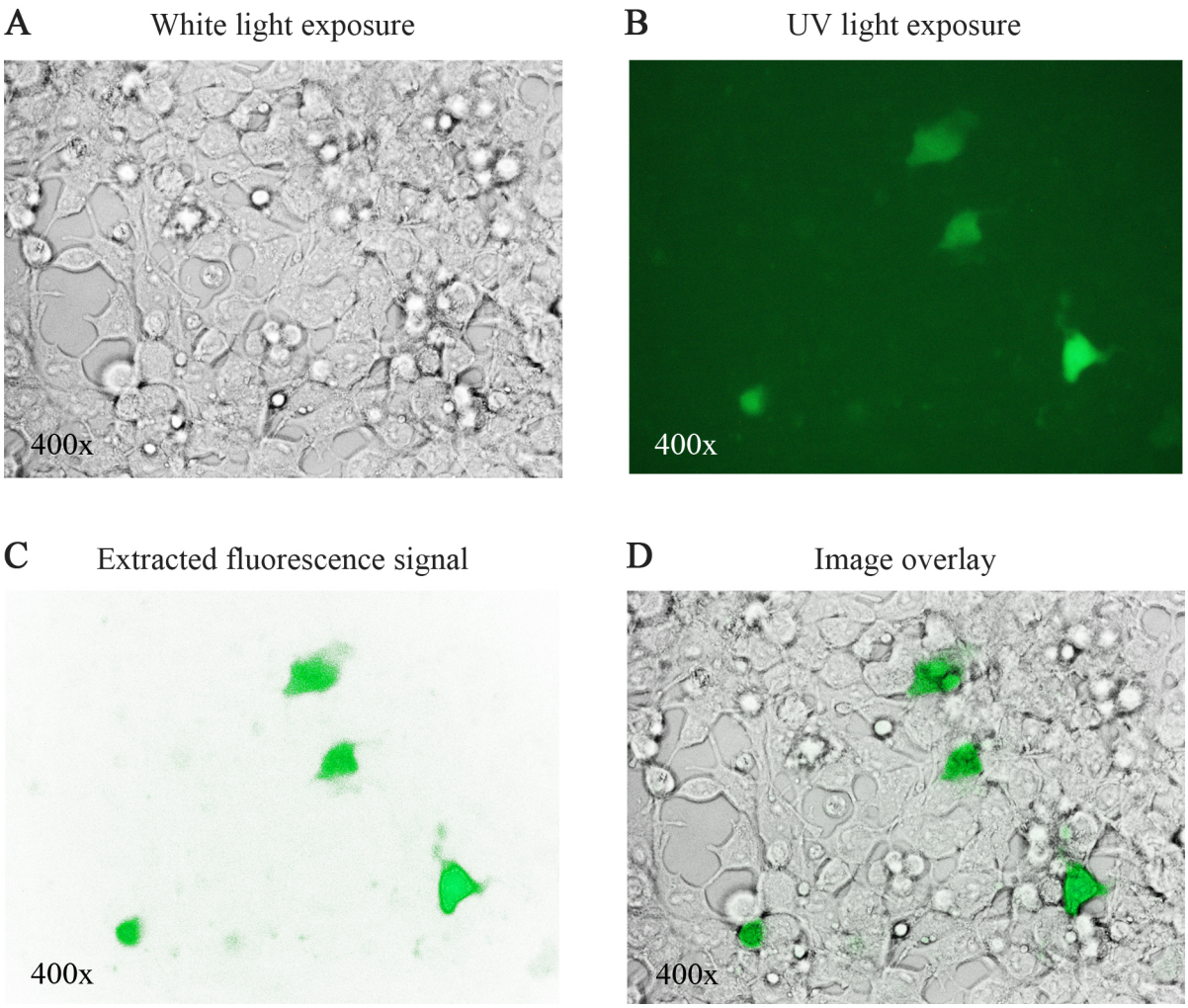


Figure 5: Reporter gene expression in transfected HEK293T cells.
To produce the distinct H22-Ang variants (III.1.1), individual pMS expression vectors (II.1.7) were generated (II.2.1, II.2.8) and used for the transfection of HEK293T cells (II.1.6, II.3.2). Zeocin™ was applied to the culture medium for selection (II.3.1). The CFPs were transiently co-expressed along with eGFP that could be visualized under UV light exposure (II.1.7). Shown are HEK293T cells transfected with pMS-L-H22-Ang QG_{mut} plasmid DNA three days after induction of selective conditions. Images were captured with 400x magnitude under white light (**A**) and UV light (**B**), respectively (II.3.4). The fluorescence signals were extracted using Adobe Photoshop CS5.1 software (**C**) and overlaid with the white light image (**A**) to visualize fluorescent cells after transfection (**D**). Abbreviations: Ang, Angiogenin; CFP, Cytolytic fusion protein; eGFP, Enhanced green fluorescent protein.

Protein purifications from cell culture supernatants were carried out using IMAC (II.4.1) following analysis of the collected fractions via SDS-PAGE and Coomassie Brilliant Blue staining (II.4.2). Elution fractions containing proteins at the expected size were pooled and working solutions were prepared by protein concentration, dialysis and sterile filtration (II.4.3). The working solutions were again analyzed by SDS-PAGE (Figure 6A) and CFPs were

specifically detected on a nitrocellulose membrane after western blotting (II.4.2) using mouse-anti-penta-his and goat-anti-mouse-HRPO antibodies (II.1.8) as shown in Figure 6B. Each CFP was detected at its theoretical size of ~45 kDa. The estimated protein purities were 60-90% based on SDS gel staining with Coomassie Brilliant Blue (II.1.4, Table 5) and evaluation using AIDA software. Yields between 1.5 and 2.8 mg per liter cell culture supernatant were calculated after determination of CFP concentrations (II.4.4). The fusion protein H22-Ang GGRR$_{mut}$ provided lower yields of approximately 0.4 mg/L.

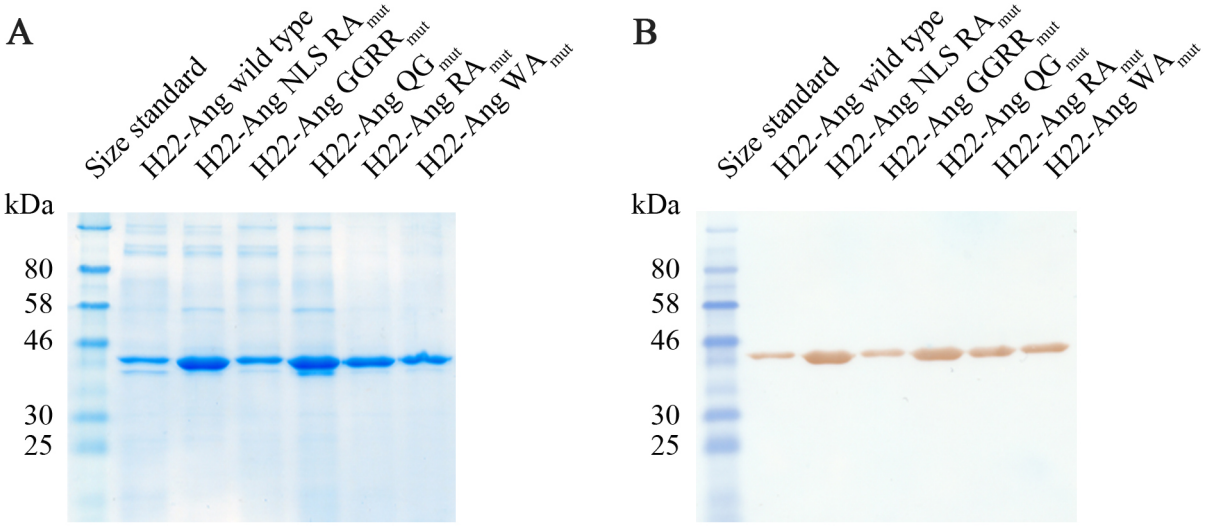


Figure 6: SDS-PAGE and western blot analysis of purified H22-Ang variants.
The DNA sequence of H22-Ang wild type (II.1.7) was modified by site-directed mutagenesis (II.2.1, Table 8). After sequencing (II.2.8), HEK293T cells (II.1.6) were transfected (II.3.2) and the H22-Ang variants were transiently expressed (II.3.1). Purification from cell culture supernatants was carried out using IMAC (II.4.1) following preparation of working solutions (II.4.3). Protein samples were analyzed by SDS-PAGE (II.4.2) and Coomassie Brilliant Blue staining (**A**). Immunodetection was carried out on a nitrocellulose membrane after western blotting using anti-penta-his and goat-anti-mouse-HRPO antibodies (II.1.8) as described in II.4.2 (**B**). Applied size standard: Prestained Protein Marker, Broad Range (NEB). Abbreviations: Ang, Angiogenin; IMAC, Immobilized metal ion affinity chromatography; HRPO, Horseradish peroxidase.

III.1.2 Binding analysis of CFPs by flow cytometry

The specific binding activity of CFPs (III.1.1) on IFNγ-stimulated HL-60 cells (II.1.6) was demonstrated by flow cytometry (II.5) using L-540cy cells as negative control (Figure 7). Briefly, 1 µg CFPs (II.4.4) were incubated with the cells for 20 min on ice and binding activities were visualized in the FL1-H channel using an anti-penta-his ALEXA Fluor® 488 detection antibody (II.1.8).

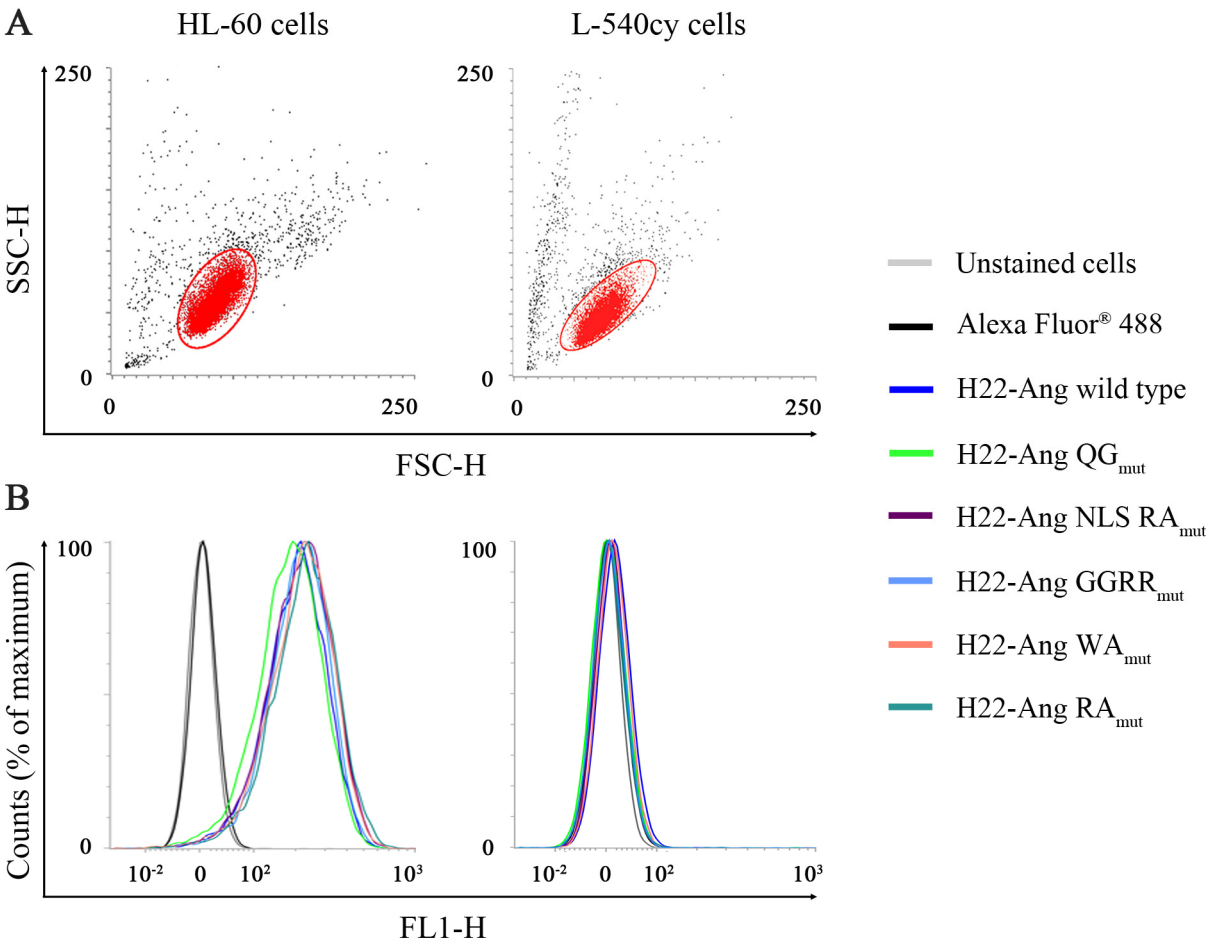


Figure 7: Cell-specific binding analysis of H22-Ang variants.
HL-60 cells (II.1.6) were stimulated with 300 U/mL IFNγ 24 h prior to use and the binding of 1 µg H22-Ang variants (III.1.1) was demonstrated by flow cytometry analysis (II.5). L-540cy cells (II.1.6) were used as negative control. The fusion proteins were incubated with the cells for 20 min on ice and 1 µg/mL anti-penta-his ALEXA Fluor® 488 detection antibody (II.1.8) was applied for 15 min. Gated target cell populations are highlighted in red (**A**). Fluorescence shifts were detected in the FL1-H channel, respectively. The background signal of anti-penta-his ALEXA Fluor® 488 alone (black) is shown as reference (**B**). Abbreviations: Ang, Angiogenin; IFNγ, Interferon gamma; SSC-H, Sideward scatter; FSC-H, Forward scatter.

All tested CFPs demonstrated a similar binding activity on IFNγ-stimulated HL-60 cells whereas no binding was observed on the negative control cell line L-540cy (Figure 7B).

III.1.3 CFP-mediated reduction of HL-60 cell viability

The reduction of cell viability upon CFP exposure was demonstrated using XTT viability assays (II.9). IFNγ-stimulated HL-60 cells (II.1.6) were exposed to serial CFP dilutions (III.1.1)

for 72 h under standard conditions (II.3.1). The cell line L-540cy (II.1.6) was used as negative control. The addition of zeocin™ and sterile DPBS buffer to the cells revealed 0% and 100% cell viability, respectively. Colorimetric detection of viable cells was mediated by the mitochondrial conversion of XTT tetrazolium salt (II.1.4, Table 5) and dose-responses were fitted as representatively shown in Figure 8.

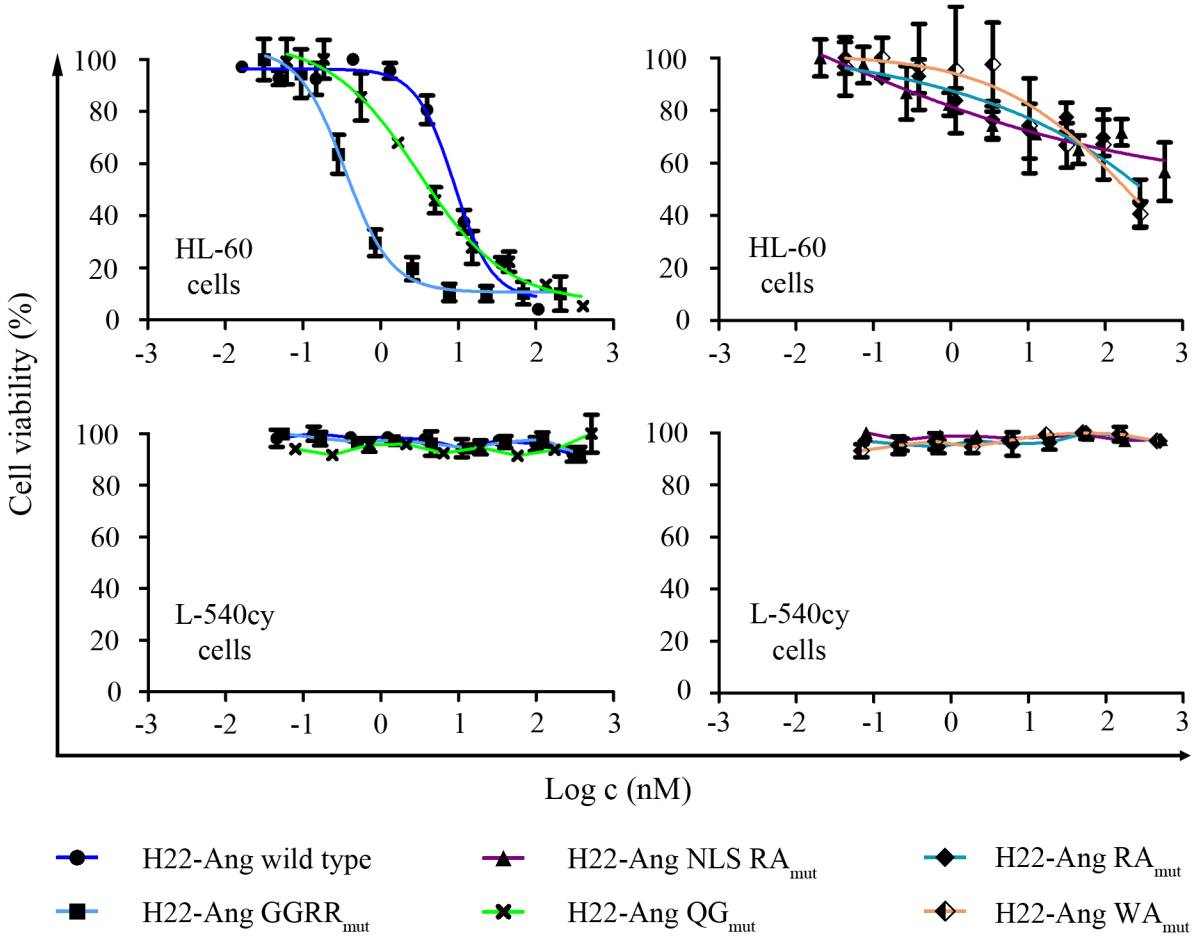


Figure 8: Representative reduction of cell viability upon exposure to H22-Ang variants.
HL-60 cells (II.1.6) were stimulated with 300 U/mL IFNγ 24 h prior to use. Cultivation of cells was carried out in the presence of serial dilutions of fusion proteins (III.1.1) for 72 h under standard conditions (II.3.1, II.9). $CD64^-$ L-540cy cells (II.1.6) were used as negative control. The dose-dependent reduction of cell viability was colorimetrically visualized by the addition of XTT tetrazolium salt (II.1.4, Table 5). Cells exposed to zeocin™ and sterile DPBS buffer indicated 0% and 100% cell viability, respectively. Sigmoidal dose-response fits with variable slope were carried out using GraphPad Prism 5 software. Indicated values express means of triplicates ± SD. Abbreviations: Ang, Angiogenin; IFNγ, Interferon gamma; c, Concentration.

On stimulated HL-60 cells, H22-Ang RA_{mut} and H22-Ang WA_{mut} demonstrated inconsistent efficacies and no appropriate dose-response could be fitted in most of the experiments (Figure 8, upper right). Compared to the other tested CFPs, both reduced the target cell viability less efficient leading to their exclusion from further experiments. H22-Ang NLS RA_{mut} demonstrated a dose-dependent cytotoxicity (Figure 8, upper right) but the amount of treatment-surviving cells was usually higher than observed after application of H22-Ang wild type. Compared to H22-Ang $GGRR_{mut}$ and H22-Ang QG_{mut} (Figure 8, upper left), H22-Ang NLS RA_{mut} reduced the total cell viability ~10-fold less efficient (n = 3).

H22-Ang $GGRR_{mut}$ and H22-Ang QG_{mut} both outperformed the efficacy of H22-Ang wild type on stimulated HL-60 cells and reduced the cell viability to 5-10% at the highest tested concentrations (Figure 8, upper left). This indicated the feasibility of increasing the cytotoxicity of Ang by protein engineering approaches.

The ^{Ang}G85R/G86R and the ^{Ang}Q117G mutations were joined in the second mutagenesis round to aim synergistic or at least cooperative effects (III.2.1). Chapter III.2 outlines the detailed *in vitro* characterization of H22-Ang $GGRR_{mut}$, H22-Ang QG_{mut} and H22-Ang $GGRR/QG_{mut}$ in comparison to H22-Ang wild type.

III.2 2nd mutagenesis and evaluation round

III.2.1 Generation, expression & purification of H22-Ang $GGRR/QG_{mut}$

H22-Ang $GGRR/QG_{mut}$ was generated by site-directed mutagenesis (II.2.1) using pMS-L-H22-Ang $GGRR_{mut}$ plasmid DNA (III.1.1) as template and the QG oligonucleotide exchange primer (II.1.9, Table 8) for mutagenesis. The inserted mutation was confirmed by DNA sequencing (II.2.8) and the CFP-encoding plasmid was used for transfection of HEK293T cells (II.3.2, II.1.6). After transient expression (II.3.1), the CFP was purified from the cell culture supernatant using IMAC (II.4.1) and prepared as described in II.4.3. Following SDS-PAGE and Coomassie Brilliant Blue staining (II.4.2), H22-Ang $GGRR/QG_{mut}$ could be visualized at the expected size of ~46 kDa (Figure 9A). The specific CFP detection was carried out on a nitrocellulose membrane (Figure 9B) using mouse-anti-hexa-his and goat-anti-mouse-HRPO antibodies (II.4.2, II.1.8). The calculated expression yield of H22-Ang $GGRR/QG_{mut}$ was 1.7 mg/L cell culture supernatant.

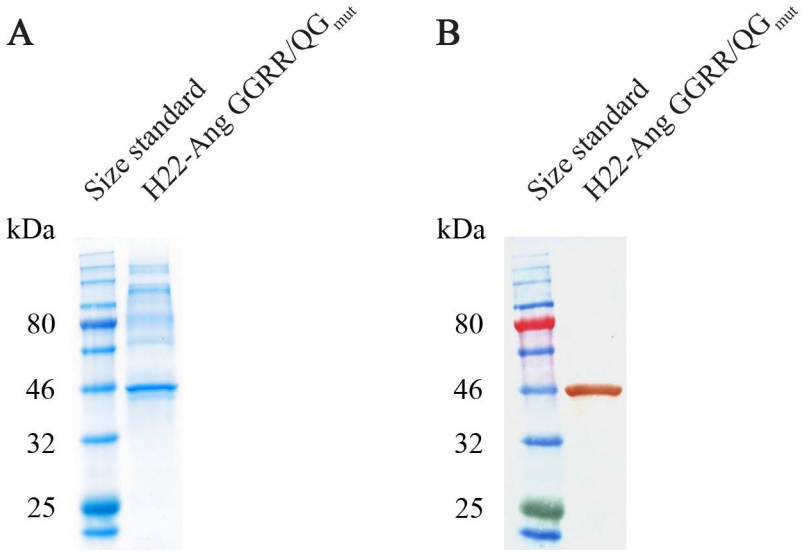


Figure 9: SDS-PAGE and western blot analysis of purified H22-Ang GGRR/QG$_{mut}$.
After generation and sequencing of the pMS-L-H22-Ang GGRR/QG$_{mut}$ expression vector (II.2.1, II.2.8), HEK293T cells (II.1.6) were transfected (II.3.2) and used for transient expression (II.3.1). H22-Ang GGRR/QG$_{mut}$ was purified from the cell culture supernatant using immobilized metal ion affinity chromatography (II.4.1). A working solution was prepared as described in II.4.3 and analyzed by SDS-PAGE (II.4.2) and Coomassie Brilliant Blue staining (**A**). Immunodetection of the cytolytic fusion protein was carried out on a nitrocellulose membrane after western blotting (II.4.2) using anti-hexa-his and goat-anti-mouse-HRPO antibodies (II.1.8) (**B**). Applied size standard: Color Prestained Protein Standard, Broad Range (NEB). Abbreviations: Ang, Angiogenin; HRPO, Horseradish peroxidase.

III.2.2 Ribonucleolytic activity and inhibition susceptibility of CFPs

The tRNA cleavage activity of CFPs (III.1.1, III.2.1) was demonstrated by the addition of decreasing protein amounts to 600 ng yeast tRNA (II.6). Incubation was carried out for 90 min at 37°C whereas RNase A or RNase cleavage buffer (II.1.4, Table 4) were applied to the substrate as controls. Undigested tRNA was visualized on an RNase-free agarose gel (II.6) by staining with ethidium bromide and exposure to UV light (Figure 10A). H22-Ang wild type and H22-Ang GGRR$_{mut}$ demonstrated a similar tRNA degradation efficacy that was apparently higher for H22-Ang QG$_{mut}$ and H22-Ang GGRR/QG$_{mut}$. Additionally, the fluorophore- and quencher-coupled RNaseAlert® substrate was cleaved by the CFPs (II.7). Only digested substrate emitted a signal at 520 nm when excited at 485 nm due to separation of the quencher. The digestion was either monitored (Figure 10B) or carried out o/n whereas the emission was normalized to the fluorescence background of dissolved substrate and the averaged emission of the H22-Ang wild type-mediated cleavage reaction (indicated 0% and 100% cleavage activity) for evaluation (Figure 10C). H22-SNAP was applied as negative control fusion protein [159].

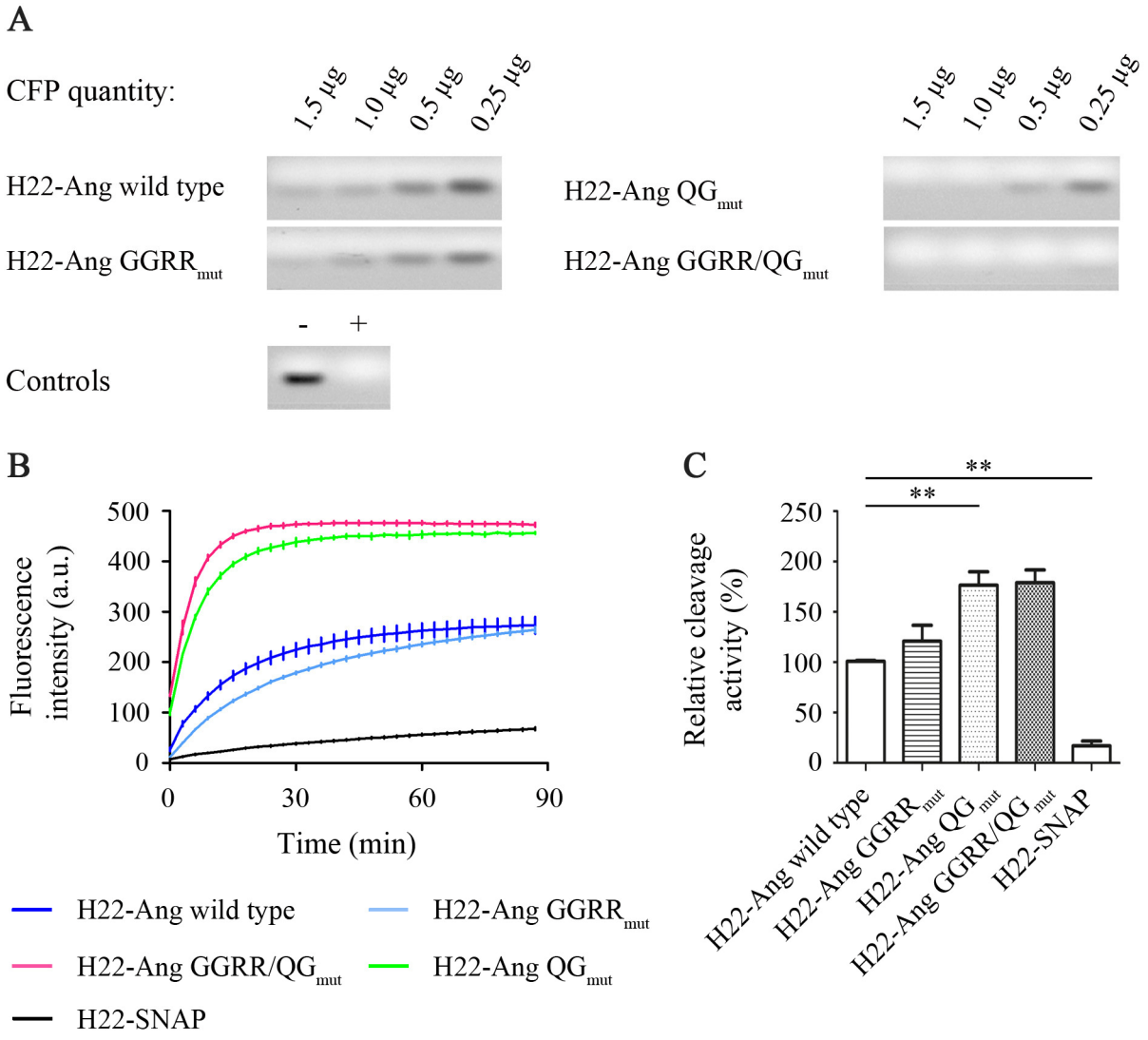


Figure 10: Ribonucleolytic activity of H22-Ang variants.
The tRNA cleavage activity of H22-Ang variants (III.1.1, III.2.1) was demonstrated by incubating decreasing fusion protein amounts with 600 ng yeast tRNA for 90 min at 37°C (II.6). Samples containing substrate with 100 ng RNase A (+) or RNase cleavage buffer (-) (II.1.4, Table 4) represented controls. Undigested tRNA was visualized on an RNase-free agarose gel (II.6) by ethidium bromide staining and UV light exposure (**A**). Additionally, 50 nM RNaseAlert® substrate was used to monitor the RNA cleavage mediated by 100 nM fusion proteins (II.7). When excited at 485 nm, only the emission of cleaved substrate is detectable at 520 nm due to the quencher separation. H22-SNAP was applied as negative control [159]. Shown are means of duplicates ± SD. Evaluation was carried out using GraphPad Prism 5 software (**B**). Illustrations A and B were modified from [1]. After overnight cleavage of RNaseAlert®, the detected signals were normalized against the emission of dissolved substrate in RNase cleavage buffer (0% relative cleavage activity) and the emission of the H22-Ang wild type-based cleavage reaction (100% relative cleavage activity). The illustration was modified from [2] whereas indicated values express means of duplicates ± SEM, n = 6-7. Individual statistical comparisons between the fusion proteins and H22-Ang wild type were carried out using GraphPad Prism 5 software and non-parametric Mann-Whitney tests, **p≤0.01 (**C**). Abbreviations: Ang, Angiogenin; tRNA, Transfer RNA.

H22-Ang QG_{mut} and H22-Ang $GGRR/QG_{mut}$ demonstrated an increased cleavage activity compared to H22-Ang wild type and H22-Ang $GGRR_{mut}$. The ribonucleolytic activity under inhibiting conditions was demonstrated by supplementing the yeast tRNA cleavage reaction (II.6) with RiboLock™ ribonuclease inhibitor as described in [1]. In comparison to the other tested CFPs, H22-Ang $GGRR_{mut}$ retained the highest enzymatic activity (Figure 11A and B).

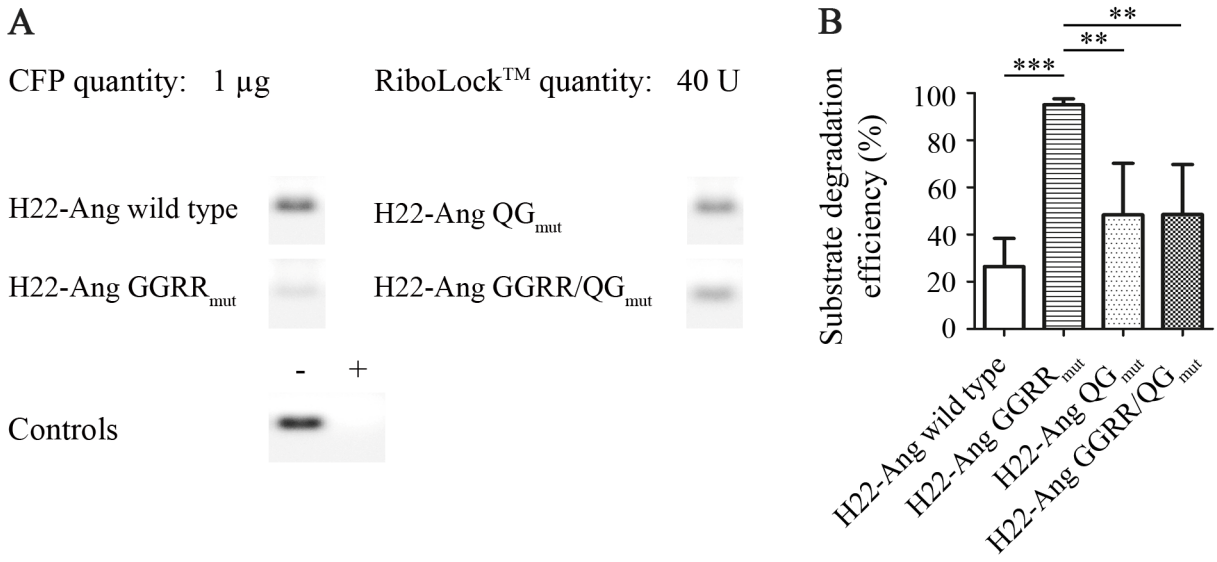


Figure 11: Substrate cleavage activity of CFPs in the presence of RiboLock™.
Yeast tRNA (600 ng) was incubated with 1 µg CFPs (III.1.1, III.2.1) and 40 U RiboLock™ inhibitor for 90 min at 37°C (II.6). RNase A (+) and RNase cleavage buffer (-) (II.1.4, Table 4) were applied as internal controls. Undigested tRNA was visualized on an RNase-free agarose gel by ethidium bromide staining and UV light exposure. The illustration was modified from [1] (**A**). For evaluation, the tRNA bands were analyzed using AIDA software and the bands intensities of controls were correlated with 0% and 100% degradation efficacy, respectively. Shown values express means ± SD, n = 10. Statistical analysis was carried out using GraphPad Prism 5 software and a Kruskal-Wallis test following Dunn's multiple comparison analysis, **p≤0.01 and ***p≤0.001 (**B**). Abbreviations: CFP, Cytolytic fusion protein; Ang, Angiogenin; tRNA, Transfer RNA.

Accordingly, the RNaseAlert®-based cleavage assay (II.7) was supplemented with increasing quantities of RiboLock™ (2-200 nM). The individual decrease of relative cleavage activities indicated the inhibition susceptibility of the CFPs, respectively (Figure 12). H22-Ang wild type, H22-Ang QG_{mut} and H22-Ang $GGRR/QG_{mut}$ demonstrated similar sensitivities towards the ribonuclease inhibitor whereas H22-Ang $GGRR_{mut}$ retained almost 80% cleavage activity at the highest tested RiboLock™ concentration.

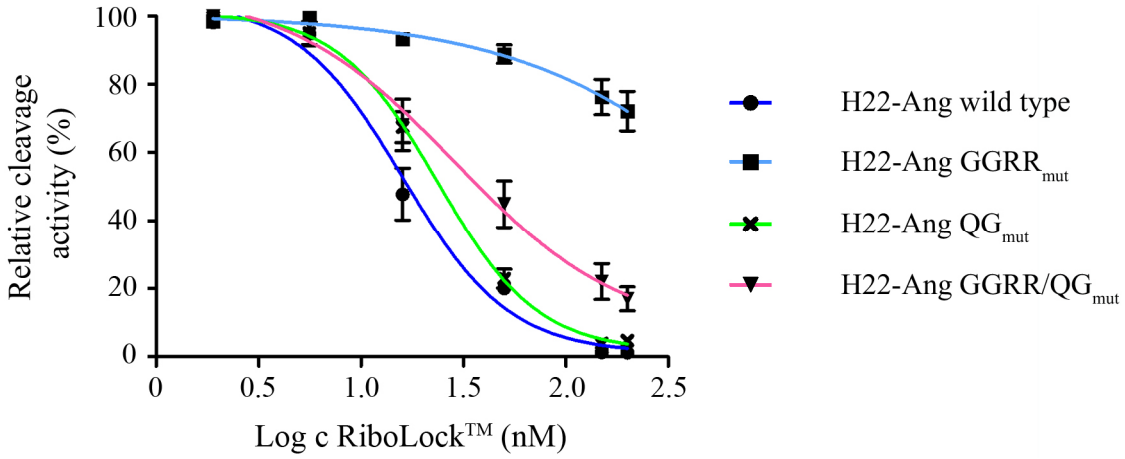


Figure 12: Inhibition susceptibility of generated cytolytic fusion proteins.
Increasing amounts of RiboLock™ ribonuclease inhibitor (2-200 nM) were incubated with 100 nM H22-Ang variants for 10 min at RT and 50 nM RNaseAlert® substrate was added for overnight digestion (II.7). Solely non-inhibited fusion proteins cleaved the substrate and separated the fluorophore and the quencher. The samples were excited at 485 nm and the emission was detected at 520 nm. Relative cleavage activities were calculated by signal normalization against the emission of dissolved substrate in RNase cleavage buffer (II.1.4, Table 4) and the individual maximal emission determined for each cleavage reaction without inhibition (indicating 0% and 100% relative cleavage activity, respectively). The relative cleavage activities were plotted against the logarithmic quantity of applied RiboLock™ and dose-responses were fitted using GraphPad Prism 5 software and a log (inhibitor) vs. response algorithm with variable slope. Indicated values express means of duplicates ± SEM, n = 3. The illustration was modified from [2]. Abbreviations: Ang, Angiogenin; RT, Room temperature; c, Concentration.

III.2.3 The binding of CFPs to genomic DNA

Inhibition of Ang by RNH1 abolishes its angiogenic activity and thus its ability to interact with gDNA [137]. Using EMSA experiments (II.8), the individual and dose-dependent loss of binding activity towards gDNA (II.2.4) of A431 cells (II.1.6) was demonstrated for the H22-Ang variants (III.1.1, III.2.1) in the presence of increasing RiboLock™ amounts. The binding of 15 pmol CFPs to 170 ng genomic DNA was allowed for 30 min at 37°C. Free DNA and such bound to the CFPs could be differentiated by agarose gel electrophoresis in consideration of varying migration velocities (Figure 13). The experiments confirmed that the inhibition of H22-Ang wild type and H22-Ang QG$_{mut}$ by RiboLock™ prevented the binding of gDNA in a dose- and affinity-dependent manner. H22-Ang QG$_{mut}$ retained an apparently higher binding activity than H22-Ang wild type under similar conditions. H22-Ang GGRR$_{mut}$ and H22-Ang GGRR/QG$_{mut}$ both failed to bind gDNA even in the absence of the inhibitor. To investigate if the abolished binding activity of H22-Ang GGRR$_{mut}$ and H22-Ang GGRR/QG$_{mut}$

is mediated by the common ^{Ang}G85R/G86R exchanges, the fusion protein Ang GGRR$_{mut}$-H22 was tested in a direct comparison (Figure 13B). The CFP was kindly provided by Hanna Braun (Institute of Applied Medical Engineering (AME), Department of Experimental Medicine and Immunotherapy (EMI), University Hospital Aachen) [9]. The additional experiment confirmed that all CFPs carrying the GGRR mutations failed to interact with genomic DNA of A431 cells.

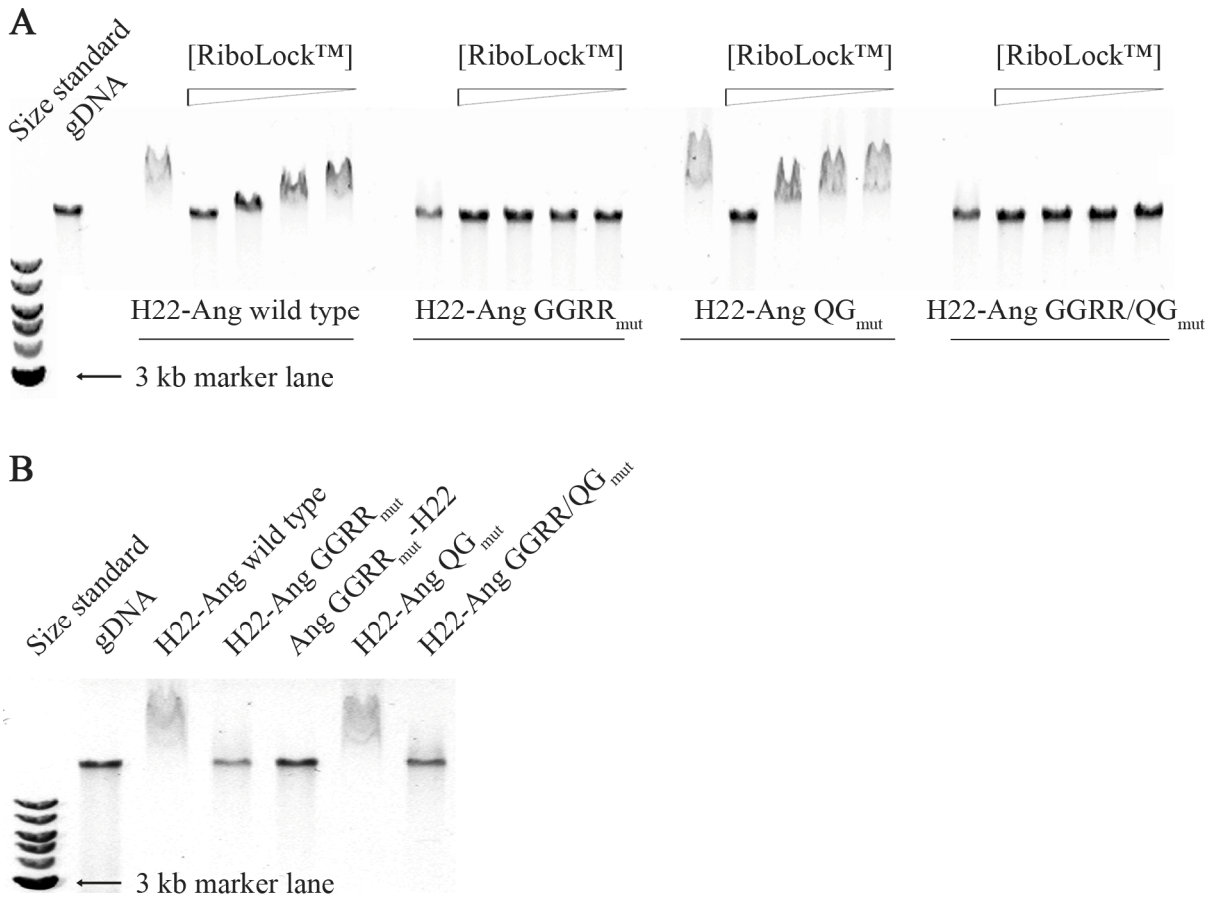


Figure 13: Binding activity of H22-Ang variants towards genomic DNA of A431 cells.
Genomic DNA of A431 cells (II.1.6) was isolated using the QIAamp® DNA Mini and Blood Mini kit (II.1.3, II.2.4) and 170 ng (II.2.4) were incubated with 15 pmol H22-Ang variants (III.1.1, III.2.1) for 30 min at 37°C to allow binding. Decreasing amounts of RiboLock™ (6, 2, 1 and 0.6 pmol) were added to inhibit Ang and thus the binding of CFPs to gDNA in an affinity-dependent manner. Electrophoretic mobility shift assays were carried out to distinguish free DNA and CFP-DNA complexes in consideration of varying migration velocities (II.8). DNA fragments were visualized by ethidium bromide under UV light exposure. Genomic DNA and complexes without inhibitor served as internal controls. The 2-log DNA ladder (NEB) was used as size standard (**A**). The fusion protein Ang GGRR$_{mut}$-H22 was kindly provided by Hanna Braun [9] and its binding activity to gDNA was competitively tested against the remaining CFPs (III.1.1, III.2.1) under conditions described above without inhibition (**B**). Abbreviations: Ang, Angiogenin; CFP, Cytolytic fusion protein; gDNA, Genomic DNA.

III.2.4 Preparation of M1 macrophages and binding analysis of CFPs

Human MΦ cells were prepared from buffy coats and polarized into the pro-inflammatory M1 subtype using IFNγ and LPS (II.3.3). The cell differentiation was associated with morphological changes as representatively illustrated in Figure 14. Shown are macrophages of a single and healthy blood donor which either remained untreated (Figure 14A) or were polarized into M1 (Figure 14B). Images were captured under white light with 400-fold magnitude, respectively (II.3.4). While untreated macrophages usually appeared circular with at most marginal developed pseudopodia, M1-polarized cells stretched and evolved distinct pseudopodia and cell extensions.

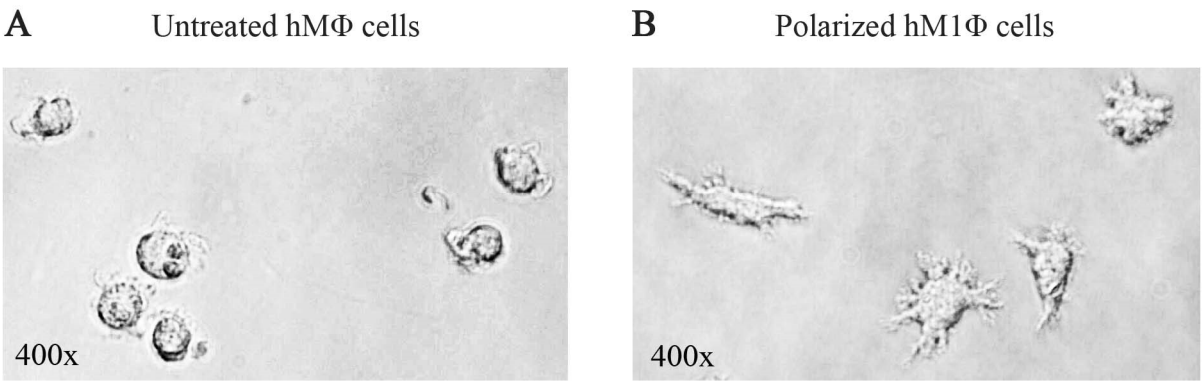


Figure 14: Morphological comparison of untreated and polarized hM1Φ cells.
Human peripheral blood mononuclear cells were isolated from buffy coats and macrophages were separated by adherent growth (II.3.3). Lipopolysaccharide and IFNγ were applied to induce the M1 polarization (II.3.3) whereas untreated cells served as reference. Images were captured under white light with 400-fold magnitude, respectively (II.3.4). Shown are hMΦ cells of a single blood donor which either remained untreated (**A**) or were polarized into the M1 subtype (**B**). Image processing was carried out using Adobe Photoshop CS5.1 extended software. Abbreviations: hMΦ cells, Human macrophages; IFNγ, Interferon gamma.

The binding activity of H22-Ang wild type, H22-Ang $GGRR_{mut}$, H22-Ang QG_{mut} and H22-Ang $GGRR/QG_{mut}$ (III.1.1, III.2.1) on stimulated HL-60 cells and polarized M1 macrophages (II.1.6, II.3.3) was demonstrated by flow cytometry (II.5). L-540cy cells were used as negative control (Figure 15). Briefly, 1 µg CFPs were incubated with the cells for 20 min and binding activities were detected in the FL1-H channel using an anti-penta-his ALEXA Fluor® 488 antibody (II.1.8). Intermediate washing was carried out using 1x PBS buffer to remove unbound proteins.

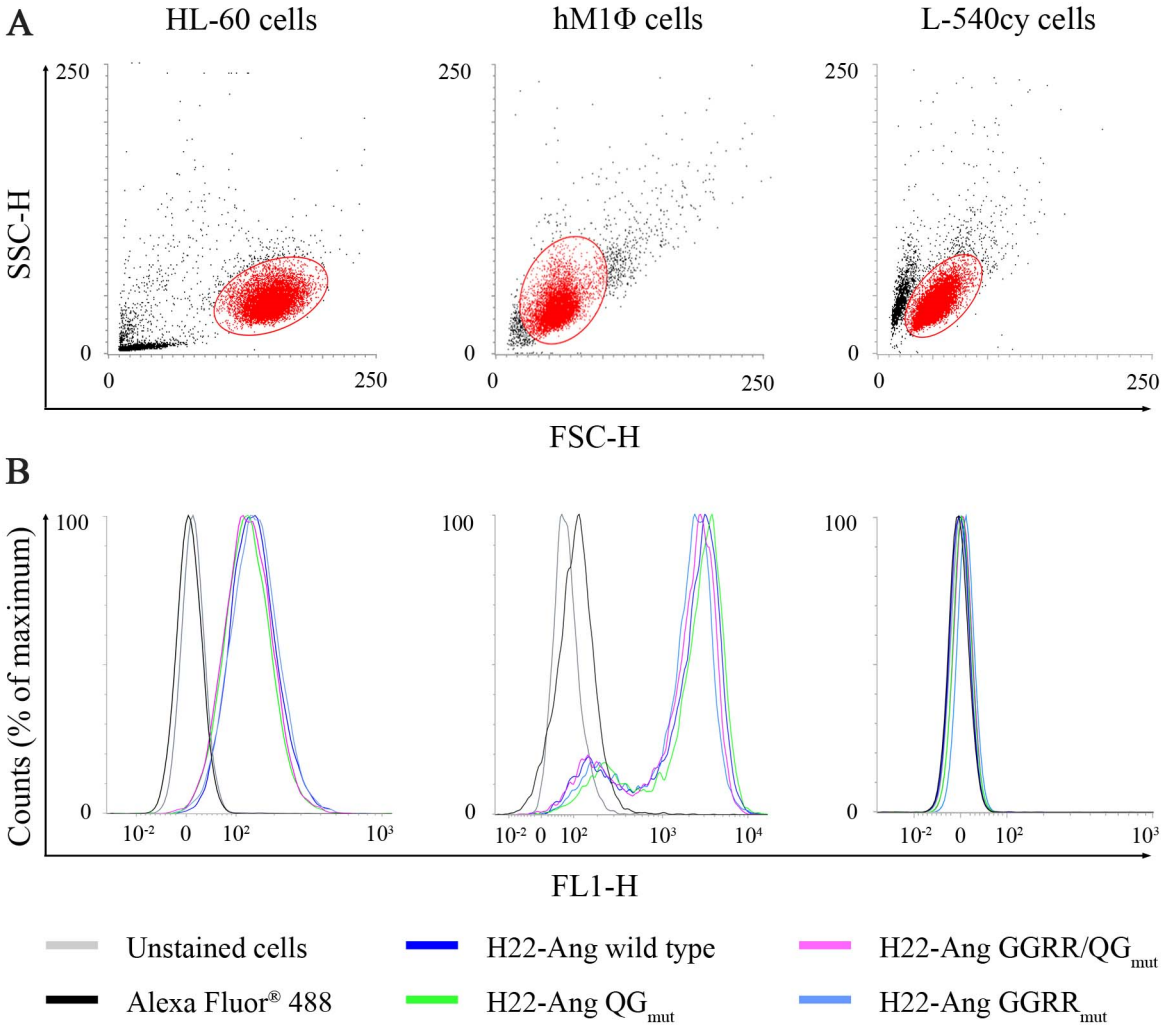


Figure 15: Binding activity of H22-Ang variants on different cell types.
The binding activity of 1 µg H22-Ang variants (III.1.1, III.2.1) was demonstrated on IFNγ-stimulated HL-60 cells (II.1.6) and hM1Φ cells (II.3.3). $CD64^-$ L-540cy cells (II.1.6) were used as negative control. The fusion proteins were incubated with the cells for 20 min on ice and 1 µg/mL anti-penta-his ALEXA Fluor® 488 detection antibody (II.1.8) was applied for 15 min. Binding activities were demonstrated using flow cytometry analysis (II.5). Gated target cell populations are highlighted in red (**A**). Fluorescence shifts were detected in the FL1-H channel, respectively (**B**). The illustration was modified from [1]. Abbreviations: hM1Φ cells, Human M1 macrophages; IFNγ, Interferon gamma; Ang, Angiogenin; SSC-H, Sideward scatter; FSC-H, Forward scatter.

III.2.5 *In vitro* cytotoxicity of CFPs

The cytotoxicity of CFPs (III.1.1, III.2.1) on stimulated HL-60 cells (II.1.6) and hM1Φ cells (II.3.3) was demonstrated by XTT viability assays (II.9). L-540cy cells were used as negative control. Following exposure to serial CFP dilutions, viable cells were colorimetrically detected by the conversion of XTT tetrazolium salt (II.1.4, Table 5). Dose-responses were fitted as representatively shown in Figure 16.

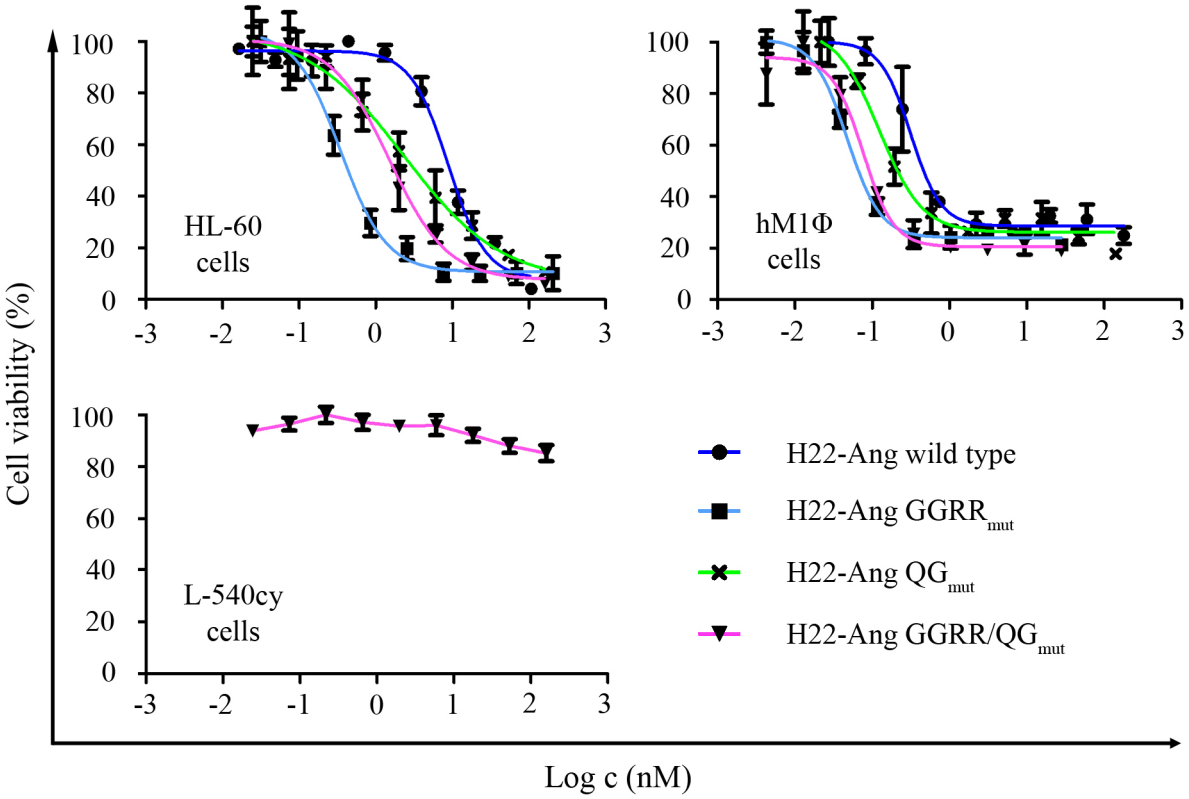


Figure 16: Representative *in vitro* cytotoxicity of CFPs.
The cytotoxic effects of the CFPs (III.1.1, III.2.1) were demonstrated on IFNγ-stimulated HL-60 cells (II.1.6) and hM1Φ cells (II.3.3) using XTT viability assays (II.9). CD64$^-$ L-540cy cells (II.1.6) were used as negative control to exclude an unspecific cytotoxic effect of H22-Ang GGRR/QG$_{mut}$. The target cell specificity of the remaining CFPs has already been demonstrated (III.1.3, Figure 8). After 72 h exposure to serial CFP dilutions, viable cells were colorimetrically detected by the addition of the tetrazolium salt XTT (II.1.4, Table 5). Cells exposed to zeocin™ and sterile DPBS buffer indicated 0% and 100% cell viability, respectively. Indicated values express means of triplicates ± SD. Sigmoidal dose-response fits with variable slope were carried out using GraphPad Prism 5 software and EC$_{50}$ values were determined. The illustration was modified from [1]. Abbreviations: hM1Φ cells, Human M1 macrophages; IFNγ, Interferon gamma; CFP, Cytolytic fusion protein; Ang, Angiogenin; c, Concentration.

Averaged EC$_{50}$ values of the CFPs are summarized in Table 12 and were obtained during the distinct evaluation rounds (III.1.3, III.2.5, III.3.4), respectively. H22-Ang GGRR/QG$_{mut}$ and H22-Ang QG$_{mut}$ were found to be more cytotoxic than the wild type-based CFP on stimulated HL-60 cells and hM1Φ cells (Figure 17, Table 12). Relative to H22-Ang GGRR$_{mut}$, H22-Ang GGRR/QG$_{mut}$ performed less efficient on stimulated HL-60 cells than on M1 macrophages. H22-Ang GGRR$_{mut}$ demonstrated the strongest cytotoxicity on both target cell types. M1 macrophages were found to be more sensitive towards the CFP treatment than stimulated HL-60 cells.

Table 12: *In vitro* cytotoxicity of H22-Ang variants
Averaged EC_{50} values on stimulated HL-60 cells (n = 7-18) and on hM1Φ cells (n = 6-7) were obtained during the distinct evaluation rounds (III.1.3, III.2.5, III.3.4), respectively [4]. Abbreviations: CFP, Cytolytic fusion protein; Ang, Angiogenin; hM1Φ cells, Human M1 macrophages.

CFP	EC_{50} values (nM) ± SEM		Improvement (x-fold) Referred to H22-Ang wild type	
	HL-60 cells	hM1Φ cells	HL-60 cells	hM1Φ cells
H22-Ang wild type	6.1 ± 1.2	0.47 ± 0.10		
H22-Ang $GGRR_{mut}$	0.6 ± 0.1	0.09 ± 0.03	8 - 12	4 - 7
H22-Ang QG_{mut}	4.1 ± 0.9	0.25 ± 0.08	1 - 2	1 - 3
H22-Ang $GGRR/QG_{mut}$	3.0 ± 0.6	0.09 ± 0.02	~2	4 - 7

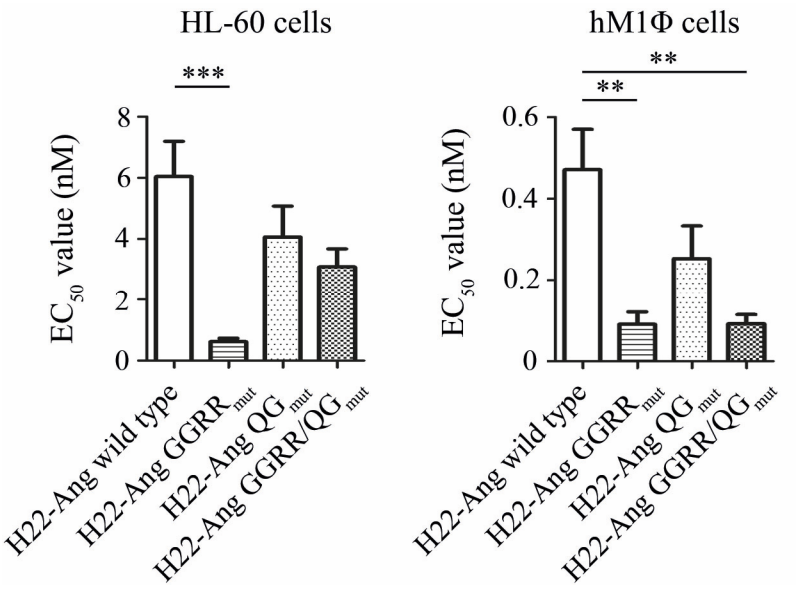


Figure 17: EC_{50} values of CFPs on stimulated HL-60 cells and human M1 macrophages.
Averaged EC_{50} values were obtained during the distinct evaluation rounds (III.1.3, III.2.5, III.3.4) and express means ± SEM, n = 7-18 on HL-60 cells and n = 6-7 on hM1Φ cells. Statistical analysis was carried out using GraphPad Prism5 software and a Kruskal-Wallis test following Dunn's multiple comparison analysis, **p≤0.01 and ***p≤0.001 [4]. Abbreviations: Ang, Angiogenin; hM1Φ cells, Human M1 macrophages.

III.2.6 Molecular dynamic simulation of RNH1-Ang interactions

MD simulations were carried out by Dr. Xiaojing Cong (German Research School for Simulation Sciences, Department of Computational Biophysics, Forschungszentrum Jülich) to demonstrate the individual interactions between RNH1 and Ang wild type, Ang $GGRR_{mut}$, Ang QG_{mut} and Ang $GGRR/QG_{mut}$. The H22 sequence of the CFPs was excluded to reduce the simulation complexity. Instead, all variants comprised three and four additional

amino acids at the N- and C-terminus corresponding to the CFP sequence, respectively (VII.5). The simulations revealed three main interaction clusters (Figure 18). Cluster I involves helix 2 of Ang which interacts with the N-terminus of RNH1 (blue-framed). The green-framed interaction cluster II contains the ^{Ang}G85/G86 residues at a surface loop. Cluster III represents an interaction surface that involves the C-terminus of Ang (red-framed). The simulation results have been published in a collaborative manuscript [4].

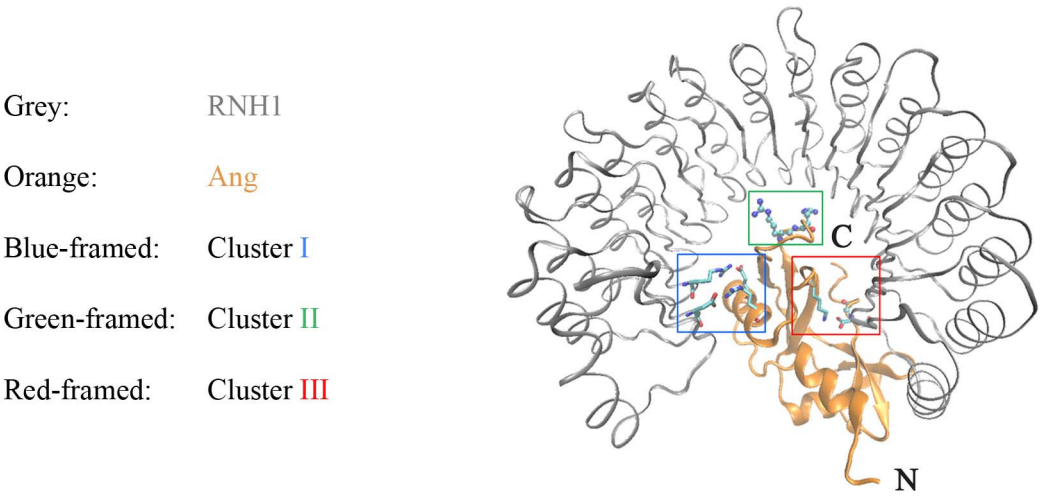


Figure 18: Interaction surfaces of RNH1 and human angiogenin.
Molecular dynamic simulations were carried out for RNH1 (grey) in complex with Ang (yellow). The latter comprised three and four additional amino acids at the N- and C-terminus corresponding to the CFP sequence, respectively. Three prominent interaction clusters could be figured out that are highlighted by colored frames. The raw figure was kindly provided by Dr. Xiaojing Cong (German Research School for Simulation Sciences, Department of Computational Biophysics, Forschungszentrum Jülich). Abbreviations: Ang, Angiogenin; RNH1, Ribonuclease inhibitor; CFP, Cytolytic fusion protein.

Determination of individual protein flexibilities during RNH1-Ang interaction

Root mean square deviations (RMSD) were determined and indicate global changes in the three-dimensional protein structures during interaction (Figure 19A). The inhibitor conformation remained almost stable in complex with Ang wild type, Ang QG$_{mut}$ and Ang GGRR/QG$_{mut}$. In contrast, it demonstrated a remarkable flexibility during interaction with Ang GGRR$_{mut}$. Cα's root mean square fluctuations (RMSF) indicate local backbone flexibilities (Figure 19B). The RMSF values for RNH1 were almost similar to each other, independent from the Ang variant it interacts with. This also applied for Ang wild type and Ang GGRR/QG$_{mut}$ in complex with RNH1. Ang QG$_{mut}$ appeared even more stable than Ang wild type during interaction whereas certain subdomains of Ang GGRR$_{mut}$ showed an enhanced flexibility.

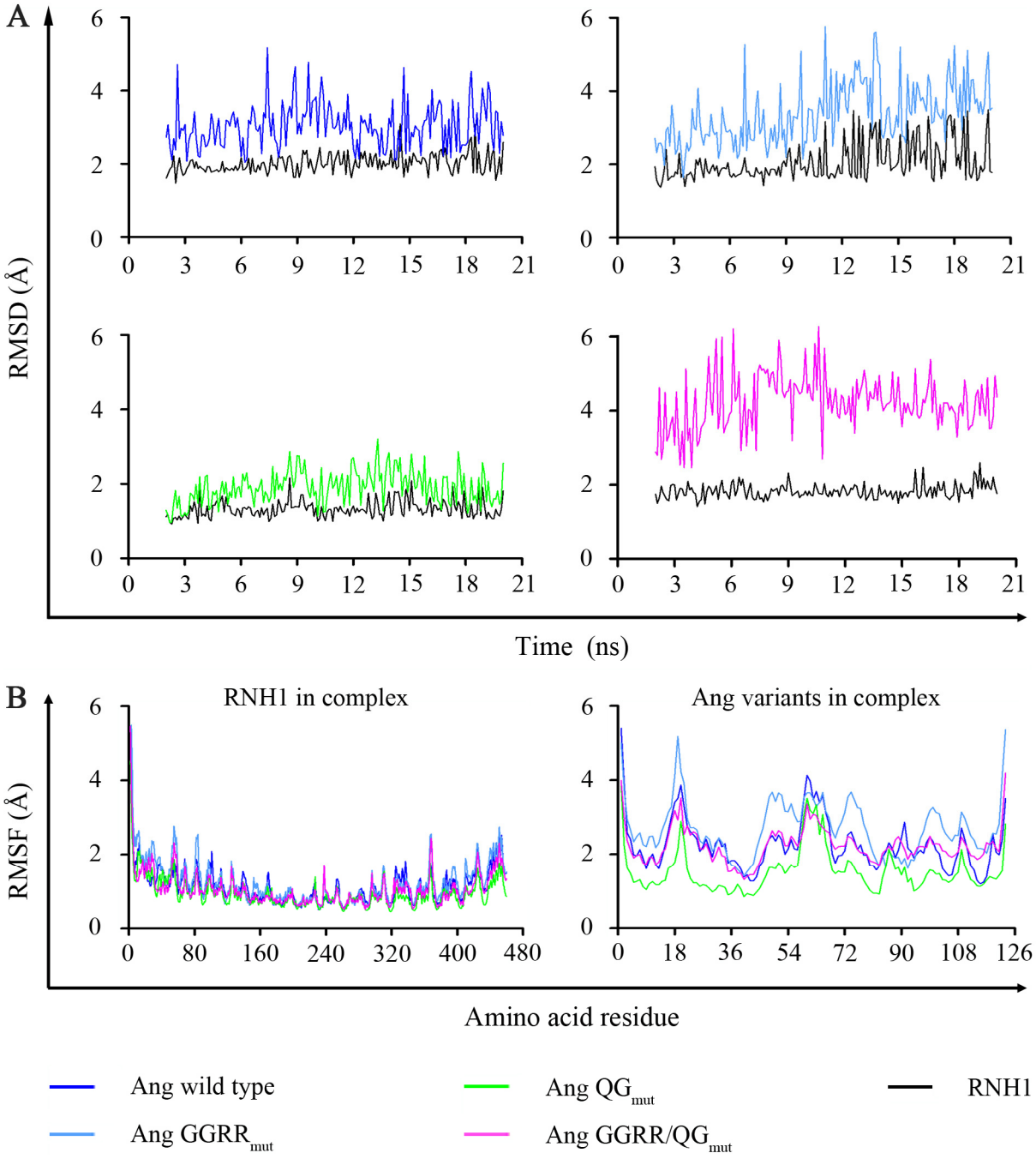


Figure 19: Individual RMSD and RMSF values of simulated RNH1-Ang complexes.
Molecular dynamic simulations (21 ns x 32 replicas) were carried for RNH1 in complex with the distinct Ang variants. The latter comprised three and four additional amino acids at the N- and C-terminus corresponding to the CFP sequence, respectively. The scFv sequence was excluded to reduce complexity. RMSD values were determined and indicate changes in total protein flexibilities during interaction (**A**) whereas RMSF values indicate local backbone flexibilities of the interacting proteins (**B**). Molecular dynamic simulations were carried out by Dr. Xiaojing Cong and the illustration was modified from a collaborative manuscript [4]. Raw data were kindly provided for figure preparation. Abbreviations: Ang, Angiogenin; RNH1, Ribonuclease inhibitor; CFP, Cytolytic fusion protein; scFv, Single chain variable fragment; RMSD, Root mean square deviation; RMSF, Cα's root mean square fluctuation.

Simulation of the RNH1-Ang wild type interaction

Helix 2 of Ang tightly interacts with N-terminal amino acids of RNH1 at cluster I (Figure 18, not shown in higher resolution here). At interaction cluster II, ^{Ang}G86 forms hydrogen bonds with the ^{RNH1}Q346 side chain (Figure 20) and to a lesser extent with ^{RNH1}S289 (not illustrated). During interaction with the inhibitor, the C-terminal ^{Ang}Q117 side chain at cluster III forms a hydrogen bond with ^{RNH1}D435. However, it also forms intramolecular H-bonds with ^{Ang}I42 and ^{Ang}T44, respectively. This conformation stabilizes the C-terminus in front of the active center and aggravates the substrate accessibility.

Simulation of the RNH1-Ang GGRR$_{mut}$ interaction

The ^{Ang}G85R/G86R exchanges cause a rearrangement of bonds at cluster 2 and a dislocation of Ang from RNH1 (Figure 20). In contrast to the wild type enzyme, ^{Ang}R85 forms salt bridges with ^{RNH1}E149 and E206 while ^{Ang}R86 builds up salt bridges with ^{RNH1}E206 and E264. Beyond, the dislocation weakens the interactions at cluster III by largely disrupting the network of salt bridges and hydrogen bonds. This increases the distance between the C-terminus of Ang and RNH1. The ^{Ang}Q117 side chain conformation is destabilized and swings between the native position and a solvent-exposed one. The GGRR exchanges further destabilize cluster I (not shown) whereas the sum of weakened interactions cooperatively reduces the affinity for RNH1.

Simulation of the RNH1-Ang QG$_{mut}$ interaction

The interactions at cluster II are similar to those found in the RNH1-Ang wild type complex (Figure 20). At the C-terminus, the ^{Ang}Q117G mutation eliminates the glutamine side chain and thus the hydrogen bonds initially formed with the surrounding residues ^{Ang}I42 and ^{Ang}T44. The weakened interactions destabilize the C-terminus orientation and facilitate the conformational rearrangement essential for substrate binding. In comparison to the wild type ribonuclease, the ^{Ang}R121 side chain was found to form a stronger salt bridge and hydrogen bond with ^{Ang}D41 and ^{Ang}G117, respectively. This reinforces the α-helix structure in the C-terminus of Ang. At interaction cluster I, the Ang QG variant was found to form stronger salt bridges with RNH1 residues than the wild type enzyme does (not shown).

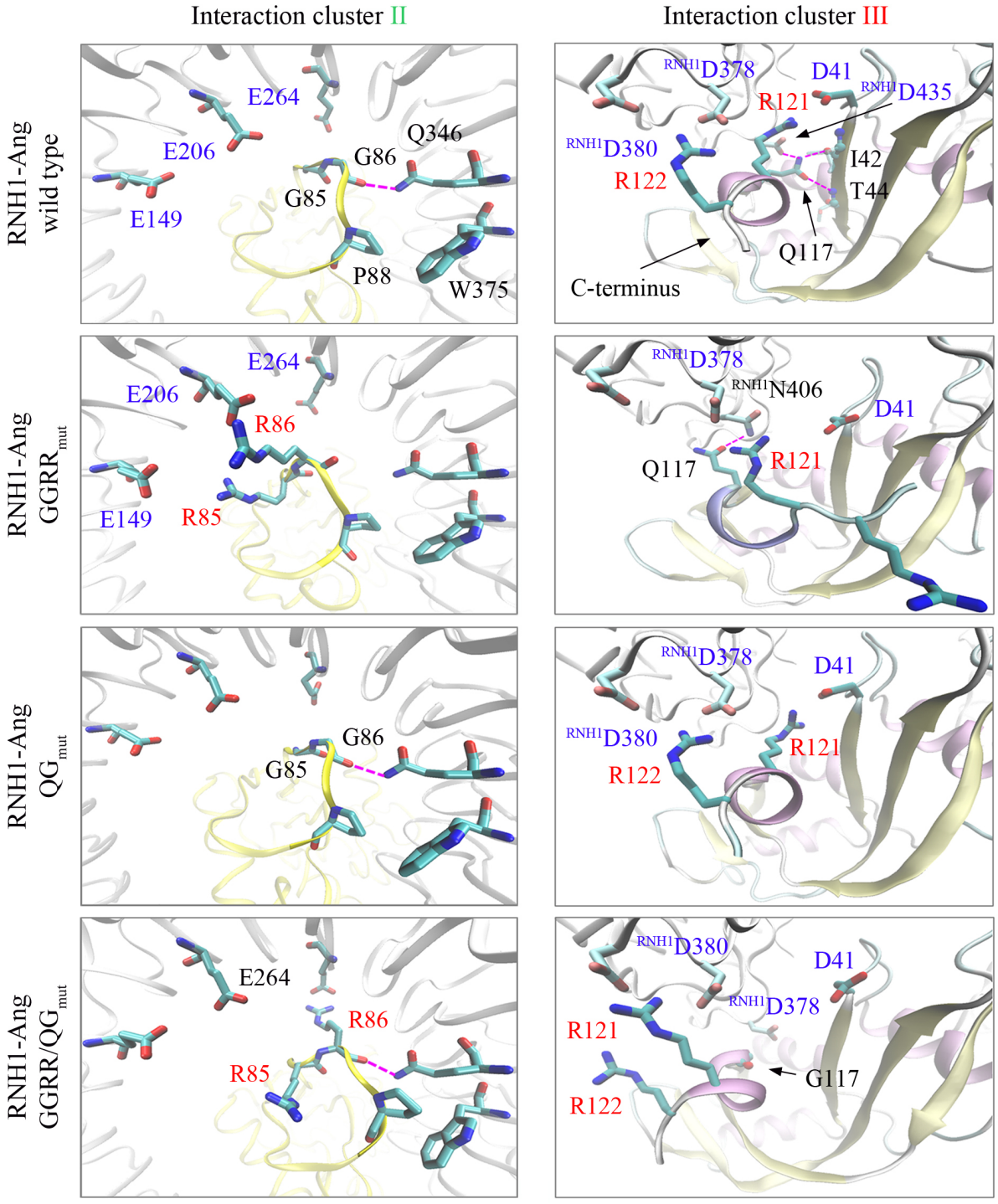


Figure 20: Molecular interactions between Ang variants and RNH1.
Molecular dynamic simulations were carried out by Dr. Xiaojing Cong for RNH1 (grey) in complex with the distinct Ang variants (colored). Shown are interactions at clusters II and III (Figure 18) of the RNH1-Ang complexes. The Ang variants comprised three and four additional amino acids at the N- and C-terminus corresponding to the CFP sequence. Hydrogen bonds involved in the interaction of both proteins are shown as dashed magenta lines. The label color of amino acids indicates the side chain charge at physiological pH: red, positively charged; blue, negatively charged; black, neutral. Salt bridges appear as combination of hydrogen bonding and electrostatic interaction between residues of opposite charges. The illustration was modified from [4]. Abbreviations: Ang, Angiogenin; CFP, Cytolytic fusion protein; RNH1, Ribonuclease inhibitor.

Simulation of the RNH1-Ang GGRR/QG$_{mut}$ interaction

The interactions at cluster I (not shown) and II (Figure 20) are weakened in the RNH1-Ang GGRR/QG$_{mut}$ complex, respectively. However, essential differences were found at cluster III in comparison to the RNH1-Ang GGRR$_{mut}$ complex. The QG exchange endows the C-terminus of Ang with enhanced flexibility due to the lacking hydrogen bonds initially formed with ^{Ang}Q117. Thus, it is able to readjust its position relative to RNH1 and allowed to form more stable salt bridges between ^{Ang}R121, ^{RNH1}D378 and ^{RNH1}D380. This markedly increases the RNH1 affinity of the variant in comparison to Ang GGRR$_{mut}$.

Concluded strategies to abolish the affinity of Ang GGRR/QG$_{mut}$ for RNH1

Three strategies were considered to disrupt the recovered RNH1 affinity of Ang GGRR/QG$_{mut}$ while still maintaining the improved enzymatic activity mediated by Q117G:

1. Aiming the disruption of cluster I by exchanging corresponding amino acids that are involved in the interaction with RNH1.
2. Replacing cluster-independent amino acids that participate in RNH1 binding and that are expected to cooperatively contribute to a subsequent affinity reduction.
3. Interfering with the C-terminal readjustment by exchanging charged amino acids in the C-terminus to prevent the recovery of cluster III.

III.3 3rd mutagenesis and evaluation round

The literature was screened for mutations that matched the considered strategies in III.2.6 and selected ones are listed in Table 13. The R5A and H8A mutations are located next to cluster I and were expected to weaken the RNH1 affinity appropriately. ^{Ang}K40 is described to crucially participate in the inhibitor interaction. ^{Ang}D116H is adjacent to the already introduced Q117G exchange and expected to interfere with the C-terminal readjustment of Ang GGRR/QG$_{mut}$ during interaction with RNH1. Even the mutation is not described to reduce the inhibitor affinity of Ang wild type, it replaces a negatively-charged aspartic acid by a positively-charged histamine at the C-terminus. The third mutagenesis and evaluation round was carried out in cooperation with Hanna Braun as part of her master's thesis under my technical supervision [9]. Data that have been published in a collaborative manuscript are cited accordingly [2].

Table 13: Selected mutations to weaken the RNH1-Ang GGRR/QG$_{mut}$ interaction
Abbreviations: Ang, Angiogenin; RNH1, Ribonuclease inhibitor.

Mutation	Ang variant	Described effect on wild type Ang	Reference
R5A	GGRR/QG/RA$_{mut}$	Decreases the RNH1-Ang binding energy by 2.3 kcal/mol	[164]
H8A	GGRR/QG/HA$_{mu}$	Decreases the RNH1-Ang binding energy by 0.9 kcal/mol	[165]
K40Q	GGRR/QG/KQ$_{mu}$	Decreases the RNH1-Ang binding energy by 4.2 kcal/mol	[164, 165]
D116H	GGRR/QG/DH$_{mu}$	Increases the enzymatic activity ~18-fold	[166]

III.3.1 Generation, expression and purification of novel H22-Ang variants

The mutations (III.3, Table 13) were introduced into H22-Ang GGRR/QG$_{mut}$ (III.2.1, II.1.7) using SOE-PCR (II.2.1), respectively [2]. Transient CFP expression using HEK293T cells (II.1.6, II.3.2, II.3.1), IMAC purification (II.4.1) and the preparation of working solutions (II.4.3) was carried out by Hanna Braun under my technical supervision [9]. SDS-PAGE and western blot analysis (II.4.2) confirmed the presence of the CFPs (Figure 21).

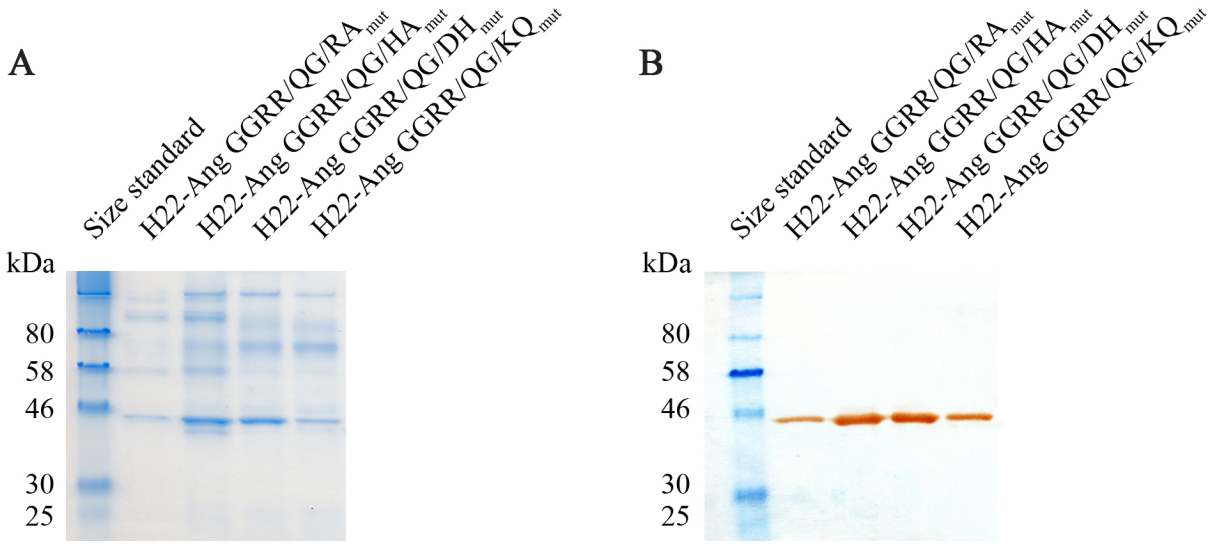


Figure 21: SDS-PAGE and western blot analysis of H22-Ang variants.
The H22-Ang variants were transiently expressed using HEK293T cells (II.3.1, II.1.6) and purified from the cell culture supernatants by IMAC (II.4.1). Working solutions were prepared (II.4.3) and analyzed by SDS-PAGE and Coomassie Brilliant Blue staining (**A**). Immunodetection was carried out after western blotting (II.4.2) using anti-penta-his and goat-anti-mouse-HRPO antibodies (II.1.8) (**B**). Applied size standard: Prestained Protein Marker, Broad Range (NEB). The work was carried out by Hanna Braun under my technical supervision and the illustration was modified from [9]. Abbreviations: Ang, Angiogenin; IMAC, Immobilized metal ion affinity chromatography; HRPO, Horseradish peroxidase.

Yields between 0.1 and 0.9 mg per liter cell culture supernatant were calculated after determination of CFP concentrations (II.4.4).

III.3.2 Enzymatic activity and inhibition resistance of the generated CFPs

The ribonucleolytic activity of CFPs (III.1.1, III.3.1) was demonstrated by incubating varying protein amounts with yeast tRNA for 90 min (II.6) as described previously [2, 9]. Undigested tRNA was visualized by RNase-free agarose gel electrophoresis. H22-Ang GGRR/QG/RA_{mut}, H22-Ang GGRR/QG/DH_{mut} and H22-Ang GGRR/QG/HA_{mut} demonstrated a higher tRNA cleavage activity than H22-Ang wild type and H22-Ang GGRR/QG/KQ_{mut}, respectively (Figure 22A). In the presence of 5 U RiboLock™ inhibitor, H22-Ang GGRR/QG/DH_{mut} did show almost unaffected substrate cleavage which was apparently reduced for the remaining fusion proteins (Figure 22B).

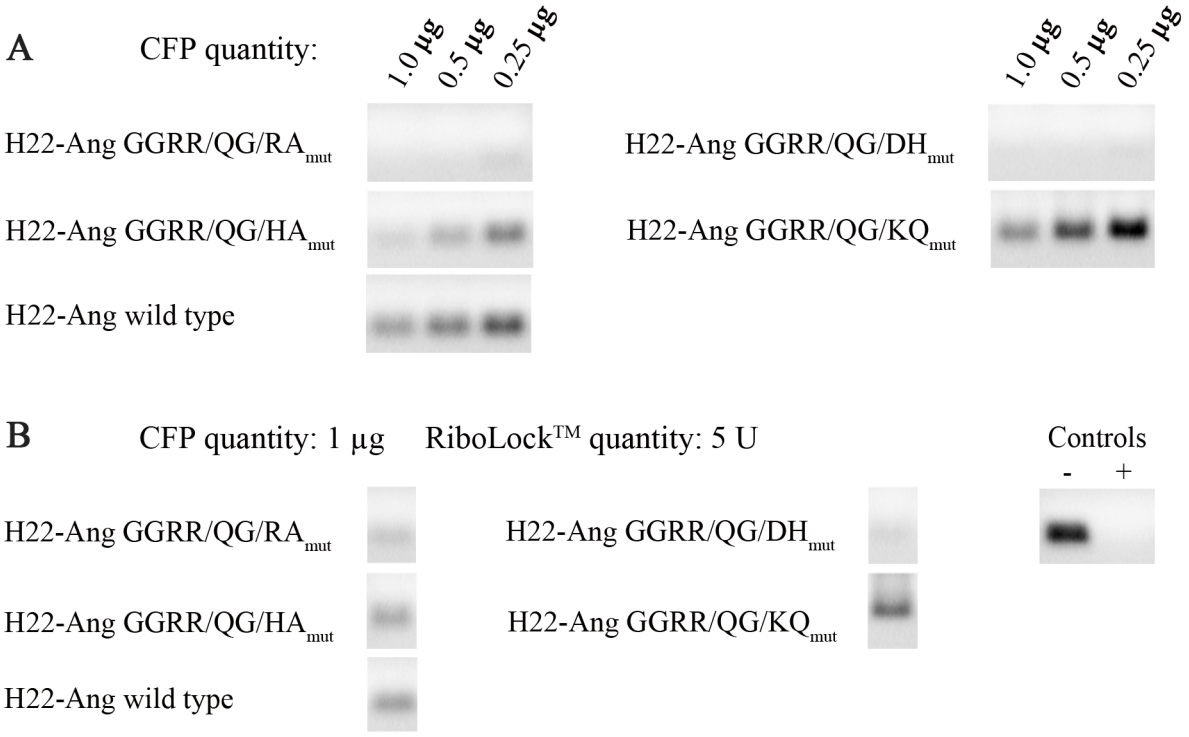


Figure 22: CFP-mediated cleavage of yeast tRNA under varying conditions.
Decreasing amounts of CFPs (III.1.1, III.3.1) were incubated with 600 ng yeast tRNA for 90 min at 37°C (II.6). H22-Ang wild type was used as reference fusion protein. Samples containing substrate with 100 ng RNase A (+) or RNase cleavage buffer (-) (II.1.4, Table 4) represented internal controls. Undigested tRNA was visualized on an RNase-free agarose gel (II.6) by ethidium bromide staining and UV light exposure (**A**). Five units RiboLock™ were applied to the cleavage reactions containing 1 µg CFPs to establish inhibiting conditions (**B**). The illustration was modified from [2]. Abbreviations: Ang, Angiogenin; CFP, Cytolytic fusion protein; tRNA, Transfer RNA.

The digestion of RNaseAlert® substrate (II.7) revealed distinct cleavage activities of the CFPs (III.1.1, III.3.1) that slightly varied between different preparations and experiments (Figure 23A). In comparison to H22-Ang wild type, all tested CFPs carrying the Q117G exchange demonstrated an increased enzymatic activity (Figure 23A and B).

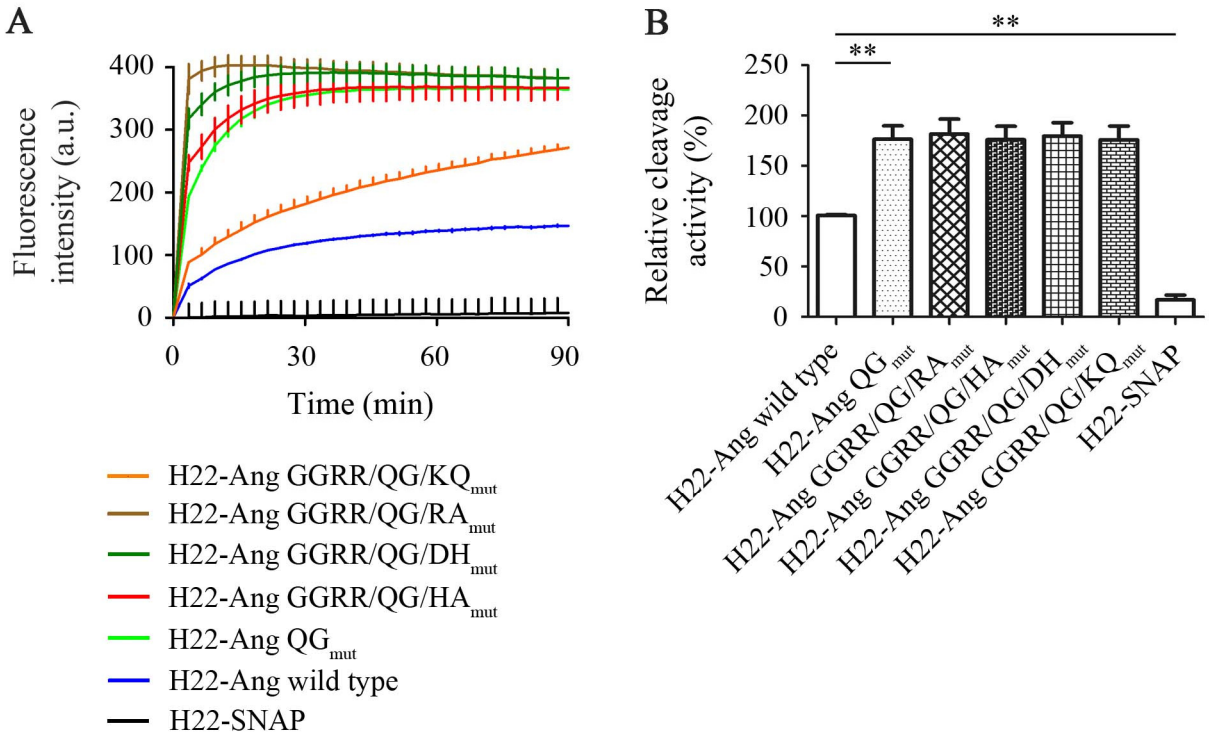


Figure 23: CFP-mediated digestion of RNaseAlert® substrate.
RNaseAlert® substrate (50 nM) was used to visualize the cleavage activity of 100 nM CFPs (III.1.1, III.3.1, II.7). H22-SNAP was applied as negative control [159]. The samples were excited at 485 nm whereas solely digested substrate emitted a signal at 520 nm due to separation of the quencher. Measurements were carried out in 3-min intervals. Shown are means of duplicates ± SD (**A**). Following overnight digestion of RNaseAlert®, the measured fluorescence intensities were normalized against the emission of substrate dissolved in RNase cleavage buffer (II.1.4, Table 4) and the H22-Ang wild type-mediated cleavage signal indicating 0% and 100% relative cleavage activity, respectively. The illustration was modified from [2] whereas shown values express means of duplicates ± SEM, n = 6-7. Individual statistical comparisons between fusion proteins and H22-Ang wild type were carried out using non-parametric Mann-Whitney tests, **p≤0.01. (**B**). The GraphPad Prism 5 software was used for evaluation. Abbreviations: Ang, Angiogenin; CFP, Cytolytic fusion protein.

To investigate the inhibition susceptibility of the CFPs (III.3.1), the RNaseAlert® substrate was used to reveal the individual cleavage efficacies in the presence of varying RiboLock™ concentrations (II.7). After overnight incubation, the emitted signals were converted into relative cleavage activities and plotted against the amount of applied inhibitor (Figure 24).

H22-Ang wild type, H22-Ang GGRR/QG$_{mut}$ and H22-Ang GGRR$_{mut}$ served as reference CFPs (III.1.1, III.2.1, III.2.2, Figure 11). H22-Ang GGRR/QG/RA$_{mut}$ and H22-Ang GGRR/QG/HA$_{mut}$ demonstrated a half maximal inhibition at equivalent RiboLock™ concentrations compared to H22-Ang wild type but both retained a higher relative activity at lower inhibitor amounts. Inactivation occurred rapidly after a critical inhibitor content was exceeded whereas H22-Ang wild type remained more active. H22-Ang GGRR/QG/KQ$_{mut}$ demonstrated a slightly lower inhibition resistance in a direct comparison. Full enzymatic activity even at high inhibitor quantities was observed for H22-Ang GGRR/QG/DH$_{mut}$. Nevertheless, inactivation took place after exceeding a critical inhibitor concentration whereas H22-Ang GGRR$_{mut}$ was the only CFP that still retained its enzymatic activity.

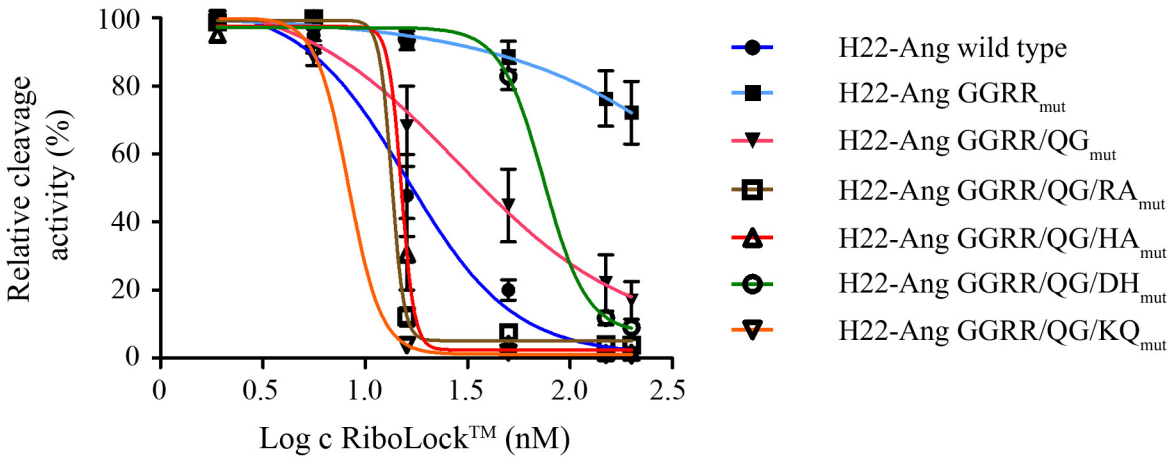


Figure 24: Inhibition susceptibility of generated H22-Ang variants.
Increasing RiboLock™ amounts (2-200 nM) were pre-incubated with 100 nM CFPs (III.1.1, III.2.1, III.3.1) at RT and 50 nM RNaseAlert® substrate was added for overnight cleavage (II.7). The samples were excited at 485 nm and the fluorescence was measured at 520 nm. Relative cleavage activities were calculated by signal normalization against the emission of substrate dissolved in RNase cleavage buffer (II.1.4, Table 4) and the maximal signals revealed for the distinct cleavage reactions without inhibition (indicating 0% and 100% relative cleavage activity, respectively). The logarithmic quantity of applied RiboLock™ was plotted against the relative cleavage activities of CFPs and individual dose-responses were fitted using GraphPad Prism 5 software and a log (inhibitor) vs. response algorithm with variable slope. Values express means of duplicates ± SEM, n = 3. The illustration was modified from [2]. Abbreviations: Ang, Angiogenin; RT, Room temperature; c, Concentration.

III.3.3 *In vitro* binding activity of the CFPs

The binding activity of CFPs (III.3.1) on IFNγ-stimulated HL-60 cells (II.1.6) and M1 macrophages (II.3.3) was demonstrated by flow cytometry (II.5) using L-540cy cells (II.1.6) as

negative control [9]. Gated target cell populations are indicated in red (Figure 25A). Briefly, 1 µg CFPs were incubated with the cells for 20 min on ice and binding activities were detected in the FL1-H channel using an anti-penta-his ALEXA Fluor® 488 antibody (II.1.8). Similar binding activities could be observed for all CFPs on stimulated HL-60 cells and M1Φ cells whereas no binding was recognized on L-540cy cells, respectively (Figure 25B).

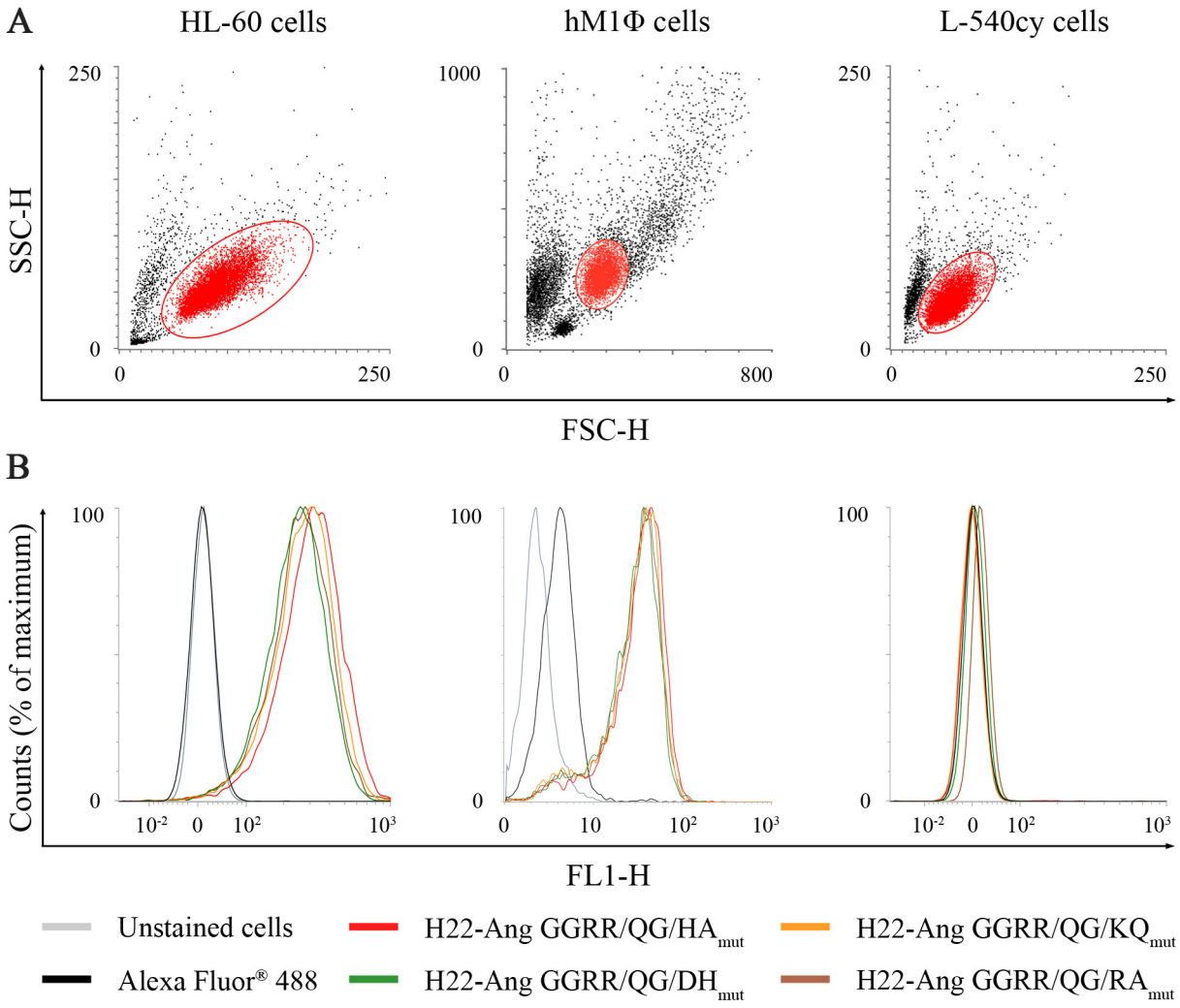


Figure 25: Flow cytometry-based binding analysis of CFPs.
IFNγ-stimulated HL-60 cells (II.1.6) and hM1Φ cells (II.3.3) were incubated with 1 µg CFPs (III.3.1) for 20 min on ice to allow binding. CD64$^-$ L-540cy cells (II.1.6) were used as negative control. The anti-penta-his ALEXA Fluor® 488 antibody (II.1.8) was applied to detect the binding of fusion proteins via flow cytometry (II.5). Defined target cell populations used for evaluation are indicated in red (**A**). Fluorescence shifts were detected in the FL1-H channel, respectively (**B**). The binding analysis on hM1Φ cells was carried out by Hanna Braun under my technical supervision [9]. Raw data were processed using BD FACSuite™ software for figure preparation. The illustration was modified from [2]. Abbreviations: IFNγ, Interferon gamma; CFP, Cytolytic fusion protein; hM1Φ cells, Human M1 macrophages; Ang, Angiogenin; SSC-H, Sideward scatter; FSC-H, Forward scatter.

III.3.4 CFP-mediated cytotoxic effects on different cell types *in vitro*

The *in vitro* cytotoxicity of the CFPs (III.1.1, III.3.1) was evaluated by XTT viability assays (II.9) on IFNγ-stimulated HL-60 cells (II.1.6) and human M1 macrophages (II.3.3). The L-540cy cell line (II.1.6) was used as negative control. Viable cells were colorimetrically detected after exposure to serial CFP dilutions and controls for 72 h and dose-responses were fitted (Figure 26). All CFPs induced a dose-dependent and specific reduction of target cell viability. Averaged EC_{50} values listed in Table 14 were obtained during the third evaluation round. Indicated values on M1 macrophages include such that have been generated under my technical supervision (66%) [9].

Table 14: EC_{50} values of CFPs obtained in the third evaluation round
EC_{50} values were obtained during the third evaluation round, n = 5-8 on HL-60 cells. Indicated values on hM1Φ cells include such that have been generated by Hanna Braun under my technical supervision (66%) [9], n = 5-7. The table was modified from [2]. Abbreviations: CFP, Cytolytic fusion protein; Ang, Angiogenin; hM1Φ cells, Human M1 macrophages.

CFP	EC_{50} values (nM) ± SEM		Improvement (x-fold) Referred to H22-Ang $GGRR_{mut}$	
	HL-60 cells	hM1Φ cells	HL-60 cells	hM1Φ cells
H22-Ang wild type	4.19 ± 1.31	0.75 ± 0.09	-	-
H22-Ang $GGRR_{mut}$	0.88 ± 0.26	0.53 ± 0.18		
H22-Ang GGRR/QG/RA_{mut}	1.65 ± 0.36	0.68 ± 0.13	-	-
H22-Ang GGRR/QG/HA_{mut}	1.00 ± 0.21	0.37 ± 0.06	-	1 - 2
H22-Ang GGRR/QG/DH_{mut}	0.52 ± 0.17	0.26 ± 0.05	1 - 2	2 - 3
H22-Ang GGRR/QG/KQ_{mut}	1.63 ± 0.79	0.54 ± 0.13	-	-

H22-Ang GGRR/QG/DH_{mut} was the only CFP that outperformed the pro-apoptotic potency of H22-Ang $GGRR_{mut}$ on stimulated HL-60 cells and hM1Φ cells (Table 14 and Figure 27). Based on EC_{50} values obtained in the third evaluation round, H22-Ang GGRR/QG/DH_{mut} and H22-Ang $GGRR_{mut}$ substantially outperformed the efficacy of H22-Ang wild type on both target cell types (Table 15). M1 macrophages were found to be less sensitive towards the CFP treatment than observed previously (Table 12) but still demonstrated a higher sensitivity than stimulated HL-60 cells.

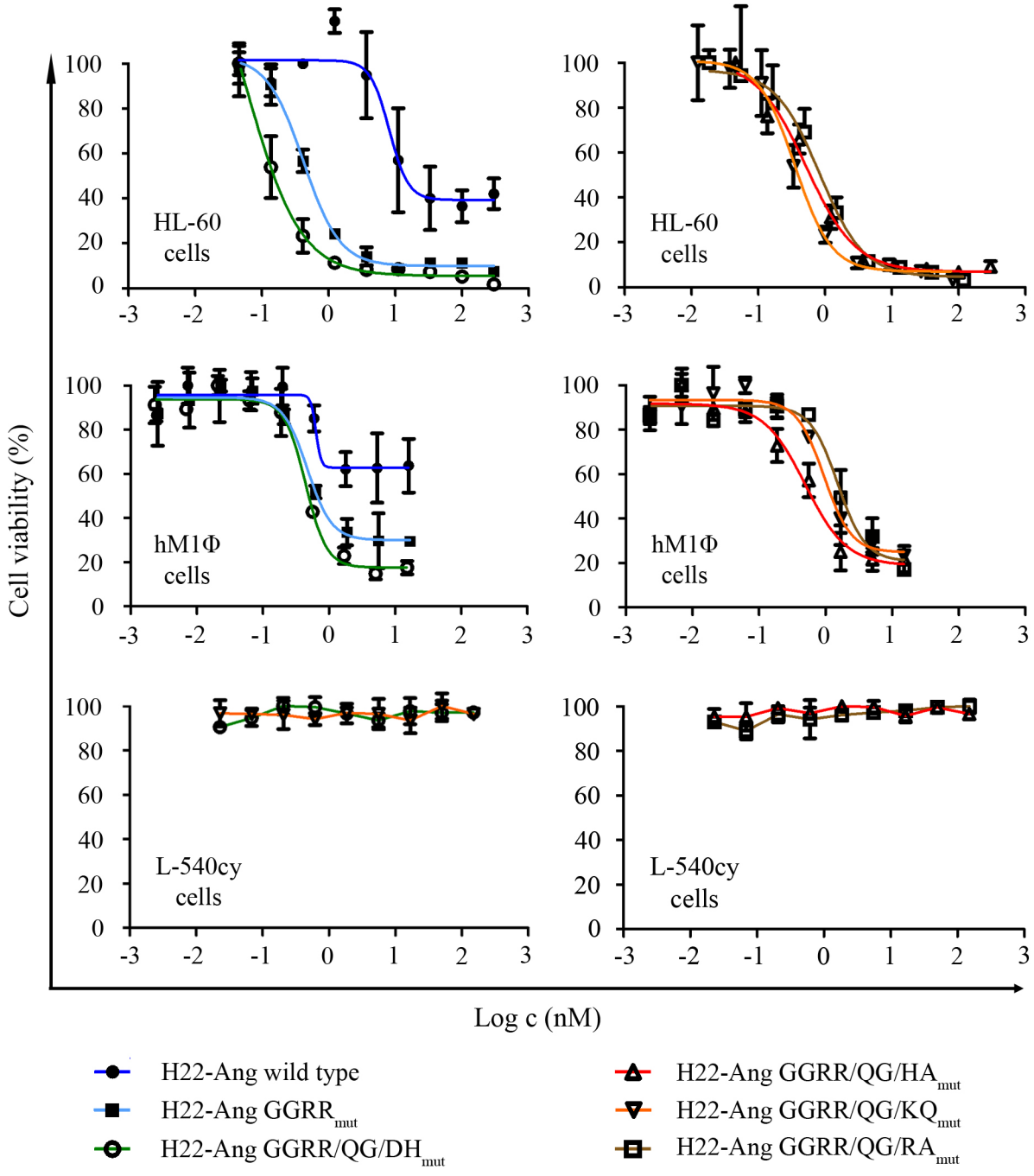


Figure 26: Dose-dependent cytotoxicity of CFPs on different cell types.
The cytotoxicity of CFPs (III.1.1, III.3.1) was evaluated on IFNγ-stimulated HL-60 cells (II.1.6) and human M1 macrophages (II.3.3) using XTT viability assays (II.9). H22-Ang wild type and H22-Ang GGRR$_{mut}$ served as reference fusion proteins whereas CD64^{-} L-540cy cells (II.1.6) were used as negative control. Cells exposed to either zeocin™ or sterile DPBS buffer indicated 0% and 100% cell viability, respectively. Serial CFP dilutions were incubated with the cells for 72 h and viable cells were detected by the conversion of XTT tetrazolium salt (II.1.4, Table 5). Sigmoidal dose-response fits with variable slope were carried out using GraphPad Prism 5 software and EC_{50} values were determined, respectively. Indicated viabilities express means of triplicates ± SD. Dose-responses on hM1Φ cells and L-540cy cells were generated by Hanna Braun under my technical supervision [9]. The illustration was modified from a collaborative manuscript [2]. Abbreviations: hM1Φ cells, Human M1 macrophages; IFNγ, Interferon gamma; Ang, Angiogenin; CFP, Cytolytic fusion protein; c, Concentration.

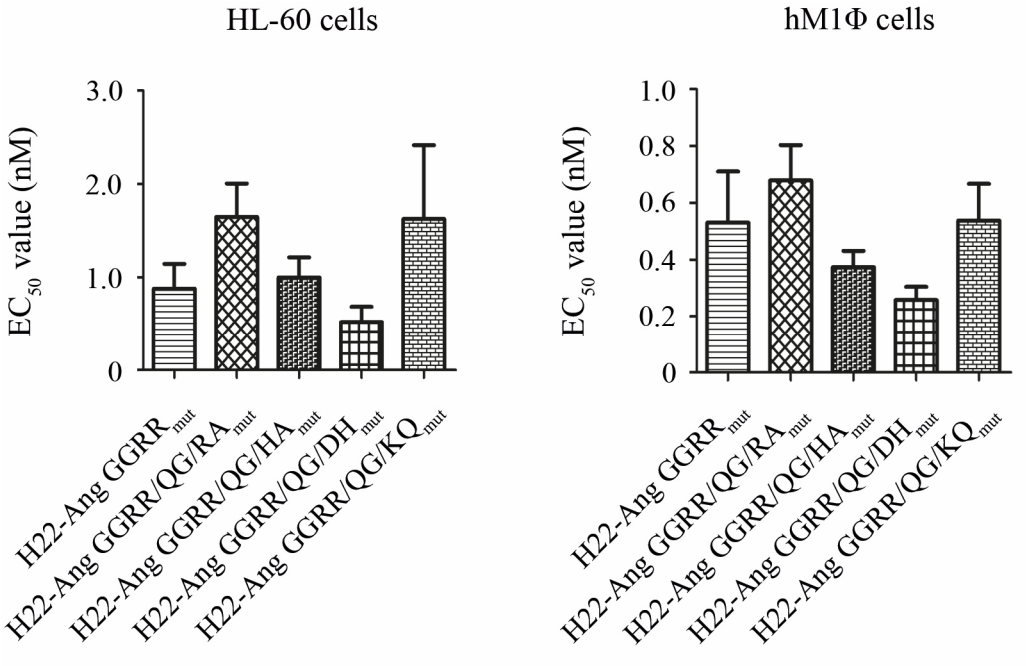


Figure 27: *In vitro* cytotoxicity of fusion proteins in the third evaluation round.
Indicated EC_{50} values represent means ± SEM and were calculated from fitted dose-responses of XTT viability assays (II.9) carried out in the third evaluation round, n = 5-8 on HL-60 cells. Averaged values on hM1Φ cells include such that have been generated by Hanna Braun under my technical supervision (66%) [9], n = 5-7. The illustration was modified from [2] whereas the Kruskal-Wallis test did not reveal significant differences between the distinct CFPs. Abbreviations: hM1Φ cells, Human M1 macrophages; Ang, Angiogenin.

Table 15: Improvement of cytotoxicity in comparison to H22-Ang wild type
The calculated improvements base on indicated EC_{50} values ± SEM in Table 14. Abbreviations: CFP, Cytolytic fusion protein; Ang, Angiogenin; hM1Φ cells, Human M1 macrophages.

CFP	Improvement compared to H22-Ang wild type (x-fold)	
	HL-60 cells	hM1Φ cells
H22-Ang $GGRR_{mut}$	5 - 8	~2
H22-Ang $GGRR/QG/DH_{mut}$	5 - 12	~3

III.4 Stability of CFPs in human and mouse serum

The serum stability of H22-Ang wild type, H22-Ang $GGRR_{mut}$ (III.1.1) and H22-Ang $GGRR/QG/DH_{mut}$ (III.3.1) was competitively investigated (II.11). One µg CFPs were incubated in human and mouse serum (diluted 1:1 with DPBS buffer) for 0.5-6 h at 37°C. Then the remaining binding activities on IFNγ-stimulated HL-60 cells (II.1.6) were analyzed using the anti-penta-his ALEXA Fluor® 488 antibody (II.1.8) and flow cytometry (II.5). Only the binding of intact CFPs could be detected (Figure 28).

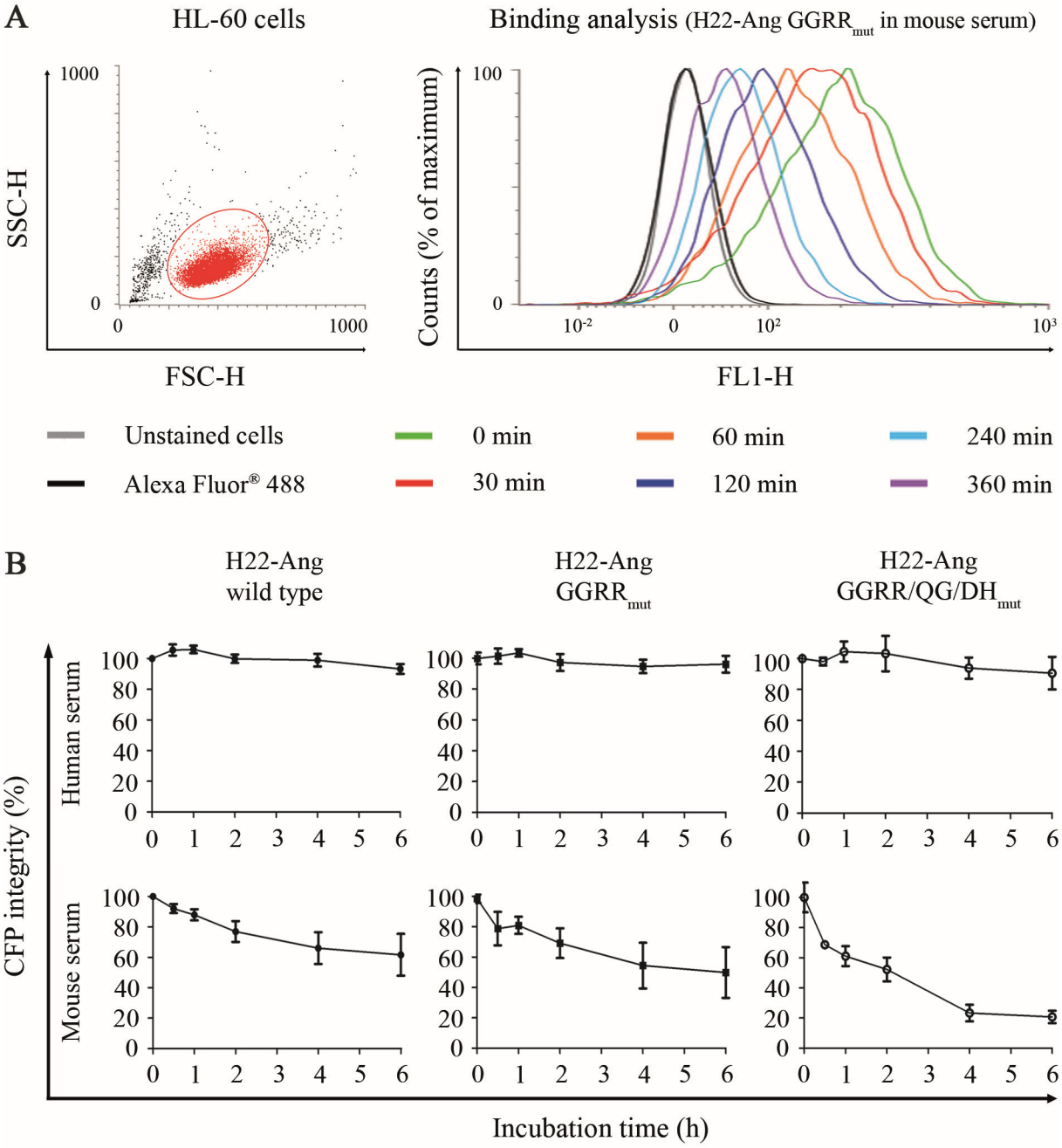


Figure 28: Degradation susceptibility of CFPs in human and mouse serum.
One µg CFPs (III.1.1, III.3.1) were incubated in human and mouse serum (diluted 1:1 with DPBS buffer) at 37°C for 0.5-6 h (II.11) and the remaining binding activities on IFNγ-stimulated HL-60 cells (II.1.6) were evaluated by flow cytometry (II.5). Only the binding of intact CFPs towards a predefined target cell population could be detected using an anti-penta-his ALEXA Fluor® 488 antibody (II.1.8) (**A**). Normalization of MFI values was carried out against the fluorescence signal of anti-penta-his ALEXA Fluor® 488 alone (indicated 0% CFP integrity) and reference samples prepared similarly without incubation (0 min sample, indicated 100% CFP integrity). Shown values express means of duplicates ± SEM, n = 3 whereas two experiments were carried out for H22-Ang GGRR/QG/DH$_{mut}$ in mouse serum (**B**). Abbreviations: Ang, Angiogenin; CFP, Cytolytic fusion protein; IFNγ, Interferon gamma; SSC-H, Sideward scatter; FSC-H, Forward scatter; MFI, Mean fluorescence intensity.

Measured MFI values were normalized to the fluorescence background of the anti-penta-his ALEXA Fluor® 488-labeled antibody (II.1.8) and the binding signal of reference samples prepared without incubation, revealing 0% and 100% CFP integrity, respectively. All tested CFPs were stable in human serum for at least 6 h at 37°C. In contrast, remarkable CFP degradation was observed in mouse serum with the highest for H22-Ang GGRR/QG/DH_{mut}.

III.5 Targeted *ex vivo* depletion of leukemia cells with H22-Ang variants

Blood and bone marrow specimens of CMML and AML patients were kindly provided by the Department of Hematology and Oncology (University Hospital Aachen, Internal Medicine IV) after being pre-screened for the availability of CD64. None of the patients received any treatment prior to sample donation. Clinically relevant patient data are summarized in Table 16. Isolation of mononuclear leukemia cells (II.3.3), verification of the CD64 availability (II.5), demonstration of binding activities (II.5) and apoptosis assays (II.10) were carried out with the assistance of Hanna Braun, Lea Schenke (both AME, EMI) and Radoslav Mladenov (Fraunhofer IME, PPD). Data that have been published in a collaborative manuscript are cited accordingly [2].

Table 16: Clinically relevant patient data
Abbreviations: CMML, Chronic myelomonocytic leukemia; AML, Acute myeloid leukemia; WBC, White blood cell; FAB, French-American-British cooperative group classification.

Patient characteristics	Number	Provided specimen
Total patient number	5	
Average age	73 ± 15	
Gender		
Male	3	
Female	2	
Specimen classification (FAB)		
CMML	1	Bone marrow
AML-M4	2	Peripheral blood
AML-M4/M5	1	Peripheral blood
AML-M5	1	Peripheral blood
WBC (g/L)	99 ± 15	
Monocytes (%)	1 - 44	
Hemoglobin (g/L)	10 - 116	
Platelet count (g/L)	31 - 134	

III.5.1 Preparation of leukemia cells and flow cytometry analyses

Mononuclear cells were prepared from provided specimens of leukemia patients (Table 16) using density gradient centrifugation (II.3.3). The availability of CD64 was confirmed by staining the cells with anti-CD64-FITC and anti-CD33-APC antibodies (II.1.8) following flow cytometry analysis (II.5). As representatively shown for samples A and E in Figure 29 (III.5, Table 17), varying frequencies of CD64-positive cells were found in the distinct preparations that are listed in Table 17.

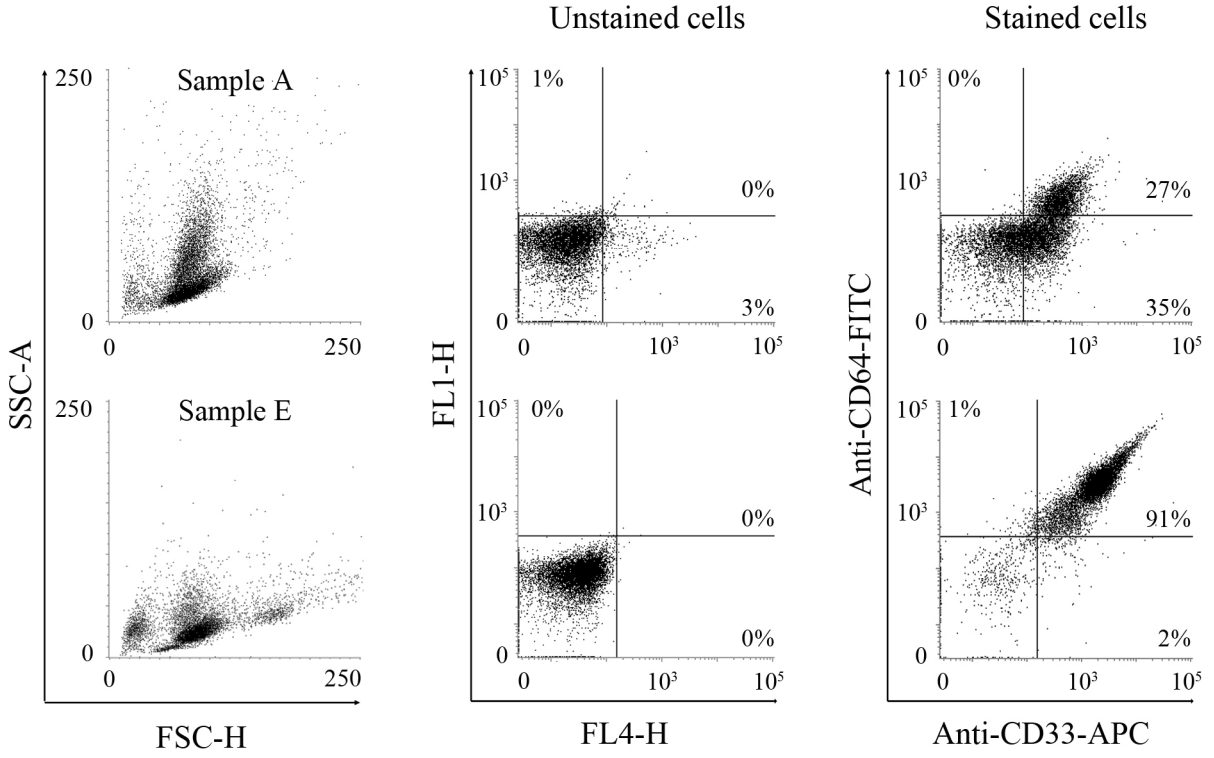


Figure 29: Representative determination of CD64 frequency on leukemia cells.
Mononuclear cells were isolated from specimens of leukemia patients (II.3.3, III.5, Table 16) and 5 x 10^5 cells were stained with anti-CD64-FITC and anti-CD33-APC antibodies (II.1.8) for 20 min. The binding was detected by flow cytometry (II.5) in comparison to an unstained control sample as representatively shown for leukemia samples A and E (III.5, Table 17). CD64 frequencies were calculated, respectively. Flow cytometry analyses were carried out with the assistance of Hanna Braun, Lea Schenke (both Institute of Applied Medical Engineering, Department of Experimental Medicine and Immunotherapy, University Hospital Aachen) and Radoslav Mladenov (Fraunhofer Institute for Molecular Biology and Applied Ecology IME, Department of Pharmaceutical Product Development, Aachen). Abbreviations: SSC-H, Sideward scatter; FSC-H, Forward scatter; FITC, Fluorescein isothiocyanate; APC, Allophycocyanin.

The binding activity of 1 µg fusion proteins (III.1.1, III.2.1, III.3.1, II.10) to leukemia cells was demonstrated by flow cytometry (II.5) as representatively shown for sample E in Figure 30.

Table 17: Determined CD64 frequencies of prepared leukemia cells
Abbreviations: FAB, French-American-British cooperative group classification; AML, Acute myeloid leukemia; CMML, Chronic myelomonocytic leukemia.

Sample	FAB classification	CD64 frequency (%)
A	AML-M4	26
B	AML-M5	36
C	CMML	61
D	AML-M4/M5	71
E	AML-M4	92

H22-ETA' and anti-Her2-Ang $GGRR_{mut}$ (II.10) were kindly provided by Anh-Tuan Pham (AME, EMI) and Radoslav Mladenov (Fraunhofer IME, PPD). Fusion proteins were incubated with 1% (v/v) heat-inactivated human serum to increase the binding specificity whereas the anti-penta-his ALEXA Fluor® 488 antibody (II.1.8) was applied for detection. Observed fluorescence shifts of H22-based fusion proteins widely correlated with the varying CD64 frequencies found on the distinct cell preparations (Table 17). No binding was detected for applied negative control proteins with irrelevant binding moieties, respectively.

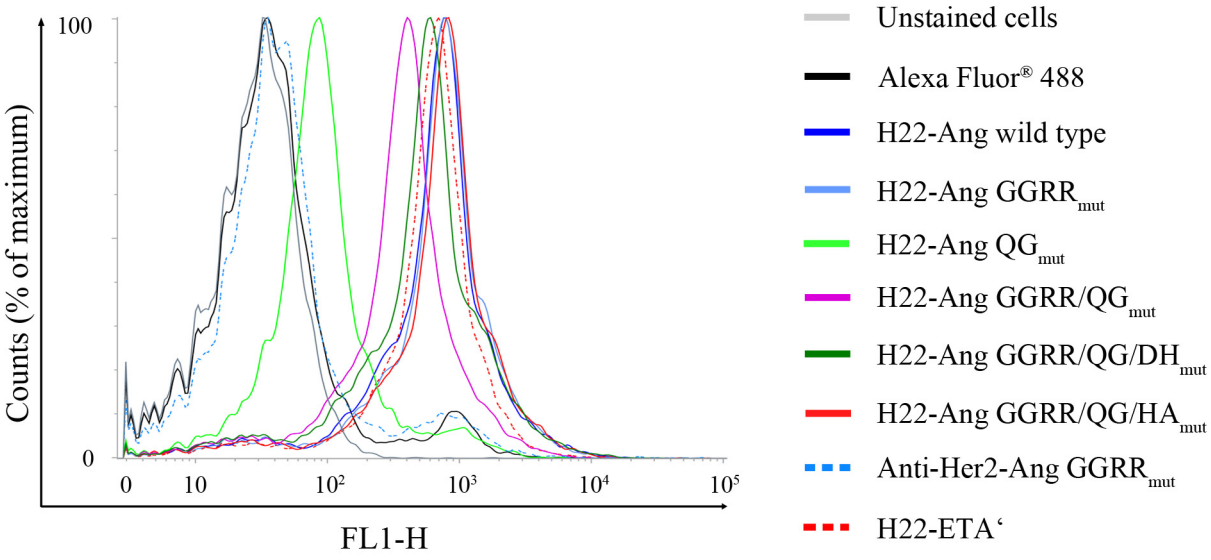


Figure 30: Binding analysis of fusion proteins on leukemia cells.
One µg fusion proteins (III.1.1, III.2.1, III.3.1, II.10) were incubated with leukemia cells (II.3.3, III.5.1) for 20 min in the presence of 1% (v/v) heat-inactivated human serum. The anti-penta-his ALEXA Fluor® 488 antibody (II.1.8) was used to detect the binding. Fluorescence shifts were obtained in the FL1-H channel using flow cytometry analysis (II.5) as representatively shown on AML-M4 cells (sample E, III.5.1, Table 17). The experiment was carried out with the assistance of Hanna Braun, Lea Schenke and Radoslav Mladenov. The illustration was modified from a collaborative manuscript [2]. Abbreviations: Ang, Angiogenin; AML, Acute myeloid leukemia.

III.5.2 Pro-apoptotic effects of CFPs on leukemia cells *ex vivo*

Leukemia cells (III.5.1, Table 17) were incubated with 200 nM fusion proteins (III.1.1, III.2.1, III.3.1, II.10) for 12 h in the presence of 100 U/mL IFNγ and 10% (v/v) heat-inactivated human serum. Afterwards, apoptotic cells were detected by flow cytometry (II.5) using annexin V-eGFP/PI staining. The sums of annexin V-eGFP-positive cells were calculated and plotted against untreated cells and such exposed to control fusion proteins (Figure 31 and 32). Untreated cells indicated the appearance of treatment-independent apoptosis induction. H22-ETA', anti-Her2-Ang $GGRR_{mut}$ and anti-EpCAM-ETA' were kindly provided by Anh-Tuan Pham (AME, EMI) and Radoslav Mladenov (Fraunhofer IME, PPD) whereas 2112(scFv)-Ang $GGRR_{mut}$ and MOG-Ang wild type were kindly provided by Dr. Judith Niesen (Fraunhofer IME, PPD) and Melanie Neß [7], respectively (II.10).

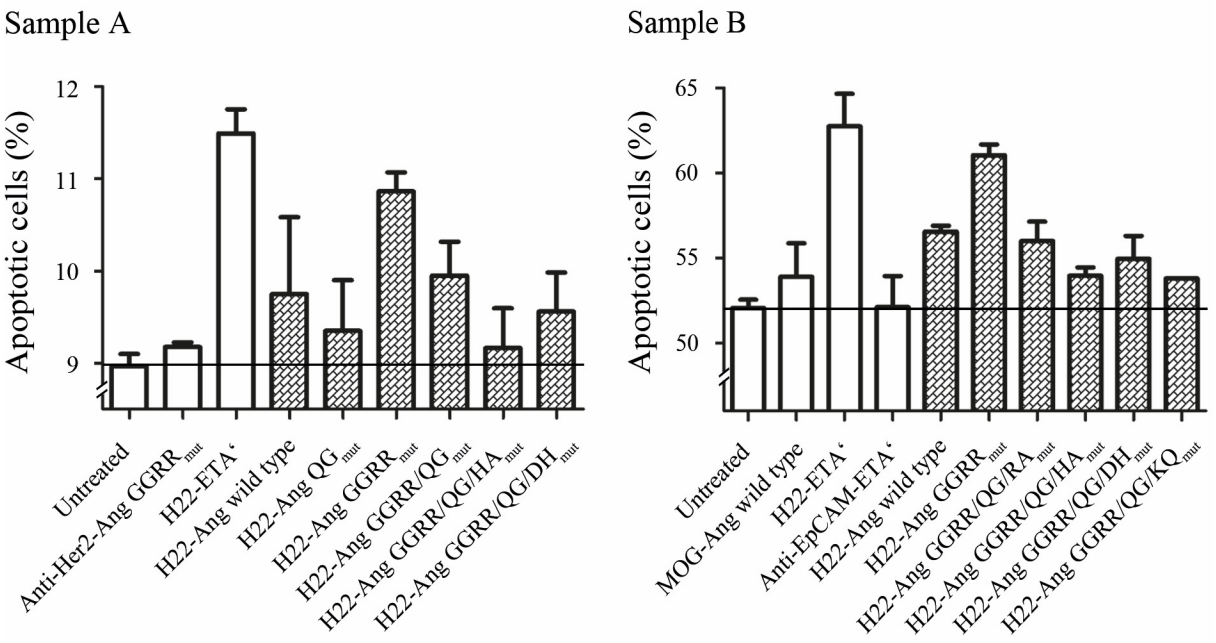


Figure 31: CFP efficacies on leukemia cells with CD64 frequencies below 40%.
Cells were isolated from peripheral blood of leukemia patients (II.3.3, III.5.1, Table 17) and cultivated in the presence of 200 nM fusion proteins, 100 U/mL IFNγ and 10% (v/v) heat-inactivated human serum for 12 h at 37°C (II.10). Untreated cells were cultured similar without exposure to fusion proteins. H22-ETA' was applied as positive control whereas anti-Her2-Ang $GGRR_{mut}$, MOG-Ang wild type and anti-EpCam-ETA' were used as negative control proteins. The cellular CD64 frequencies were 26% (sample A) and 36% (sample B). Apoptotic cells were detected by annexin V-eGFP/PI staining (II.5) and flow cytometry analysis. The appearance of apoptosis without treatment and effects mediated by control proteins are indicated by white bars. Pro-apoptotic effects mediated by H22-Ang variants are shown as dark bars. Values express means of duplicates of annexin V-eGFP-positive cells ± SD. The experiments were carried out with the assistance of Hanna Braun, Lea Schenke and Radoslav Mladenov. The illustration was modified from [2]. Abbreviations: Ang, Angiogenin; eGFP, Enhanced green fluorescent protein; PI, Propidium iodide; IFNγ, Interferon gamma; ETA', Exotoxin A (truncated variant).

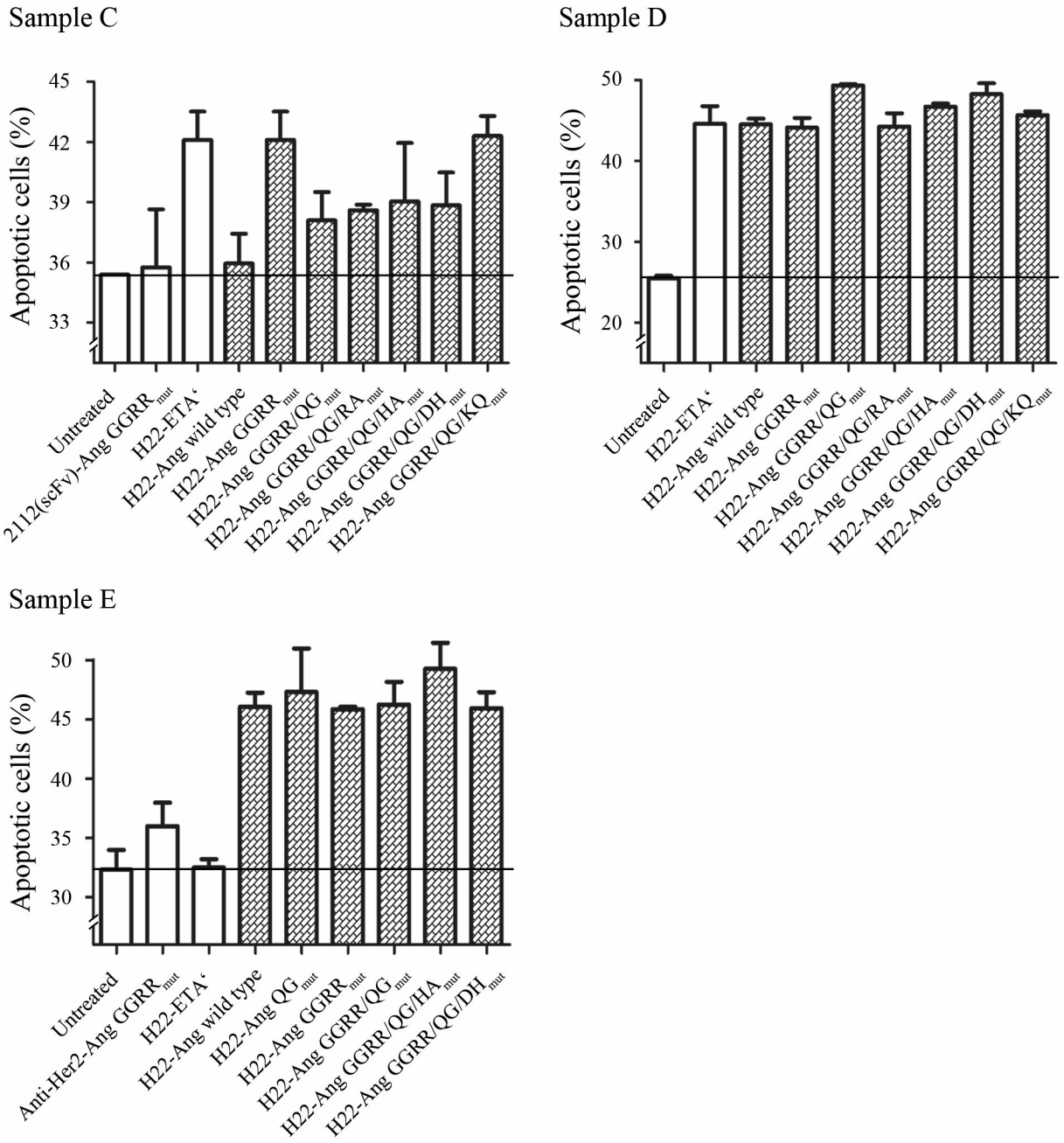


Figure 32: CFP efficacies on leukemia cells with CD64 frequencies of at least 60%.
Mononuclear cells were isolated from bone marrow (sample C) or peripheral blood (samples D and E) of leukemia patients (II.3.3, III.5.1, Table 17) and cultivated for 12 h in the presence of 200 nM fusion proteins, 100 U/mL IFNγ and 10% (v/v) heat-inactivated human serum (II.10). Untreated cells were cultured similar without fusion proteins. H22-ETA' was applied as positive control whereas 2112(scFv)-Ang $GGRR_{mut}$ and anti-Her2-Ang $GGRR_{mut}$ were used as negative control proteins. The cellular CD64 frequencies were 61% (sample C), 71% (sample D) and 92% (sample E). Apoptotic cells were detected by flow cytometry using annexin V-eGFP/PI staining (II.5). The appearance of apoptosis without treatment and effects mediated by applied control proteins are indicated by white bars. Pro-apoptotic effects mediated by H22-Ang variants are shown as dark bars. Values express means of duplicates of annexin V-eGFP-positive cells ± SD. The experiments were carried out with the assistance of Hanna Braun, Lea Schenke and Radoslav Mladenov. The illustration was modified from [2]. Abbreviations: Ang, Angiogenin; scFv, Single chain variable fragment; eGFP, Enhanced green fluorescent protein; PI, Propidium iodide; IFNγ, Interferon gamma; ETA', Exotoxin A (truncated variant).

The pro-apoptotic activities of the CFPs correlated with the determined CD64 frequencies in the cell preparations (III.5.1, Table 17) and the associated binding activities (representatively shown for sample E, Figure 30). An apparent CD64 frequency of at least 30-40% favored the induction of distinct cytotoxic effects within 12 h CFP exposure (Figure 31 vs. 32). H22-ETA' induced reproducible pro-apoptotic effects except on cells of sample E (Figure 32). H22-Ang GGRR$_{mut}$ demonstrated similar efficacy as H22-ETA' and even induced apoptosis where H22-ETA' failed. The remaining CFPs did show varying efficacies that ranged from marginal effects (Figure 31, sample A) to at least similar performances as H22-Ang GGRR$_{mut}$ or H22-ETA' (Figure 32, samples D and E). Cells cultivated in the presence of fusion proteins with irrelevant binding moieties did show a similar appearance of apoptosis than untreated cells (Figure 31 and 32).

III.6 The effect of CatAd on the cytotoxicity of H22-Ang GGRR$_{mut}$

The synthetic adapter CatAd [69] was incorporated into H22-Ang GGRR$_{mut}$ (III.1.1) to improve the endosomal release of the CFP [8]. H22-CatAd-Ang GGRR$_{mut}$ was transiently expressed in HEK293T cells (II.3.1, II.3.2) and yielded 0.5 mg protein per liter cell culture supernatant. *In vitro* characterizations revealed the functionality of the CFP (data not shown) and XTT viability assays (II.9) were carried out on stimulated HL-60 cells and hM1Φ cells (II.1.6, II.3.3) to evaluate the efficacies of H22-Ang GGRR$_{mut}$ and H22-CatAd-Ang GGRR$_{mut}$ (Figure 33). The L-540cy cell line was used as negative control to exclude an unspecific cytotoxicity of H22-CatAd-Ang GGRR$_{mut}$. The adapter-based CFP decreased the viability of stimulated HL-60 cells more efficient than its adapter-less counterpart. However, the calculated EC$_{50}$ values on stimulated HL-60 cells and especially on hM1Φ cells indicated a lower potency in comparison to H22-Ang GGRR$_{mut}$ (Table 18).

Table 18: *In vitro* cytotoxicity of H22-Ang GGRR$_{mut}$ and H22-CatAd-Ang GGRR$_{mut}$
Indicated EC$_{50}$ values were generated by Tim Vierbuchen under my technical supervision [8], n = 3. Abbreviations: Ang, Angiogenin; CFP, Cytolytic fusion protein; hM1Φ cells, Human M1 macrophages.

CFP	EC$_{50}$ values (nM) ± SEM		CatAd-mediated impairment (x-fold)	
	HL-60 cells	hM1Φ cells	HL-60 cells	hM1Φ cells
H22-Ang GGRR$_{mut}$	0.50 ± 0.04	0.05 ± 0.004	-	-
H22-CatAd-Ang GGRR$_{mut}$	0.64 ± 0.05	0.79 ± 0.147	1.2 - 1.4	14 - 18

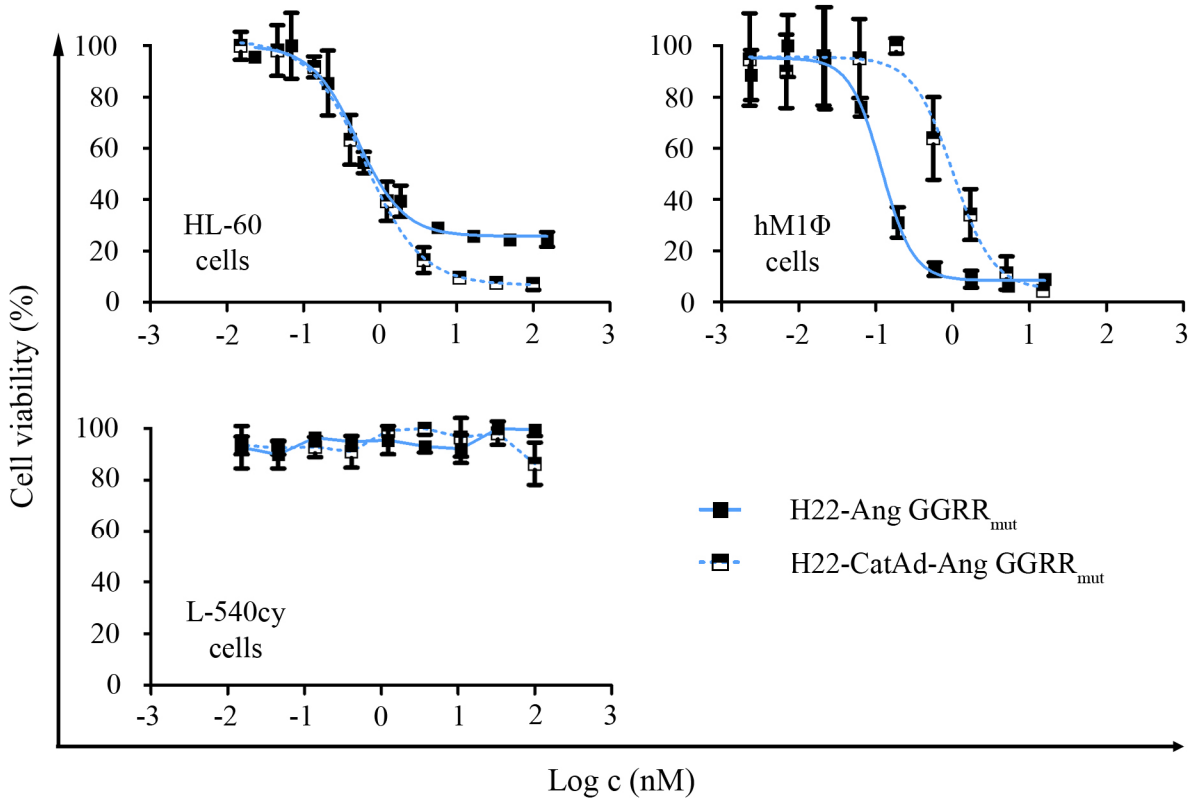


Figure 33: The effect of CatAd on the *in vitro* cytotoxicity of H22-Ang GGRR$_{mut}$.
XTT viability assays (II.9) were carried out on IFNγ-stimulated HL-60 cells (II.1.6) and hM1Φ cells (II.3.3) to competitively evaluate the cytotoxicity of H22-Ang GGRR$_{mut}$ (III.1.1) and H22-CatAd-Ang GGRR$_{mut}$. L-540cy cells (II.1.6) were used as negative control. The cells were exposed to serial CFP dilutions for 72 h whereas the addition of either zeocin™ or sterile DPBS buffer indicated 0% and 100% cell viability, respectively. Viable cells were detected by the addition of XTT tetrazolium salt (II.1.4, Table 5) and sigmoidal dose-responses with variable slope were fitted using GraphPad Prism 5 software. Shown viabilities express means of triplicates ± SD. The experiments were carried out by Tim Vierbuchen under my technical supervision [8]. Raw data were kindly provided for figure preparation. Abbreviations: hM1Φ cells, Human M1 macrophages; IFNγ, Interferon gamma; Ang, Angiogenin; c, Concentration.

III.7 Summarized performance of H22-Ang variants

Table 19 summarizes the individual properties of characterized Ang variants as effector domains in fusion to H22(scFv). The strongest pro-apoptotic activity of Ang is mediated by inhibition resistance as indicated by the consistent performance of H22-Ang GGRR$_{mut}$ *in vitro* and *ex vivo*. Nevertheless, also variants featuring a higher inhibition susceptibility than the wild type can induce remarkable pro-apoptotic effects when equipped with a strong enzymatic activity. On leukemia cells, either H22-Ang GGRR$_{mut}$ alone was effective or all CFPs performed almost similar depending on the respective specimen.

Table 19: Properties of H22-Ang variants in comparison to H22-Ang wild type
Abbreviations: n.c., Not changed substantially; +, Improved; −, Decreased; Ang, Angiogenin.

H22-Ang variant	Expression yield	Substrate cleavage activity	Inhibitor resistance	*In vitro* efficacy	*Ex vivo* efficacy
$GGRR_{mut}$	−	n.c.	++	+++	+
QG_{mut}	n.c.	+	n.c.	+	n.c.
$GGRR/QG_{mut}$	n.c.	+/++	n.c.	+ / ++	n.c.
$GGRR/QG/RA_{mut}$	−	+/++	−	++	n.c.
$GGRR/QG/HA_{mut}$	−	+	−	++	n.c.
$GGRR/QG/DH_{mut}$	−	+/++	+	+++	n.c.
$GGRR/QG/KQ_{mut}$	−	+	−	++	n.c.

III.8 IFNγ sensitizes target cells for the depletion with H22-Ang

The M1 polarization of macrophages is associated with an upregulated expression of CD14 and CD64 [158]. To confirm the presence of M1 macrophages after induced cell polarization (II.3.3), treated and untreated cells were stained with anti-CD14-FITC and anti-CD64-APC antibodies (II.1.8) following flow cytometry analysis (II.5). The M2-specific marker CD206 and CD301 [158] were stained as controls using anti-CD206-FITC and anti-CD301-APC antibodies (II.1.8). In comparison to untreated cells, the M1-polarization increased the percentage of CD64-positive macrophages (Figure 34B) whereas the amount of $CD206^+$ macrophages remained almost unchanged. The percentages of macrophages which were positive for CD14 and CD301 tend to increase following M1 polarization, respectively.

Similarly, the IFNγ-dependent expression levels of CD14 and CD64 were evaluated on HL-60 cells (II.1.6) which have been cultivated with or without 300 U/mL IFNγ for 24 h. Flow cytometry analyses (II.5) revealed a basal CD64 expression on unstimulated HL-60 cells while the IFNγ-treatment increased the binding activity of anti-CD64-APC (II.1.8) by almost 5-fold (Figure 35A and B). The expression of CD14 was absent on unstimulated HL-60 cells and could be induced by IFNγ in approximately 8% of the cells (Figure 35A and C).

For HL-60 cells and macrophages in common, it could be recognized that a variable percentage of cells did not respond to IFNγ since no modulation of CD64 expression could be recognized (Figure 34B and 35C).

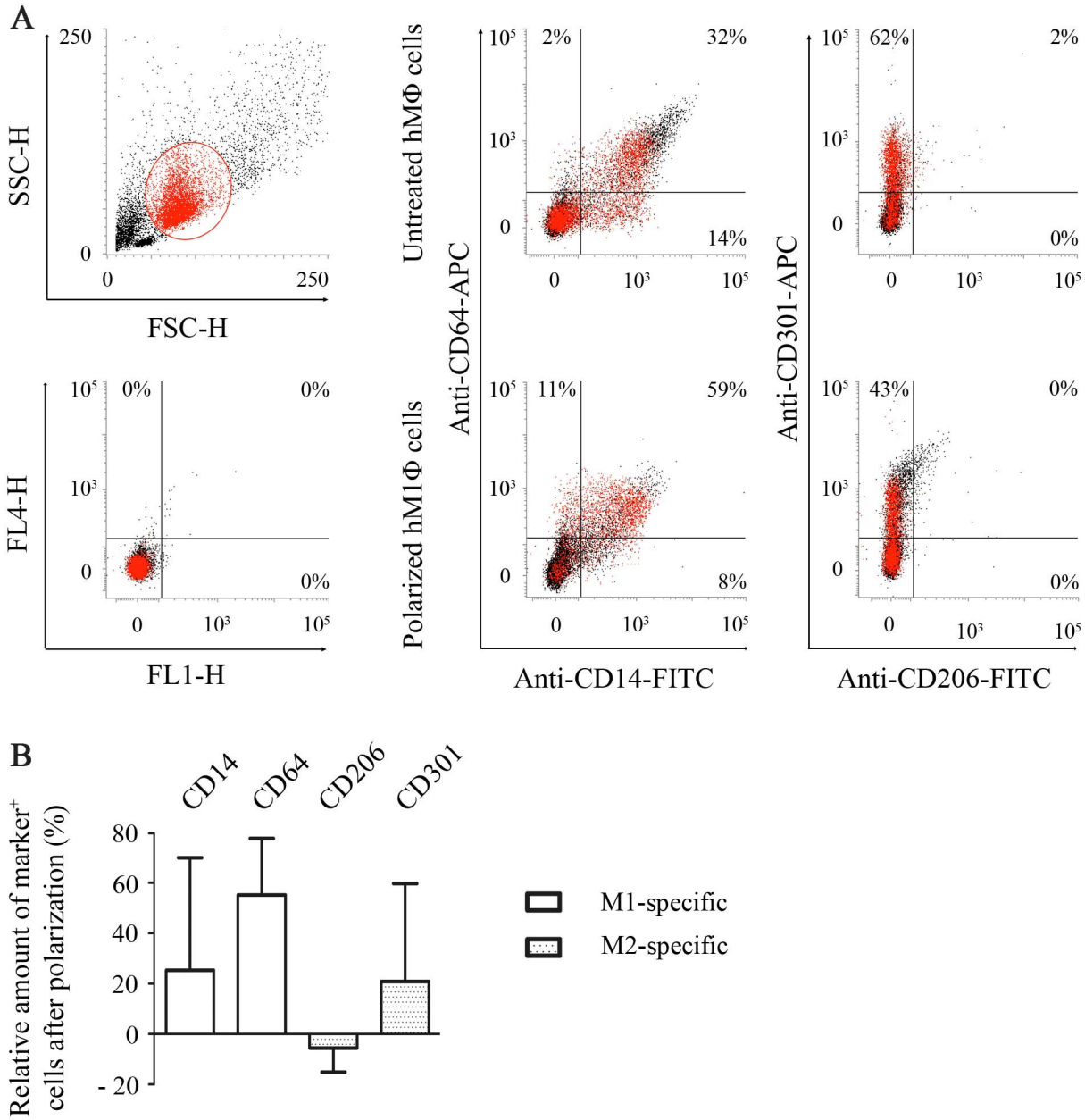


Figure 34: Evaluation of hM1Φ cell polarization.
Peripheral blood mononuclear cells were isolated from buffy coats and macrophages were separated by adherent growth (II.3.3). Lipopolysaccharide and IFNγ were used to induce the M1 polarization whereas untreated hMΦ cells served as reference. To evaluate the cell differentiation, the M1-specific marker CD14 and CD64 as well as the M2-specific marker CD206 and CD301 [158] were stained with combinations of anti-CD14-FITC/anti-CD64-APC and anti-CD206-FITC/anti-CD301-APC antibodies (II.1.8) for 20 min on ice. The binding towards a predefined cell population (indicated in red) was detected by flow cytometry (II.5) using the FL1-H and FL4-H channels for evaluation (**A**). Shown are percentages of marker-positive macrophages after M1 polarization relative to untreated cells. Indicated values express means ± SD, n = 5 (**B**). Abbreviations: SSC-H, Sideward scatter; FSC-H, Forward scatter; FITC, Fluorescein isothiocyanate; APC, Allophycocyanin; hM1Φ cells, Human M1 macrophages; IFNγ, Interferon gamma.

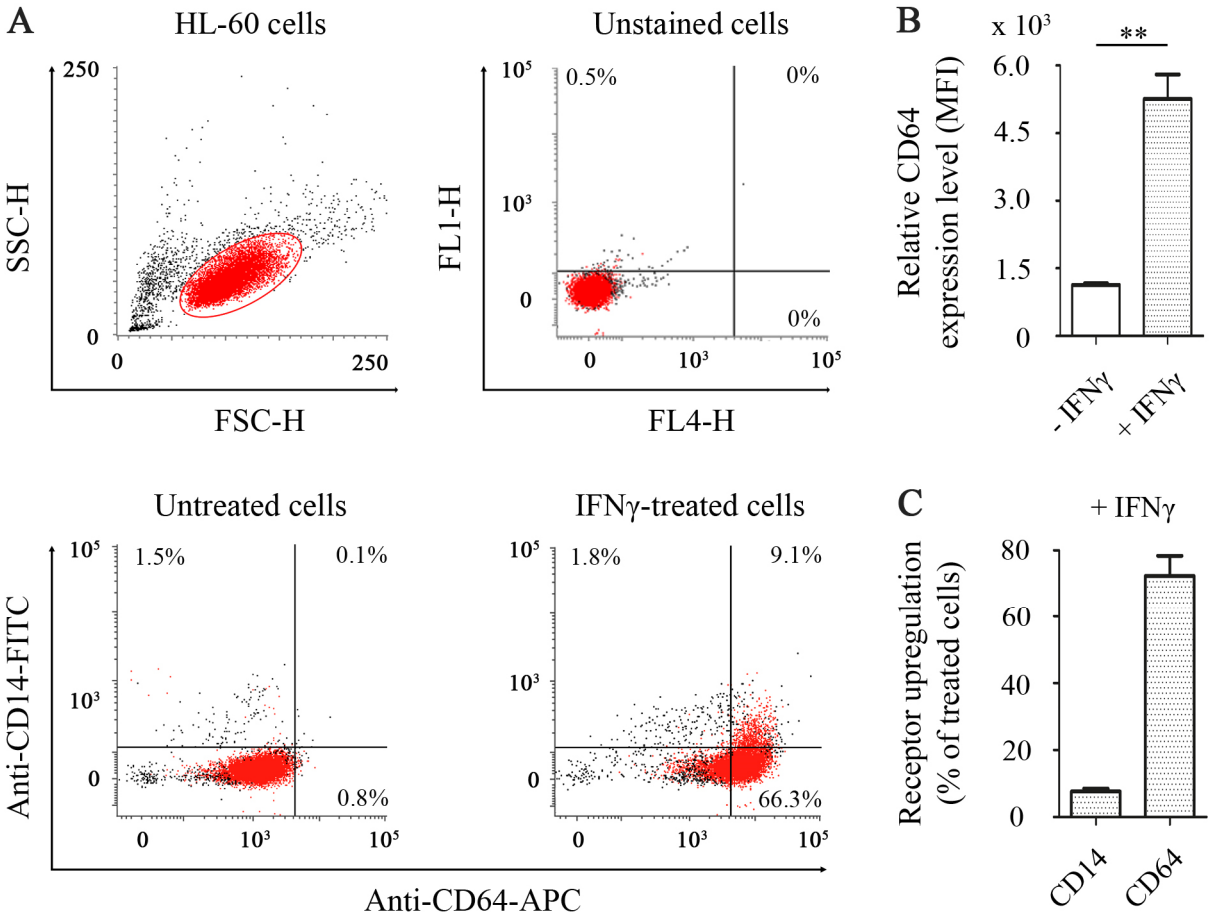


Figure 35: IFNγ-dependent expression of CD14 and CD64 on HL-60 cells.
HL-60 cells (II.1.6) were cultured under standard conditions (II.3.1) either with or without 300 U/mL IFNγ. After 24 h, 5 x 10^5 cells per sample were stained with anti-CD14-FITC and anti-CD64-APC antibodies (II.1.8) for 20 min on ice. The binding was analyzed by flow cytometry (II.5) using unstained cells as control. Gated target cell populations are indicated in red (**A**). To quantify the CD64 upregulation following IFNγ exposure, the MFI values for anti-CD64-APC were determined on untreated and stimulated HL-60 cells. Shown are means of duplicates ± SEM, n = 6. The statistical analysis was carried out using GraphPad Prism 5 software and a non-parametric Mann-Whitney test, **p≤0.01 (**B**). The percentages of target cells that demonstrated an increased expression of CD14 or CD64 after IFNγ exposure were calculated, respectively. Untreated cells served as reference. Shown are means of duplicates ± SEM, n = 6 (**C**). Abbreviations: SSC-H, Sideward scatter; FSC-H, Forward scatter; FITC, Fluorescein isothiocyanate; APC, Allophycocyanin; IFNγ, Interferon gamma; MFI, Mean fluorescence intensity.

IFNγ regulates the binding activity of H22-Ang by modulating the expression level of CD64. Representatively, one µg H22-Ang wild type (III.1.1) was applied to HL-60 cells (II.1.6) which have either been stimulated with 300 U/mL IFNγ for 24 h or remained untreated. The binding activity was demonstrated using flow cytometry (II.5) and the anti-penta-his ALEXA Fluor® 488 detection antibody (II.1.8) as shown in Figure 36A. The stimulation of HL-60 cells was found to increase the binding activity of H22-Ang wild type by almost 4-fold (Figure 36B).

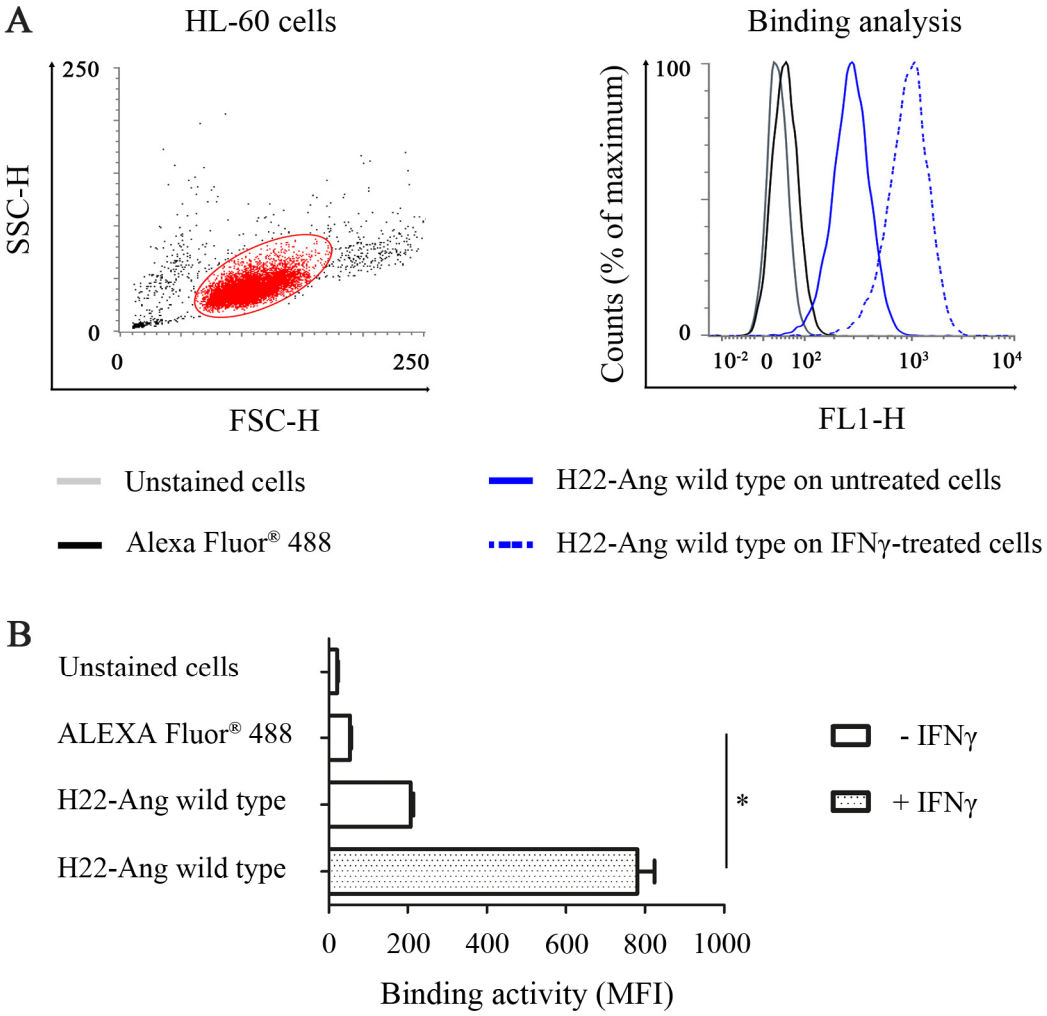


Figure 36: IFNγ modulates the binding activity of H22-Ang towards HL-60 cells.
HL-60 cells (II.1.6) were cultured under standard conditions (II.3.1) either with or without 300 U/mL IFNγ for 24 h. Then 5 x 10^5 cells per sample were incubated with 1 µg H22-Ang wild type (III.1.1, II.4.4) for 20 min on ice. The binding was detected using an anti-penta-his ALEXA Fluor® 488 antibody (II.1.8) and flow cytometry analysis (II.5). The predefined target cell population used for evaluation is indicated in red. Fluorescence shifts were detected in the FL1-H channel and MFI values were determined, respectively (**A**). Shown are means of duplicates ± SEM, n = 6. Statistical analysis was carried out using GraphPad Prism 5 software and a Kruskal-Wallis test following Dunn's multiple comparison analysis, *p≤0.05 (**B**). Abbreviations: Ang, Angiogenin; IFNγ, Interferon gamma; SSC-H, Sideward scatter; FSC-H, Forward scatter; MFI, Mean fluorescence intensity.

The activity of the RiboLock™ ribonuclease inhibitor was investigated under varying redox conditions (II.13). Briefly, 3.65 nM RNase A was used to cleave 50 nM RNaseAlert® substrate. Increasing RiboLock™ amounts were added to inhibit the cleavage reaction in a dose-dependent manner whereas a serial dilution of hydrogen peroxide (30%) was used to inactivate the inhibitor in its highest concentration. Fluorescence emissions were measured at 520 nm

while exciting the samples at 485 nm. Relative cleavage activities were calculated by signal correlation against the emission of substrate dissolved in RNase cleavage buffer (0% activity) and the emission obtained for the RNase A-mediated substrate cleavage without inhibition and H_2O_2 supplementation (100% relative cleavage activity). The presence of 330 nM RiboLock™ reduced the relative cleavage activity of RNase A to approximately 10% whereas the addition of hydrogen peroxide efficiently restored the cleavage activity of the ribonuclease in a dose-dependent manner (Figure 37).

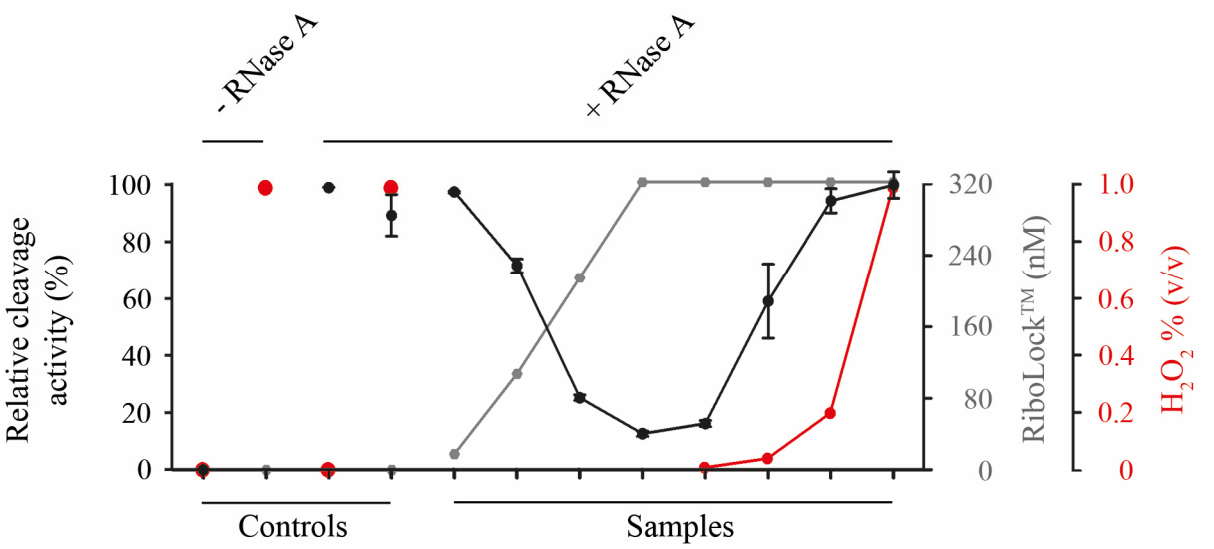


Figure 37: Redox-dependent activity of the RiboLock™ inhibitor.
RNase A (3.65 nM) was used to digest 50 nM RNaseAlert® substrate and increasing amounts of the RiboLock™ inhibitor (18-330 nM) were applied to prevent the cleavage reaction in a dose-dependent manner (II.13). A serial 1:5 dilution of 30% hydrogen peroxide, corresponding to 1-0.0016% (v/v), was used to inactivate 330 nM of the inhibitor while further reaction conditions were maintained. Relative cleavage activities were calculated by signal normalization against the emission of substrate dissolved in RNase cleavage buffer (0% cleavage activity) and the emission of an RNase A-mediated cleavage reaction without inhibition and H_2O_2 supplementation (100% relative cleavage activity). Values express means of duplicates ± SEM, n = 3.

To reveal varying RNH1 contents in stimulated HL-60 cells and polarized M1Φ cells (II.3.3), cell lysates were prepared (II.12) and separated by SDS-PAGE (II.4.2). After western blotting on a nitrocellulose membrane, RNH1 and β-actin were specifically detected using mouse-anti-RNH1, goat-anti-mouse-HRPO and mouse-anti-β-actin-HRPO antibodies (II.1.8). Protein bands were quantified using AIDA software and inhibitor contents were normalized to 100 a.u. β-actin, respectively (Figure 38). The inhibitor quantity in hM1Φ cells was found to be lower than in stimulated HL-60 cells.

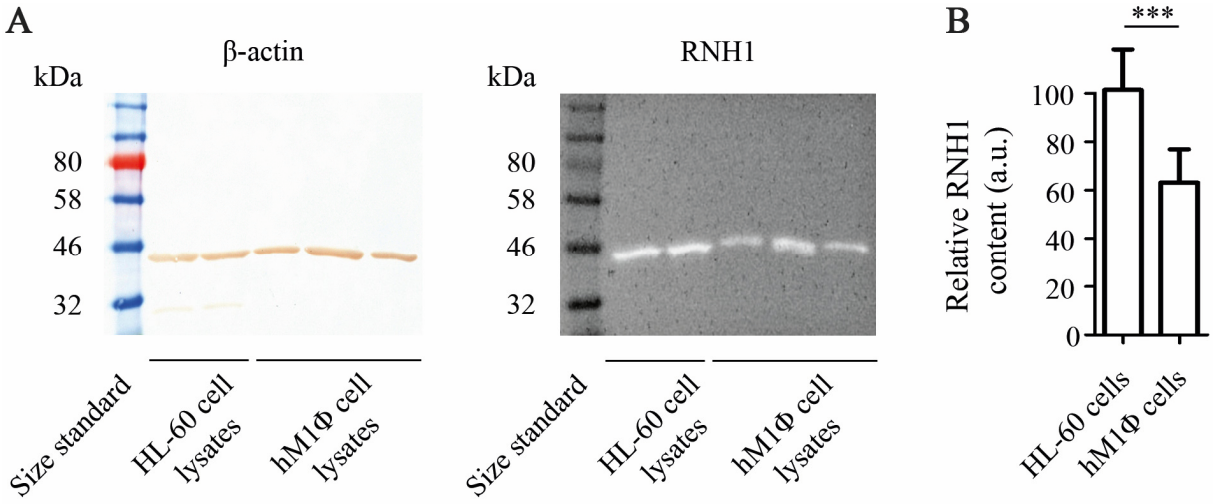


Figure 38: RNH1 contents in stimulated HL-60 cells and hM1Φ cells.
HL-60 cells (II.1.6) were cultured under standard conditions (II.3.1) and stimulated with 300 U/mL IFNγ for 24 h. Human M1Φ cells were prepared as described in II.3.3. After harvesting, cell lysates were prepared (II.12) and separated by SDS-PAGE (II.4.2). The Color Protein Standard, Broad Range (NEB) was used as internal size standard. The proteins were transferred onto a nitrocellulose membrane and mouse-anti-RNH1, goat-anti-mouse-HRPO and mouse-anti-β-actin-HRPO antibodies (II.1.8) were applied as described in II.4.2. RNH1 and β-actin were visualized by the addition of Pierce™ ECL Western Blotting Substrate and SIGMA*FAST*™ 3,3'-Diaminobenzidine tablets, respectively (**A**). Protein band intensities were quantified by AIDA software and RNH1 quantities were normalized to 100 a.u. β-actin. The illustration was modified from [1] whereas values express means ± SD, n = 9. The statistical analysis was carried out using GraphPad Prism 5 software and a non-parametric Mann-Whitney test, ***p≤0.001 (**B**). Abbreviations: RNH1, Ribonuclease inhibitor; hM1Φ cells, Human M1 macrophages; IFNγ, Interferon gamma; HRPO, Horseradish peroxidase.

Additionally, the dose-dependent effect of IFNγ on the intracellular RNH1 content was demonstrated. HL-60 cells (II.1.6) were cultured under standard conditions (II.3.1) and in the presence of either 0, 300 or 600 U/mL IFNγ, respectively. Cell harvesting was carried out after 15, 18, 21 and 24 h. Lysates were prepared and separated by SDS-PAGE following transfer of the proteins onto a nitrocellulose membrane (II.12, II.4.2). RNH1 and β-actin were specifically detected (II.1.8, II.12) and the protein bands were quantified using AIDA software. For evaluation, the inhibitor contents were normalized to 100 a.u. β-actin, respectively (Figure 39). The presence of 300 U/mL IFNγ in the culture medium was found to reduce the RNH1 content in HL-60 cells in a time-dependent manner whereas the protein accumulated in the presence of 600 U/mL IFNγ. The highest quantity was found 21 h after stimulation whereas the level decreased to that of untreated cells after 24 h.

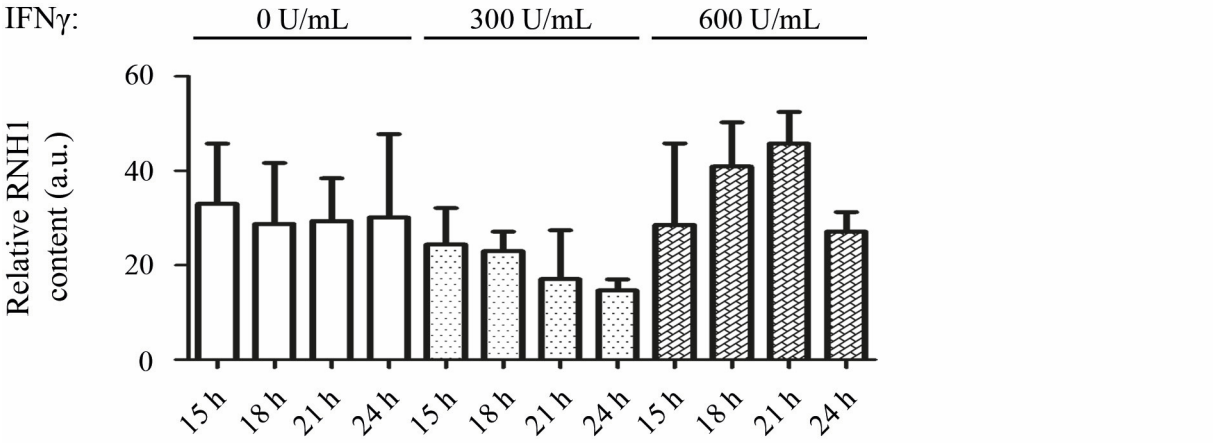


Figure 39: IFNγ-mediated effects on the intracellular RNH1 content of HL-60 cells.
HL-60 cells (II.1.6) were cultured in the presence of 0, 300 and 600 U/mL IFNγ (II.3.1) and harvested 15, 18, 21 and 24 h after stimulation. Cell lysates were prepared (II.12) and ten µl of each sample was separated by SDS-PAGE (II.4.2). The proteins were transferred onto a nitrocellulose membrane and mouse-anti-RNH1, goat-anti-mouse-HRPO and mouse-anti-β-actin-HRPO antibodies (II.1.8) were used to specifically detect RNH1 and β-actin. Protein bands were quantified by AIDA software and RNH1 quantities were normalized to 100 a.u. β-actin, respectively. Evaluation was carried out using GraphPad Prism 5 software. Shown values express means ± SD, n = 3. Abbreviations: RNH1, Ribonuclease inhibitor; IFNγ, Interferon gamma.

IV Discussion

IV.1 Expression and purification of H22-Ang variants

Upon the generation of novel H22-Ang variants by site-directed mutagenesis and their transient expression in HEK293T cells, the recombinant fusion proteins were purified from the cell culture supernatant by affinity chromatography. As some metal ions are described to affect the ribonucleolytic activity of angiogenin, Cu^{2+} and Zn^{2+} ions being the most potent inhibitors diminishing the ribonucleolytic activity >99% and 93% [167], the choice of metal ions for affinity chromatography is critical. No inhibiting effect has been described for Ni^{2+} ions leaving the enzymatic activity of human Ang unaffected. However, encountering traces of inhibiting ions during *in vitro* experiments may impair the activity of angiogenin substantially. Purified protein samples were analyzed by SDS-PAGE and western blot (Figure 6A, 9A and 21A) revealing the appearance of co-purified proteins in varying intensities corresponding to the determined CFP purities of 60-90% (III.1.1). The proteins of 60-160 kDa in size most probably derive from the supplemented serum in the cell culture supernatant. However, their appearance was not considered to affect cellular assays as the used eukaryotic culture media contain serum proteins as well (Table 3). An increased imidazole concentration in the 1x incubation buffer might have increased the binding stringency during purification but this was not carried out due to varying elution susceptibilities of individual CFPs. Similarly, an enhanced washing stringency during IMAC purification usually results in a remarkable yield reduction due to the increased loss of the target protein. Regarding the CFP yields determined in the third evaluation round (0.1-0.9 mg/L, III.3.1), the application of alternative purification strategies is recommended to obtain higher protein purities. Expression yields of 1.5-2.8 mg protein per liter cell culture supernatant were obtained for CFPs containing the Ang variants QG_{mut}, NLS RA_{mut}, RA_{mut}, WA_{mut}, GGRR/QG_{mut} and the wild type matching with expression yields of other Ang wild type-based CFPs using bacterial expression systems [53, 69]. CFPs containing the Ang variants $GGRR_{mut}$, GGRR/QG/RA_{mut}, GGRR/QG/HA_{mut}, GGRR/QG/DH_{mut} and GGRR/QG/KQ_{mut} provided lower yields not exceeding 0.9 mg protein per liter cell culture supernatant (III.3.1). Those were similar to such already described for the wild type angiogenin-based Ki-4-Ang, Ang-Ki-4, Ang-MJ7, MJ7-Ang and RFB4-Ang [132, 134, 135]. It could be noticed that CFPs with increased potency compared to H22-Ang wild type usually provided lower yields (Table 19) suggesting that the expression of Ang variants somehow affects the

cellular host. This assumption is supported by the expression yield of 8 mg/L for H22(scFv)-SNAP in the HEK293T expression system [159]. Angiogenin is expected to interfere with the protein biosynthesis of target cells when delivered as effector domain and its efficacy strongly depends on individual enzymatic properties. Similar effects on HEK293T cells might explain this observation. The N-terminal Ig-kappa leader of the CFPs (II.1.7) mediates translation at the rough endoplasmic reticulum (rER) and the secretion of proteins via the trans-Golgi pathway [168]. The absent expression of CD64 on HEK293T cells makes internalization after secretion unlikely. We presume that a proportion of CFPs is able to escape the secretory vesicles prior to fusion with the plasma membrane. It has recently been shown that ERB-hRNase, a CFP comprising of a human ErbB2-specific scFv fused to HPR, can reach the cytosol of target cells from endosomes right after internalization [55]. Native Ang is expected to cross the membranes of early endosomes after cell entry in a similar manner [117]. The ability of RNases to destabilize lipid vesicles was found to depend on their electrostatic conditions whereas a positive net charge enhances the capability to aggregate, fuse and affect the fluidity of negatively-charged membrane bilayers [169]. The alteration of electrostatic properties, especially the increase of the positive net charge mediated by GGRR, might facilitate the secretory escape of CFPs allowing the effector domains to interfere with the HEK293T cell metabolism according to their enzymatic properties. This drawback might be circumvented by using a ‘non-human’ expression system since Ang is not posttranslationally modified and its activity was found to be species-dependent [51]. Reduced productivities that depend on a different codon usage might be faced by an appropriate modification and optimization of the CFP encoding sequence. Chinese hamster ovary (CHO) clones are promising to get access to sufficient CFP amounts for extensive *in vitro* and *in vivo* studies. A yield of 25 mg/L cell culture supernatant has been reported for stable expressed anti-ErbB2(scFv)-Fc-IL2 in CHO cells [170]. However, the generation of CHO clones by methotrexate selection is a time-consuming and cost-intensive process suggesting that optimization of the production process is reasonable after having identified the most cytotoxic Ang variant. Alternatively, bacterial fermentation platforms may promise higher yields but the notable loss of target protein during the purification steps has to be considered. An insufficient removal of endotoxins may additionally affect target cell sensitivities *in vitro* (IV.4) and could cause severe side effects upon *in vivo* application [171].

IV.2 *In vitro* characteristics and pro-apoptotic potencies of CFPs

IV.2.1 CD64-specific binding activity of H22-Ang variants

Target cell binding and internalization are the first bottlenecks for the pro-apoptotic potential of CFPs. All generated fusion proteins demonstrated a similar binding activity on stimulated HL-60 cells and M1 macrophages whereas no binding could be observed on the negative control cell line L-540cy (Figure 15 and 25). This is in line with previous observations [9]. Distinct background signals for anti-his ALEXA Fluor® 488 were obtained rarely and are expected to be caused by unspecific binding events. Binding analyses on hM1Φ cells usually revealed a weak binding signal that slightly exceeded the background fluorescence of the anti-his ALEXA Fluor® 488 antibody and a distinct peak indicating binding of CFPs (Figure 15 and 25). Since only gated cells were analyzed in the experiments, it suggests the presence of a subpopulation within the defined target cell gate with almost absent CD64 expression. This might reflect the heterogeneity of macrophages even after polarization. As shown in Figure 34B, a variable amount of macrophages was $CD301^+$ and did not increase the expression of CD64 after the addition of IFNγ and LPS. Thus, they still represent undifferentiated macrophages or a subtype other than M1 demonstrating a basal CD64 expression [158]. Consequently, macrophage subpopulations that escaped the M1 polarization most probably cause the additional small peaks observed in the respective dot plots. Different binding activities on individual leukemia cell preparations (data not shown) are primarily caused by the varying CD64 frequencies (Table 17). Beside inconsistent appearances of monocytes in the used specimens (1-44%, Table 16), the distinct expression levels of CD64 differed. Additionally, certain amounts of granulocytes and erythrocytes could remain in the interphase following centrifugation or might be co-transferred from the Biocoll phase during interphase separation (Figure 29). Since the counted cell number without gating was constant in the individual experiments, a higher persistence of non-target cells correlated with lower binding activities in general. Varying binding activities of CFPs within one experiment, as recognized for H22-Ang QG_{mut} in Figure 30, might result from the stringent binding conditions. Heat-inactivated human serum was added to block CD64 receptors on the cell surface thus preventing the cross-reaction with Fc domains of detection antibodies and increasing binding specificity [172]. However, the enhanced stringency may have weakened the binding strength of CFPs and lead to higher susceptibility of protein loss during the washing procedure. Alternatively, the C-terminal degradation of CFPs may mediate

the loss of the histidine tag that is finally required for immunodetection. The binding activity and internalization of H22-Ang variants might be improved by using a bivalent H22(scFv) construct. This strategy has already been shown for H22(scFv)$_2$-ETA', a bivalent IT that is featured by a 10-fold higher cytotoxicity on U937 cells than its monovalent counterpart [20].

IV.2.2 Preventing the nuclear translocation of H22-Ang has no favorable effect

The pro-apoptotic potential of Ang is believed to depend on the cleavage of cytoplasmic tRNA and its efficacy can be hampered by the translocation into the nucleus. Even the nuclear uptake is a well regulated process, the translocation takes place constitutively in some cancer cells to acquire the high metabolic demands [121]. The mechanism has already been described for solid tumors and a correlative effect cannot be excluded when Ang is delivered to leukemia cells or HL-60 cells using H22(scFv). To reveal an effect of enforced cytoplasmic retention, the NLS sequence of Ang was disrupted by the R33A exchange (Ang NLS RA$_{mut}$, Table 11) [161]. The corresponding fusion protein was tested for its pro-apoptotic potency on HL-60 cells whereas usually higher amounts of viable target cells were found after treatment in comparison to H22-Ang wild type and especially H22-Ang QG$_{mut}$ and H22-Ang GGRR$_{mut}$ (Figure 8). This might correlate with the finding that ^{Ang}R33 is important for the ribonucleolytic activity of Ang, albeit non-crucial [173]. Nevertheless, a slightly reduced tRNA cleavage efficiency compared to Ang wild type might allow more target cells to remain viable even in the presence of high CFP concentrations. It further suggests that after H22(scFv)-mediated delivery, the amount of wild type Ang remaining in the cytosol of stimulated HL-60 cells is sufficient to mediate appropriate substrate cleavage and apoptosis induction. Hence, the nuclear translocation does not take place or the effect is negligible. EMSA experiments revealed that ^{Ang}G85R/G86R prevents the binding of Ang to genomic DNA (Figure 13), a process that is required to activate the ribosomal DNA promotor [119]. Consequently, the stimulation of cell proliferation by upregulating protein biosynthesis in target cells as antagonizing side effect can be excluded for all variants carrying the GGRR exchanges, given that nuclear uptake even occurs. The introduced mutation also lowers the positive net charge of the surface-exposed NLS sequence (^{31}RRRGL^{35}) and thus might reduce the endosomal release efficacy as discussed previously (IV.1). Since the ^{Ang}R33A mutation did not substantially increase the efficacy of Ang wild type in comparison to Ang QG$_{mut}$ and Ang GGRR$_{mut}$, it was not further evaluated.

IV.2.3 The impact of enzymatic activity and inhibition susceptibility

The Q117G mutation aimed to increase the cleavage activity of Ang which is rather low compared to RNase A since the active center is obstructed by Q117 making a conformational reorientation of the C-terminus necessary to allow substrate accessibility and cleavage [174]. Intracellular digestion of tRNAs occurs at the 3'-CCA termini and within particular anticodon loops. The removal of the 3'-terminus, that is required to attach amino acids, allows the rapid and reversible repression of translation as the damage can be quickly repaired by tRNA nucleotidyltransferases (CCA-adding enzymes) [122, 175, 176]. The cleavage of anticodon loops takes place more slowly and affects only a subset of tRNAs [122]. Accordingly, the total intracellular tRNA pool is only reduced by 1-2% upon stress-induced cleavage indicating amplifying or signal-related effects of the generated fragments [125]. Indeed, 5'-tiRNAs efficiently inhibit cap-dependent and -independent global protein translation including such regulated by weak IRES. Genes translated by strong IRES sequences are not affected and are usually associated with cell survival [126]. Nevertheless, the translation of proteins to maintain a minimal metabolic activity for survival requires a certain pool of functional tRNAs with attached amino acids. Therefore, the persisting and extensive removal of 3'-CCA termini is expected to antagonize with CCA-adding enzymes and might result in cell death if the cell metabolism is suppressed below a critical level. Alkylated onconase with ~2% of its initial enzymatic activity or cationic variants of bovine RNase A and human RNase 1 exhibiting less than 0.01% enzymatic activity were all not found to be cytotoxic [177]. However, onconase is highly cytotoxic despite of its low enzymatic activity [178]. These findings indicate that only a certain ribonucleolytic activity is required to induce apoptosis but it is essential and must be achievable in the presence of RNH1. Onconase and Ang are also known to digest rRNA that has been linked to the inactivation of the protein biosynthesis machinery [179, 180]. The performed cleavage assays revealed that all CFPs carrying the Q117G exchange demonstrated increased cleavage efficacy compared to H22-Ang wild type and H22-Ang $GGRR_{mut}$ (Figure 10 and 23). As recognized for H22-Ang $GGRR/QG/KQ_{mut}$ in Figure 22 and 23, varying activities observed in some experiments may be caused by inaccurate protein concentrations, pipetting errors and different CFP preparations. Nevertheless, the obtained tRNA cleavage activities of the CFPs (Figure 22) were similar to such described previously [2, 9]. Photobleaching effects during short-interval measurements may additionally hamper RNaseAlert® signals following digestion by enzymes with lower activity.

This effect was circumvented by overnight incubation of the cleavage reactions allowing variants with lower cleavage activities to convert higher amounts than initially observed. However, removal of the active center obstruction improved the substrate cleavage activity of respective variants and contributed to an increased potency, respectively. Despite of RNH1 sensitivities similar to the wild type-based CFP, H22-Ang QG_{mut} and H22-Ang GGRR/QG_{mut} demonstrated increased cytotoxicity compared to H22-Ang wild type that was defined by their higher substrate cleavage activities (Table 12, Figure 10-12). Determined EC_{50} values for H22-Ang wild type, H22-Ang QG_{mut} and H22-Ang GGRR/QG_{mut} were similar to such reported for Gb-H22 on CD64-positive U937 cells and Gm-H22 on HL-60 cells [49, 50].

The resistance towards inhibition was found to be a key feature for the cytotoxicity of Ang. Although H22-Ang $GGRR_{mut}$ retains the ribonucleolytic activity of the wild type-based fusion protein (Figure 10), it markedly outperforms the *in vitro* efficacy of H22-Ang wild type (Table 12 and 14) since it digests tRNA even in the presence of extensive inhibitor concentrations (Figure 11) due to its remarkable RNH1 insensitivity (Figure 12). The combination of GGRR and QG mutations aimed to join increased enzymatic activity and the inhibition resistance. As mentioned above, the inhibition susceptibility of H22-Ang GGRR/QG_{mut} was found to be similar to the wild type variant (Figure 12) as confirmed by MD simulations (Figure 19). The RNH1-Ang wild type complex is stabilized by three tight interaction clusters whereas the GGRR exchanges cause a dislocation at cluster II that weakens cluster I and prevents cluster III assembly. This markedly impairs the affinity for RNH1. In Ang GGRR/QG_{mut}, the additional Q117G mutation endows the C-terminus of Ang with an enhanced flexibility and allows it to almost reassemble cluster III. Accordingly, the D116H mutation was introduced into the C-terminus of Ang GGRR/QG_{mut} to exchange a negatively charged aspartic acid by a positively charged histamine (III.3). The altered electrostatic conditions were expected to interfere with the C-terminal readjustment and thus the recovery of cluster III. Indeed, H22-Ang GGRR/QG/DH_{mut} demonstrated a lower inhibition susceptibility than H22-Ang GGRR/QG_{mut} (Figure 24) but it was still inhibited when a critical inhibitor concentration was exceeded while H22-Ang $GGRR_{mut}$ remained active. Nevertheless, it slightly outperformed the *in vitro* cytotoxicity of H22-Ang $GGRR_{mut}$ (Figure 26 and Table 14) most probably due to its higher cleavage activity (Figure 10 and 23). The cytotoxicity of H22-Ang $GGRR_{mut}$ and

H22-Ang GGRR/QG/DH$_{mut}$ were almost similar to such reported for monovalent H22-ETA' on U937 cells and M1 macrophages [20, 51].

The ^{Ang}R5A and ^{Ang}H8A mutations were introduced into H22-Ang GGRR/QG$_{mut}$ to weaken the interactions at cluster I (Table 13) while ^{Ang}G85R/G86R still promote the dislocation at cluster II. However, both variants appeared to be more susceptible towards inhibition than H22-Ang wild type (Figure 24). A weakened but not disrupted cluster I might allow both variants to eradicate the steric incompatibility caused by GGRR and to intensify cluster III interactions. The same applied for H22-Ang GGRR/QG/KQ$_{mut}$ suggesting that the missing interaction of RNH1 and ^{Ang}K40 has a similar effect in combination with the remaining mutations that were already introduced. Unexpectedly, H22-Ang GGRR/QG/RA$_{mut}$, H22-Ang GGRR/QG/HA$_{mut}$ and H22-Ang GGRR/QG/KQ$_{mut}$ still demonstrated a notable *in vitro* cytotoxicity (Table 14).

Although the observed CFP efficacies towards leukemia cells seem variable, they allow making essential conclusions. Independent from CD64 frequency, H22-Ang GGRR$_{mut}$ induced pro-apoptotic effects on all tested leukemia cell preparations with similar efficacy as H22-ETA' (Figure 31 and 32). Furthermore, the fusion protein efficiently eliminated cells that could not be depleted by H22-ETA' (Figure 32, sample E). The phenomenon of ETA resistance was first reported to appear in children with acute lymphoblastic leukemia and is caused by a deletion in the *WDR85* gene [181]. These observations are consistent with a study describing the *ex vivo* efficacy of an inhibitor-resistant Gb variant fused to H22(scFv) on leukemia cells [86]. In contrast to H22-Ang GGRR$_{mut}$, all RNH1-sensitive H22-Ang variants (Figure 12 and 24) mediated only marginal pro-apoptotic effects on cells with moderate CD64 frequency (Figure 31) supporting the significance of inhibition resistance. However, on cells with high CD64 frequency they performed at least similar to H22-ETA' and H22-Ang GGRR$_{mut}$ (Figure 32, samples D and E) indicating a stronger impact of the distinct ribonucleolytic activities (Figure 10 and 23) while the inhibiting effect of RNH1 was less important. These observations are in line with the determined *in vitro* efficacies of H22-Ang GGRR/QG/RA$_{mut}$, H22-Ang GGRR/QG/HA$_{mut}$ and H22-Ang GGRR/QG/KQ$_{mut}$ on HL-60 cells (Table 14) that likewise demonstrate a high CD64 frequency after stimulation (Figure 35). Since RNH1 is continuously expressed and represents 0.01-0.1% of the total eukaryotic protein content [142], a regulatory mechanism is likely (IV.3) that affects the CD64 frequency and the RNH1 activity in common.

IV.2.4 Endowing H22-Ang GGRR$_{mut}$ with CatAd does not increase its potency

Incorporation of the CatAd adapter sequence has previously been described to enhance the *in vitro* efficacy of H22-Ang wild type on U937 cells by 20-fold [69]. However, the cell-specific cytotoxicity of H22-CatAd-Ang GGRR$_{mut}$ on stimulated HL-60 cells did not support this observation since it was not able to outperform H22-Ang GGRR$_{mut}$ (Table 18). This observation might be related to the different target cell lines used for evaluation or the Ang mutant that was selected as effector domain. With respect to its increased positive net charge (IV.1), we assume that Ang GGRR$_{mut}$ has an improved translocation activity across membrane bilayers. This might have the similar effect than the incorporation of the CatAd adapter sequence. Hence, a lacking cooperativity might allow both CFPs to escape endosomes with a similar efficacy. An increased reduction of HL-60 cell viability by the adapter-based fusion protein in comparison to H22-Ang GGRR$_{mut}$ (Figure 33) was compensated by a similar unspecific effect on the CD64-negative L-540cy cell line as revealed by apoptosis assays (data not shown) [8]. On pro-inflammatory macrophages, H22-CatAd-Ang GGRR$_{mut}$ demonstrated an up to 18-fold lower efficacy than H22-Ang GGRR$_{mut}$. This might be triggered by a proteolytic cleavage of CFPs. In a pro-inflammatory environment, macrophages secrete cathepsin B [182] and the culture medium during XTT viability assays was supplemented with IFNγ and LPS thus representing a pro-inflammatory microenvironment [8]. The amino acid sequence of the translocation adapter comprises three adjacent cleavage sites and the first one is specific for cathepsin B [183]. Consequently, a proteolytic cleavage of H22-CatAd-Ang GGRR$_{mut}$ may separate effector domain and scFv before internalization suggesting that CatAd-based CFPs are unfavorable for the targeted elimination of hM1Φ cells. Further experiments are necessary to clarify this issue. In addition, the adapter incorporation was reported to substantially reduce the serum stability of fusion proteins [69] markedly impairing their usability for the treatment of leukemia. No degradation was found for H22-Ang GGRR$_{mut}$ and H22-Ang GGRR/QG/DH$_{mut}$ in human serum for at least 6 h (Figure 28) favoring these fusion proteins for therapeutic application. The immunogenicity of CFPs may also increase with incorporation of a synthetic adapter peptide potentially resulting in unwanted side effects. Thus, the CatAd sequence was not considered as promising in combination with H22 and Ang GGRR$_{mut}$.

IV.3 IFNγ modulates the target cell sensitivity towards H22-Ang variants

The IFNγ-stimulation of U937 cells, HL-60 cells and macrophages is necessary to acquire sensitivity towards H22-based cytotoxic fusion proteins (personal communication with Radoslav Mladenov, Fraunhofer IME, PPD) [93, 184]. Further on, the cytokine affects the CD64 expression [185] which is assumed to correlate with the inhibitory microenvironment in the target cells (IV.2.3). This chapter will figure out cellular effects of the cytokine and discuss feasible consequences for the cytotoxicity of H22-Ang variants.

The target receptor density on the cells markedly affects the CFP efficacy since it limits the amount that can be internalized and finally be delivered into the cytosol. Beyond, a high expression level facilitates the cell targeting and thereby reduces the risk of unspecific binding and off-target cytotoxicity. The treatment of human monocytes and related cell lines such as HL-60, THP-1 and U937 with IFNγ has been described to increase the expression of CD64 up to 10-fold [185, 186]. Indeed, a distinct upregulation could be demonstrated when macrophages were polarized into M1 or when HL-60 cells were stimulated (Figure 34 and 35). The increased appearance of CD64 on target cells directly correlated with an enhanced binding activity of H22-Ang (Figure 36) and thus promoted the internalization efficacy. Nevertheless, despite of a basal CD64 expression macrophages and HL-60 cells remain resistant without IFNγ stimulation [158]. This could recently been explained by different endosomal protease activities found in distinct macrophage subtypes. M2Φ cells demonstrate a strong proteolytic activity in phagosomes suggesting the rapid degradation of internalized CFPs that renders them resistant [93, 187]. In contrast, a low proteolytic activity found in phagosomes of M1 macrophages facilitates the maintenance of CFP integrity. The inactivation of cysteine-specific cathepsin proteases in phagosomes is mediated by reversible oxidation with ROS and strongly depends on the activity of cellular NADPH oxidase [188]. During macrophage polarization with IFNγ and LPS, the oxidase is activated and generates remarkable amounts of ROS. This strongly enhances the antimicrobial activity of the cells and is known as oxidative burst [189, 190]. A similar effect has been demonstrated for HL-60 cells, THP-1 cells and peripheral blood monocytes *in vitro* [191, 192]. Consequently, the IFNγ treatment of target cells not only increases the binding activity of H22-Ang but also reduces the proteolytic CFP degradation and facilitates the delivery of intact effector domains into the cytosol.

Elevated ROS levels also affect the enzymatic activity of Ang inside target cells. The oxygen species can react with lipids, proteins and nucleic acids causing oxidative stress and damage to these macromolecules if not sufficiently removed by antioxidants [193]. One potent cellular antioxidant is the RNH1 inhibitor due to its 32 cysteine residues of which at least 30 residues are in their reduced form [194]. Thus, the protein is highly susceptible to oxidation explaining its essential role for protection of the cellular redox homeostasis [195, 196]. Most importantly, the oxidation efficiently inactivates RNH1 and promotes its degradation [143, 197]. Although it is continuously expressed, the inhibitory environment is expected to be strongly impaired in the presence of increased ROS levels. It can be concluded that the IFNγ stimulation facilitates the Ang-mediated tRNA cleavage via inactivation of RNH1, explaining its description as a "stress-activated" ribonuclease [147]. To support these coherences, the regulatory effect of ROS and IFNγ on the ribonuclease inhibitor was demonstrated. Hydrogen peroxide served as ROS representative and its dose-dependent inactivating effect on RiboLock^{TM} was obvious (Figure 37). Furthermore, it could be shown that the RNH1 content of HL-60 cells can be modulated by the prevalent IFNγ concentration (Figure 39). The cell stimulation, as carried out prior to viability assays (II.9), reduced the inhibitor content in a time-dependent manner and indicated ongoing degradation following oxidation. This is consistent with the reported decrease of RNH1 quantity in mouse embryonic fibroblasts under oxidative stress [125]. Interestingly, the inhibitor content slightly accumulated when HL-60 cells were exposed to 600 U/mL IFNγ. It most probably reflects a cellular stress response allowing to rapidly remove extensive ROS amounts by increasing the allocation of antioxidants. This assumption is supported by the peaked accumulation 18-21 h after IFNγ addition whereas after 24 h a normal inhibitor content was found. The oxidation state of accumulated RNH1 was not investigated but it is most probably inactive due to the shown regulatory coherencies (Figure 37). In a direct comparison, the inhibitor quantity in stimulated HL-60 cells was found to be higher than in M1Φ cells explaining the stronger sensitivity of the latter towards H22-Ang CFPs (Figure 38, Table 12 and 14). While HL-60 cells were only treated with IFNγ for stimulation, macrophages were additionally exposed to LPS (II.9) also inducing ROS [190]. A stronger cooperative stimulation efficacy may correlate with the lower inhibitor quantity in hM1Φ cells. Also cytochrome c represents an important antioxidant if released from the mitochondrial membrane [198]. This is important as positively-charged cytochrome c is efficiently bound by full size tRNA and tiRNA fragments after cytoplasmic

translocation [198]. The masking effect prevents the assembly with apoptotic protease-activating factor 1 (Apaf-1) required for apoptosome formation and activation of the caspase cascade. Oxidized cytochrome c remains unmasked facilitating the apoptosome formation [199]. Beyond, the appearance of ER stress in HL-60 cells and M1Φ cells could be linked to an increased NADPH oxidase activity and elevated ROS levels [200, 201].

At this point, the revealed IFNγ-mediated effects explain some observations. Pizzo *et al.* discovered that oxidative stress induces Ang to localize in the cytoplasm instead of translocating to the nucleus [146]. When Ang is delivered via H22, this abolishes the need to disrupt the NLS sequence since the nuclear import in stimulated HL-60 cells or M1 macrophages is absent or occurs with minor efficiency. H22-Ang $GGRR_{mut}$ was the only CFP that induced considerable pro-apoptotic effects on leukemia cells with low CD64 frequency (Figure 31, Table 17) because accumulated RNH1 was most probably active and inhibited sensitive variants (Figure 12 and 24). In contrast, inhibitor-sensitive H22-Ang variants performed at least similar to H22-Ang $GGRR_{mut}$ on leukemia cells with high CD64 frequency (Figure 32). This most probably reflects substantial RNH1 inactivation in the presence of increased ROS levels allowing sensitive variants to compensate their inhibition susceptibility by an increased ribonucleolytic activity (Figure 10 and 23).

Several Ang-based CFPs have been described to be even cytotoxic in the absence of IFNγ-mediated effects [53, 131-135]. This may have several reasons: First, the target receptor internalization might not be associated with phagocytosis and thus cellular endosomes may present lower proteolytic activities. Second, the target receptor density on the cell surface might be higher and even promote the internalization efficacy. Third, a more efficient CFP delivery facilitates to overcome the intracellular inhibition. Finally, non-phagocytes might exhibit lower RNH1 quantities because they have not to protect themselves against an oxidative burst.

IV.4 Therapeutic applications and the heterogeneity of target cells

It could be pointed out that cellular effects of IFNγ are essential to acquire sensitivity of phagocytic cells towards H22-Ang (IV.3). The *in vivo* polarization of macrophages into M1 takes place after exposure to Th1 helper cell cytokines such as IFNγ and tumor necrosis factor alpha in addition to LPS or endotoxins [202]. Th2 helper cells usually secrete cytokines that

mediate the macrophage polarization into the M2 subtype. Thus, Th helper cells play a crucial role in determining the present macrophage subtype that can be shifted from one into the other depending on the cytokine pattern. This may also have affected *in vitro* experiments as T cells were co-localized in the interphase following density gradient centrifugation and consequently remained in the culture medium while MΦ cells were separated by attachment to the cell culture flasks overnight (II.3.3). According to the composition of Th1/2 cells and donor-specific conditions, they might prime the subtype polarization and thereby affect the efficacy of M1 differentiation. Wermuth *et al.* described the *in vivo* differentiation of monocytes/macrophages as a fluctuating spectrum of polarization states that is constantly and reversibly modified in response to changing micro-environmental conditions [90]. In chronic skin diseases or wounds, M1Φ cells persist as response to local inflammatory conditions and prevent the resolution of inflammation [93]. Their specific elimination using H22-ETA' resolved chronic inflammations *in vivo* and *ex vivo* by shifting the balance towards regulatory M2Φ cells [93]. H22-Ang GGRR$_{mut}$ might represent a promising alternative for the IT because it demonstrates *in vitro* cytotoxicity towards hM1Φ cells (Table 12 and 14) and is expected to be less immunogenic. However, its cytotoxicity has still to be confirmed *in vivo*. Unspecific effects on non-inflammatory macrophages are unlikely since these cells are neither sensitive towards the CFPs, nor are they efficiently targeted due to the lower CD64 expression level in comparison to hM1Φ cells. The ability of local administration on the skin or on chronic wounds, for instance as supplement in ointments, facilitates *in vivo* applications and allows to expose target cells to high CFP concentrations. Pro-inflammatory macrophages are also associated with several neurodegenerative and autoimmune diseases like arthritis and type 1 diabetes [91, 92]. In this context, *in vivo* experiments have to reveal the targeting efficacy of the cells that is most likely low due to the insufficient escape from blood vessels required to reach sites of inflammation. Thus, circulating CD64^{+} leukemia cells in the blood are a more promising target.

The leukemia cells used in this work were not stimulated with IFNγ prior to apoptosis assays. Instead, the cytokine was co-supplied with the fusion proteins (II.10) to support cell sensitivity as reported previously [5, 49, 50, 86]. Since marginal effects are expected due to the limited exposure time, the observed CFP efficacies were most probably defined by the intracellular redox conditions that have already been established *in vivo*. The performed apoptosis assays

indicated a CD64 frequency of at least 30-40% to be required for detectable induction of pro-apoptotic effects within 12 h of incubation (III.5.2). However, the small number and heterogeneity of the specimens allows no detailed conclusions. Additional *ex vivo* studies may reveal critical CD64 frequencies to consider the application of H22-Ang as reasonable. The treatment length of cells during apoptosis assays was limited due to an increased appearance of treatment-independent apoptosis, most probably caused by the deprivation of essential growth factors. A prolonged exposure time *in vivo* might induce more distinct pro-apoptotic effects. The expression of CD64 was found to be absent on AML-M6 cells excluding this subtype from the treatment strategy [103]. Varying expression levels are reported for the subtypes M2, M3, M4 and especially M5 whereas CD64 appears just rarely on AML-M0 and AML-M1 cells. The heterogeneous presence of the receptor suggests the individual determination of CD64 frequencies for each patient. This also applies for CMML cells where varying expression levels of the receptor have been described [104, 105]. The sensitivity of leukemia cells towards H22-Ang might be supported by a systemic co-administration of IFNγ. A similar approach has been carried out to promote the efficacy of a drug against pulmonary tuberculosis and was evaluated in a clinical trial [203]. However, severe side effects reported by the patients lead to termination of the treatment. The impairing effect on the constitution of leukemia patients would have to be investigated. Without additional support for cell sensitization, the treatment efficacy of $CD64^+$ leukemia cells with H22-Ang depends on the cellular redox conditions (IV.3) but also on individual genetic specificities. Leukemia cells are characterized by a substantial genetic heterogeneity whereas usually signaling pathways are deregulated to promote cell survival and resistance towards apoptosis [99]. Apart from manifested mutations and genetic lesions, AML cells were found to be distinguishable into 16 subclasses according to their DNA methylation signatures and further cytogenetic and molecular subgroups [204]. CMML cells and such proceeding into AML are similarly characterized by strong heterogenic genetics. Cytogenetic aberrations were found in 46% and single nucleotide polymorphisms in even 60% of cells from 72 analyzed leukemia patients [106]. Genetic specifications of the used leukemia cells in this work (Table 16) were unknown rendering the prediction of certain CFP performances difficult. Nevertheless, a high CD64 frequency on leukemic cells might promote the specific depletion by H22-Ang in combination with conventional chemotherapy. A substitutive function for chemotherapy is inconsiderable as the therapeutic impact is supposed to be limited to well-defined cellular

conditions. Furthermore, the treatment is restricted to circulating blasts in the blood stream while originating cells in the bone marrow most probably remain unaffected due to the inaccessibility for CFPs. Nevertheless, the low immunogenicity expected for CFPs might allow the administration of high concentrations while causing at most marginal side effects. The maintained CFP stabilities for at least 6 h in human serum (Figure 28) should be sufficient to allow the targeted *in vivo* depletion of leukemia cells as H22(scFv) internalizes within 30 min after binding to CD64 [86].

IV.5 Additional strategies to increase the cytotoxicity of angiogenin

Angiogenin has a double-edged activity since it can induce translational arrest but also protect cells from apoptosis even under oxidative stress conditions [199, 205-210]. These antagonizing properties indicate that Ang has a sensory function. Most probably, it regulates if stress-associated cellular damage can be repaired during proliferative arrest or apoptosis induction is more reasonable to prevent cell transformation. Co-immunoprecipitation studies revealed at least thirteen cytoplasmic interaction partners for Ang besides RNH1 [211]. Some of these proteins are closely associated with cell survival as they are involved in anti-apoptotic signaling pathways. According to the extraordinary inhibitor affinity of Ang [136], an interaction with these proteins is most likely restricted to stress conditions that cause the release from RNH1. Thus, it might prevent the premature induction of apoptosis. A similar activity of wild type Ang as effector domain would impair the cytotoxicity of H22-Ang whereas a failing or at least diminished support of pro-survival pathways by mutants might already increase their potency without modulating RNH1 affinity or enzymatic activity. An inverse correlation is expected regarding the extent of protein modification and the retention of native interaction properties. The notable *in vitro* potency of CFPs generated in the third mutagenesis round (III.3.1, III.3.4, Figure 27) might be supported accordingly as they contain the widest modifications in the enzyme structure. A wide range of tumors overexpress the Ras GTPase-activating-like scaffold protein IQGAP1, which promotes the activation of extracellular-signal-regulated kinases (ERK) and facilitates the sequential activation and propagation of the pro-survival mitogen-activated protein kinase cascade (MAPK) [212, 213]. Activated ERK1/2 inhibits apoptosis upon various stimuli including osmotic stress and hypoxia [214] whereas the absence of IQGAP1 in cardiomyocytes facilitates apoptotic cell

death in response to oxidative stress [213]. Several circumstances suggest that Ang plays a key function in activation of this pro-survival pathway under stress conditions. First, Ang is involved in the stress response of cardiomyocytes [215]. Second, co-immunoprecipitations revealed that Ang interacts with IQGAP1 [211]. Thirdly, angiogenin is known to transiently activate ERK1/2 [216]. Fourthly, stress conditions are supposed to mediate the dissociation of Ang from RNH1 [217] and thus allow the IQGAP1 interaction and ERK 1/2 activation (IV.3). Finally, the MAPK pathway becomes activated in the presence of oxidative stress [218]. It can be assumed that the Ang-IQGAP1 interaction promotes the activation of ERK and the MAPK pathway as soon as Ang is released from RNH1 in the presence of stress-associated ROS generation. Mutants that fail to interact with IQGAP1 might bypass the MAPK pathway activation and consequently induce less pro-survival signaling compared to Ang wild type as CFP effector domain. Angiogenin was also found to interact with the E3 ubiquitin-protein ligase UHRF1 (also known as Mdm2) and the tumor suppressor protein p53 [211, 219]. Under physiological conditions, UHRF1 mediates the rapid degradation of p53 by ubiquitination. Many cancer cells overexpress the ligase to establish anti-apoptotic conditions while its knockdown suppresses cell growth [220]. Under stress conditions, p53 is phosphorylated causing aggravated ubiquitination conditions that facilitate its accumulation. This allows cells to adapt to stress conditions but also activates the expression of cell-cycle inhibitors and pro-apoptotic proteins that mediate proliferation arrest and cell death [219, 221]. Accumulated p53 can directly activate mitochondrial Bax for membrane permeabilization, cytochrome c release and apoptosis induction [222]. Sadagopan *et al.* recently proposed Ang to promote the ubiquitination of p53 [219]. This is conceivable by masking the phosphorylation site and by stabilizing the interaction of p53 and UHRF1 as a scaffold. Ang mutants with a diminished or lost interaction property for one or even both proteins might fail to support the p53 ubiquitination under stress conditions thus facilitating its cytoplasmic accumulation and associated pro-apoptotic effects. For the targeted disruption of anti-apoptotic signaling properties, natural Ang mutants detected in sporadic and familial forms of the motoneuron disease ALS might reveal promising amino acid exchanges. Angiogenin was found to be required for motoneuron survival under stress conditions and its delivery protects cultured motoneurons against stress-induced injury [209]. The neuroprotective activity includes the positive modulation of the pro-survival PI3K/Akt-1 and ERK1/2 signaling pathways [223, 224]. Wild type Ang protected cultured motoneurons against excitotoxic damage in a PI-3-kinase/Akt

kinase-dependent manner whereas knockdown of the ribonuclease facilitated cell death [224]. Engineered mutants that fail to activate the pathways but still retain enzymatic activity might outperform the cytotoxicity of the wild type accordingly.

It may also be possible that Ang has already signaling functions in the presence of cellular stress. Rny1p (RNY) is a homologue of human Ang and is expressed by the baker's yeast *Saccharomyces cerevisiae*. Its intracellular activity is regulated similar to human Ang since it is stored in vacuoles under physiological conditions but becomes released into the cytosol in the presence of oxidative stress [225]. This resembles to the relocation of Ang from the nucleus into the cytoplasm or even its cytoplasmic release from RNH1 [126]. Both RNases cleave cytosolic tRNA and rRNA to induce translational shutdown as a common stress response. Rny1p mediates cell death regardless from its catalytic activity because also inactive variants are cytotoxic after cytoplasmic translocation. Accordingly, the overexpression of wild type Rny1p or ribonucleolytic inactive variants sensitized cells to rapidly undergo apoptosis during oxidative stress, respectively [225]. This distinguishes Rny1p from other ribonucleases such as onconase, bovine RNase A or human RNase 1, which require ribonucleolytic activity for being cytotoxic [177, 178]. Similar signaling effects for released Rny1p and cytochrome c were considered as well. Due to the obvious similarities of human Ang and Rny1p, pro-apoptotic signaling activities may also apply for Ang after being released from RNH1. The targeted delivery might resemble to the overexpression of Rny1p variants. Even for onconase, tRNA cleavage-independent pro-apoptotic effects are supposed that bypass Bax and cytochrome c [226].

To summarize, the activation of anti-apoptotic signaling pathways by wild type Ang might antagonize with apoptosis induction. Preventing intracellular protein interactions of Ang by mutagenesis might represent a working point to increase its cytotoxic potential as CFP effector domain.

V Outlook

In this work, several variants of the human ribonuclease Ang were generated and fused to the CD64-specific H22(scFv) as effector domain. The characterization of these fusion proteins revealed several regulatory specificities resulting from the intrinsic combination of H22 and Ang. Those modulate the impact of individual enzymatic properties on the cytotoxicity of the ribonuclease making the evaluation of mutational effects difficult. It could be shown that an increased substrate cleavage activity promotes the pro-apoptotic efficacy of Ang and especially the insensitivity towards RNH1 equips variants with remarkable cytotoxicity (III.7, Table 19). However, cellular conditions can be established by IFNγ that already allow inhibitor-sensitive H22-Ang variants to induce distinct pro-apoptotic effects (IV.3). Since the inconsistent inhibitory microenvironment is at least a specific feature of phagocytic cells, the generated effector domains should be evaluated in fusion to another binding moiety to redefine mutational consequences. The enforced cytoplasmic retention of Ang could still be promising in combination with other binding moieties as the redox conditions might not already prevent the nuclear translocation (IV.2.2 and IV.3). The anti-CD30 scFv Ki-4 may be favorable because the fusion protein Ki-4(scFv)-Ang wild type demonstrated *in vitro* cytotoxicity [53, 132].

H22-Ang $GGRR_{mut}$ was considered to be resistant towards RNH1 due to its 'almost retained' enzymatic activity (~80%) in the presence of the highest tested RiboLock™ concentration in Figure 12. However, the inactivation of RNH1 might be strongly reduced in other target cell types than phagocytes even allowing the inhibition of Ang $GGRR_{mut}$ under these conditions. A dimeric variant might be generated as effector domain what has already been carried out using RNase A and HPR [73, 227]. According to the inhibitor resistance of a natively dimeric isoform of BS-RNase [228], corresponding amino acids were exchanged in RNase A and HPR to promote dimerization and protein folding into a RNH1-incompatible conformation while maintaining enzymatic activity. Since an increased substrate cleavage activity of Ang enhanced its cytotoxicity (IV.2.3), a dimeric variant of Ang Q117G might be promising. In this context, the increased immunogenicity has to be considered carefully as the extensive modification of the native enzyme conformation might strongly impair the usability for therapeutic applications. MD simulations might be used to predict novel mutations disrupting the Ang-RNH1 interaction surface. This can be achieved with minor changes of the enzymes structure, similar to ^{Ang}G85R/G86R. The immunogenicity of this variant is expected to be moderate due

to the primarily native structure but it is still equipped with an almost resistance against RNH1. Thus, *in silico* technology might provide an essential support.

In contrast to other ribonuclease-based effector domains such as RNase A, HPR, EDN or onconase, particular activities have to be considered for Ang due to its pro- and anti-apoptotic properties. The supposed promotion of pro-survival signaling pathways, as discussed in IV.5, might be circumvented by mutagenesis whereas promising amino acid exchanges might reveal from already characterized ALS mutants or MD simulations studies. If this strategy increases the cytotoxicity of Ang wild type, corresponding mutations might be joined with ^{Ang}G85R/G86R or ^{Ang}Q117G to aim cooperativity.

The *in vivo* efficacy of CFPs is essential for therapeutic applications suggesting competitive treatment studies with H22-Ang wild type and H22-Ang GGRR$_{mut}$. Mice with chronic skin diseases or wounds, or even severe combined immunodeficient (SCID) mice as a disseminated leukemia model are promising and were described previously [23, 93]. The competitive use of H22-ETA' as internal reference might allow estimating the treatment potential of the CFPs. To consider the ongoing development of ITs, a deimmunized variant of ETA' should be used in fusion to H22.

Finally, the expression yields have to be increased markedly to accomplish *in vivo* studies. HEK293T cells might be adapted to a serum-free expression strategy. This promises a higher CFP purify and circumvents the need of washing which often leads to substantial target protein loss. Optimized culture media might also be used to increase the productivity of the cells. Alternative expression systems, such as bacteria or CHO cells, may be promising as well. Bacteria allow to rapidly produce remarkable protein amounts but usually several purification steps are necessary to remove host proteins and endotoxins. Nevertheless, it might be promising since Ang is not posttranslationally modified. The highest yields are expected from stable expressing CHO cells. Even their generation is a time- and cost-consuming process, it may be reasonable for H22-Ang wild type and H22-Ang GGRR$_{mut}$ to generate sufficient amounts for competitive *in vivo* experiments and further preclinical trials.

VI List of references

[1] Cremer C, Vierbuchen T, Hein L, Fischer R, Barth S, Nachreiner T: Angiogenin mutants as novel effector molecules for the generation of fusion proteins with increased cytotoxic potential. *J Immunother* 2015, 38:85-95.

[2] Cremer C, Braun H, Mladenov R, Schenke L, Cong X, Jost E, Brummendorf TH, Fischer R, Carloni P, Barth S, Nachreiner T: Novel angiogenin mutants with increased cytotoxicity enhance the depletion of pro-inflammatory macrophages and leukemia cells *ex vivo*. *Cancer Immunol Immunother* 2015, 64:1575-86.

[3] Cremer C, Hehmann-Titt G, Schiffer S, Melmer G, Carloni P, Barth S, Nachreiner T: Engineered versions of granzyme B and angiogenin overcome intrinsic resistance to apoptosis mediated by human cytolytic fusion proteins. In: Verma RS, Bonavida B (eds.) Resistance to immunotoxins in cancer therapy. *Springer International Publishing Switzerland* 2015, pp. 185-219.

[4] Cong X, Cremer C, Nachreiner T, Barth S, Carloni P: Engineered human angiogenin mutations in the placental ribonuclease inhibitor complex for anticancer therapy: Insights from enhanced sampling simulations. *Protein Sci* 2016, 25:1451-60.

[5] Mladenov R, Hristodorov D, Cremer C, Hein L, Kreutzer F, Stroisch T, Niesen J, Brehm H, Blume T, Brummendorf TH, Jost E, Thepen T, Fischer R, Stockmeyer B, Barth S, Stein C: The Fc-alpha receptor is a new target antigen for immunotherapy of myeloid leukemia. *Int J Cancer* 2015, 137:2729-38.

[6] Mladenov R, Hristodorov D, Cremer C, Gresch G, Grieger E, Schenke L, Klose D, Amoury M, Woitok M, Jost E, Brummendorf TH, Fendel R, Fischer R, Stein C, Thepen T, Barth S: CD64-directed microtubule associated protein tau kills leukemic blasts *ex vivo*. *Oncotarget* 2016, 7:67166-74.

[7] Neß M: Evaluierung von ABT-737 als Additiv zur Verbesserung der Effizienz zytolytischer Fusionsproteine. (Master's thesis), RWTH Aachen University, Germany 2013.

[8] Vierbuchen T: *In vitro* characterization of novel cytolytic fusion proteins and evaluation of a synergistic treatment strategy. (Master's thesis), RWTH Aachen University, Germany 2014.

[9] Braun H: Generation and characterization of novel recombinant angiogenin mutants with improved cytotoxic potential. (Master's thesis), RWTH Aachen University, Germany 2015.

[10] Risberg K, Fodstad O, Andersson Y: Immunotoxins: a promising treatment modality for metastatic melanoma? *Ochsner J* 2010, 10:193-9.

[11] Shan L, Liu Y, Wang P: Recombinant immunotoxin therapy of solid tumors: challenges and strategies. *J Basic Clin Med* 2013, 2:1-6.

[12] Kreitman RJ: Recombinant immunotoxins containing truncated bacterial toxins for the treatment of hematologic malignancies. *BioDrugs* 2009, 23:1-13.

[13] Pastan I, Hassan R, FitzGerald DJ, Kreitman RJ: Immunotoxin treatment of cancer. *Annu Rev Med* 2007, 58:221-37.

[14] Yokota T, Milenic DE, Whitlow M, Schlom J: Rapid tumor penetration of a single-chain Fv and comparison with other immunoglobulin forms. *Cancer Res* 1992, 52:3402-8.

[15] Ahmad ZA, Yeap SK, Ali AM, Ho WY, Alitheen NB, Hamid M: scFv antibody: principles and clinical application. *Clin Dev Immunol* 2012, 2012:980250.

[16] Zhong RK, van de Winkel JG, Thepen T, Schultz LD, Ball ED: Cytotoxicity of anti-CD64-ricin A chain immunotoxin against human acute myeloid leukemia cells *in vitro* and in SCID mice. *J Hematother Stem Cell Res* 2001, 10:95-105.

[17] Tur MK, Huhn M, Thepen T, Stocker M, Krohn R, Vogel S, Jost E, Osieka R, van de Winkel JG, Fischer R, Finnern R, Barth S: Recombinant CD64-specific single chain immunotoxin exhibits specific cytotoxicity against acute myeloid leukemia cells. *Cancer Res* 2003, 63:8414-9.

[18] Tur MK, Huhn M, Jost E, Thepen T, Brummendorf TH, Barth S: *In vivo* efficacy of the recombinant anti-CD64 immunotoxin H22(scFv)-ETA' in a human acute myeloid leukemia xenograft tumor model. *Int J Cancer* 2011, 129:1277-82.

[19] Singh R, Samant U, Hyland S, Chaudhari PR, Wels WS, Bandyopadhyay D: Target-specific cytotoxic activity of recombinant immunotoxin scFv(MUC1)-ETA' on breast carcinoma cells and primary breast tumors. *Mol Cancer Ther* 2007, 6:562-9.

[20] Ribbert T, Thepen T, Tur MK, Fischer R, Huhn M, Barth S: Recombinant, ETA'-based CD64 immunotoxins: improved efficacy by increased valency, both *in vitro* and *in vivo*

in a chronic cutaneous inflammation model in human CD64 transgenic mice. *Br J Dermatol* 2010, 163:279-86.

[21] Klimka A, Barth S, Matthey B, Roovers RC, Lemke H, Hansen H, Arends JW, Diehl V, Hoogenboom HR, Engert A: An anti-CD30 single-chain Fv selected by phage display and fused to *Pseudomonas* exotoxin A (Ki-4(scFv)-ETA') is a potent immunotoxin against a Hodgkin-derived cell line. *Br J Cancer* 1999, 80:1214-22.

[22] Bruell D, Bruns CJ, Yezhelyev M, Huhn M, Muller J, Ischenko I, Fischer R, Finnern R, Jauch KW, Barth S: Recombinant anti-EGFR immunotoxin 425(scFv)-ETA' demonstrates anti-tumor activity against disseminated human pancreatic cancer in nude mice. *Int J Mol Med* 2005, 15:305-13.

[23] Barth S, Huhn M, Matthey B, Tawadros S, Schnell R, Schinkothe T, Diehl V, Engert A: Ki-4(scFv)-ETA', a new recombinant anti-CD30 immunotoxin with highly specific cytotoxic activity against disseminated Hodgkin tumors in SCID mice. *Blood* 2000, 95:3909-14.

[24] Wang D, Li Q, Hudson W, Berven E, Uckun F, Kersey JH: Generation and characterization of an anti-CD19 single-chain Fv immunotoxin composed of C-terminal disulfide-linked dgRTA. *Bioconjug Chem* 1997, 8:878-84.

[25] Niesen J, Stein C, Brehm H, Hehmann-Titt G, Fendel R, Melmer G, Fischer R, Barth S: Novel EGFR-specific immunotoxins based on panitumumab and cetuximab show *in vitro* and *ex vivo* activity against different tumor entities. *J Cancer Res Clin Oncol* 2015, 141:2079-95.

[26] Tsutsumi Y, Onda M, Nagata S, Lee B, Kreitman RJ, Pastan I: Site-specific chemical modification with polyethylene glycol of recombinant immunotoxin anti-Tac(Fv)-PE38 (LMB-2) improves antitumor activity and reduces animal toxicity and immunogenicity. *Proc Natl Acad Sci USA* 2000, 97:8548-53.

[27] Siegall CB, Liggitt D, Chace D, Tepper MA, Fell HP: Prevention of immunotoxin-mediated vascular leak syndrome in rats with retention of antitumor activity. *Proc Natl Acad Sci USA* 1994, 91:9514-8.

[28] Wayne AS, Fitzgerald DJ, Kreitman RJ, Pastan I: Immunotoxins for leukemia. *Blood* 2014, 123:2470-7.

[29] Smallshaw JE, Ghetie V, Rizo J, Fulmer JR, Trahan LL, Ghetie MA, Vitetta ES: Genetic engineering of an immunotoxin to eliminate pulmonary vascular leak in mice. *Nat Biotechnol* 2003, 21:387-91.

[30] Weldon JE, Xiang L, Zhang J, Beers R, Walker DA, Onda M, Hassan R, Pastan I: A recombinant immunotoxin against the tumor-associated antigen mesothelin reengineered for high activity, low off-target toxicity, and reduced antigenicity. *Mol Cancer Ther* 2013, 12:48-57.

[31] Mossoba ME, Onda M, Taylor J, Massey PR, Treadwell S, Sharon E, Hassan R, Pastan I, Fowler DH: Pentostatin plus cyclophosphamide safely and effectively prevents immunotoxin immunogenicity in murine hosts. *Clin Cancer Res* 2011, 17:3697-705.

[32] Pai LH, FitzGerald DJ, Tepper M, Schacter B, Spitalny G, Pastan I: Inhibition of antibody response to *Pseudomonas* exotoxin and an immunotoxin containing *Pseudomonas* exotoxin by 15-deoxyspergualin in mice. *Cancer Res* 1990, 50:7750-3.

[33] Skrlj N, Vranac T, Popovic M, Curin Serbec V, Dolinar M: Specific binding of the pathogenic prion isoform: development and characterization of a humanized single-chain variable antibody fragment. *PLoS One* 2011, 6:e15783.

[34] Mazor R, Vassall AN, Eberle JA, Beers R, Weldon JE, Venzon DJ, Tsang KY, Benhar I, Pastan I: Identification and elimination of an immunodominant T cell epitope in recombinant immunotoxins based on *Pseudomonas* exotoxin A. *Proc Natl Acad Sci USA* 2012, 109:e3597-603.

[35] Mazor R, Eberle JA, Hu X, Vassall AN, Onda M, Beers R, Lee EC, Kreitman RJ, Lee B, Baker D, King C, Hassan R, Benhar I, Pastan I: Recombinant immunotoxin for cancer treatment with low immunogenicity by identification and silencing of human T cell epitopes. *Proc Natl Acad Sci USA* 2014, 111:8571-6.

[36] Onda M, Nagata S, FitzGerald DJ, Beers R, Fisher RJ, Vincent JJ, Lee B, Nakamura M, Hwang J, Kreitman RJ, Hassan R, Pastan I: Characterization of the B cell epitopes associated with a truncated form of *Pseudomonas* exotoxin (PE38) used to make immunotoxins for the treatment of cancer patients. *J Immunol* 2006, 177:8822-34.

[37] Pavlinkova G, Colcher D, Booth BJ, Goel A, Wittel UA, Batra SK: Effects of humanization and gene shuffling on immunogenicity and antigen binding of anti-TAG-72 single-chain Fvs. *Int J Cancer* 2001, 94:717-26.

[38] Nachreiner T, Kampmeier F, Thepen T, Fischer R, Barth S, Stocker M: Depletion of autoreactive B lymphocytes by a recombinant myelin oligodendrocyte glycoprotein-based immunotoxin. *J Neuroimmunol* 2008, 195:28-35.

[39] Kreitman RJ, Wilson WH, Bergeron K, Raggio M, Stetler-Stevenson M, FitzGerald DJ, Pastan I: Efficacy of the anti-CD22 recombinant immunotoxin BL22 in chemotherapy-resistant hairy-cell leukemia. *N Engl J Med* 2001, 345:241-7.

[40] Schnell R, Borchmann P, Staak JO, Schindler J, Ghetie V, Vitetta ES, Engert A: Clinical evaluation of ricin A-chain immunotoxins in patients with Hodgkin's lymphoma. *Ann Oncol* 2003, 14:729-36.

[41] Kreitman RJ, Wilson WH, White JD, Stetler-Stevenson M, Jaffe ES, Giardina S, Waldmann TA, Pastan I: Phase I trial of recombinant immunotoxin anti-Tac(Fv)-PE38 (LMB-2) in patients with hematologic malignancies. *J Clin Oncol* 2000, 18:1622-36.

[42] Mathew M, Verma RS: Humanized immunotoxins: a new generation of immunotoxins for targeted cancer therapy. *Cancer Sci* 2009, 100:1359-65.

[43] De Poot SA, Lai KW, van der Wal L, Plasman K, Van Damme P, Porter AC, Gevaert K, Bovenschen N: Granzyme M targets topoisomerase II alpha to trigger cell cycle arrest and caspase-dependent apoptosis. *Cell Death Differ* 2014, 21:416-26.

[44] Waterhouse NJ, Sedelies KA, Browne KA, Wowk ME, Newbold A, Sutton VR, Clarke CJ, Oliaro J, Lindemann RK, Bird PI, Johnstone RW, Trapani JA: A central role for Bid in granzyme B-induced apoptosis. *J Biol Chem* 2005, 280:4476-82.

[45] Ivanov P, Emara MM, Villen J, Gygi SP, Anderson P: Angiogenin-induced tRNA fragments inhibit translation initiation. *Mol Cell* 2011, 43:613-23.

[46] Tubert P, Rodriguez M, Ribo M, Benito A, Vilanova M: The nuclear transport capacity of a human-pancreatic ribonuclease variant is critical for its cytotoxicity. *Invest New Drugs* 2011, 29:811-7.

[47] Lin Y, Hupp TR, Stevens C: Death-associated protein kinase (DAPK) and signal transduction: additional roles beyond cell death. *FEBS J* 2010, 277:48-57.

[48] Zhao J, Zhang LH, Jia LT, Zhang L, Xu YM, Wang Z, Yu CJ, Peng WD, Wen WH, Wang CJ, Chen SY, Yang AG: Secreted antibody/granzyme B fusion protein stimulates selective killing of HER2-overexpressing tumor cells. *J Biol Chem* 2004, 279:21343-8.

[49] Stahnke B, Thepen T, Stocker M, Rosinke R, Jost E, Fischer R, Tur MK, Barth S: Granzyme B-H22(scFv), a human immunotoxin targeting CD64 in acute myeloid leukemia of monocytic subtypes. *Mol Cancer Ther* 2008, 7:2924-32.

[50] Schiffer S, Letzian S, Jost E, Mladenov R, Hristodorov D, Huhn M, Fischer R, Barth S, Thepen T: Granzyme M as a novel effector molecule for human cytolytic fusion proteins: CD64-specific cytotoxicity of Gm-H22(scFv) against leukemic cells. *Cancer Lett* 2013, 341:178-85.

[51] Schiffer S, Hristodorov D, Mladenov R, Aslanian E, Huhn M, Fischer R, Barth S, Thepen T: Species-dependent functionality of the human cytolytic fusion proteins granzyme B-H22(scFv) and H22(scFv)-angiogenin in macrophages. *Antibodies* 2013, 2:9-18.

[52] Menzel C, Schirrmann T, Konthur Z, Jostock T, Dubel S: Human antibody RNase fusion protein targeting $CD30^+$ lymphomas. *Blood* 2008, 111:3830-7.

[53] Huhn M, Sasse S, Tur MK, Matthey B, Schinkothe T, Rybak SM, Barth S, Engert A: Human angiogenin fused to human CD30 ligand (Ang-CD30L) exhibits specific cytotoxicity against CD30-positive lymphoma. *Cancer Res* 2001, 61:8737-42.

[54] Hristodorov D, Amoury M, Mladenov R, Niesen J, Arens K, Berges N, Hein L, Di Fiore S, Pham AT, Huhn M, Helfrich W, Fischer R, Thepen T, Barth S: EpCAM-selective elimination of carcinoma cells by a novel MAP-based cytolytic fusion protein. *Mol Cancer Ther* 2014, 13:2194-202.

[55] De Lorenzo C, Di Malta C, Cali G, Troise F, Nitsch L, D'Alessio G: Intracellular route and mechanism of action of ERB-hRNase, a human anti-ErbB2 anticancer immunoagent. *FEBS Lett* 2007, 581:296-300.

[56] Braschoss S, Hirsch B, Dubel S, Stein H, Durkop H: New anti-CD30 human pancreatic ribonuclease-based immunotoxin reveals strong and specific cytotoxicity *in vivo*. *Leuk Lymphoma* 2007, 48:1179-86.

[57] Hristodorov D, Nordlohne J, Mladenov R, Huhn M, Fischer R, Thepen T, Barth S: Human microtubule-associated protein tau mediates targeted killing of $CD30^+$ lymphoma cells *in vitro* and inhibits tumour growth *in vivo*. *Br J Haematol* 2014, 164:251-7.

[58] Hristodorov D, Mladenov R, Pardo A, Pham AT, Huhn M, Fischer R, Thepen T, Barth S: Microtubule-associated protein tau facilitates the targeted killing of

proliferating cancer cells *in vitro* and in a xenograft mouse tumour model *in vivo*. *Br J Cancer* 2013, 109:1570-8.

[59] Brehm H, Hristodorov D, Pardo A, Mladenov R, Niesen J, Fischer R, Tur MK, Barth S: Targeted killing of rhabdomyosarcoma cells by a MAP-based human cytolytic fusion protein. *Cancer Lett* 2015, 365:149-55.

[60] Newton DL, Nicholls PJ, Rybak SM, Youle RJ: Expression and characterization of recombinant human eosinophil-derived neurotoxin and eosinophil-derived neurotoxin-anti-transferrin receptor sFv. *J Biol Chem* 1994, 269:26739-45.

[61] Antignani A, Fitzgerald D: Immunotoxins: the role of the toxin. *Toxins (Basel)* 2013, 5:1486-502.

[62] Berges N, Hehmann-Titt G, Hristodorov D, Melmer G, Thepen T, Barth S: Human cytolytic fusion proteins: modified versions of human granzyme B and angiogenin have the potential to replace bacterial toxins in targeted therapies against $CD64^+$ diseases. *Antibodies* 2014, 3:92-115.

[63] Hehmann-Titt G, Schiffer S, Berges N, Melmer G, Barth S: Improving the therapeutic potential of human granzyme B for targeted cancer therapy. *Antibodies* 2013, 2:19-49.

[64] Rutkoski TJ, Raines RT: Evasion of ribonuclease inhibitor as a determinant of ribonuclease cytotoxicity. *Curr Pharm Biotechnol* 2008, 9:185-9.

[65] Bechara C, Sagan S: Cell-penetrating peptides: 20 years later, where do we stand? *FEBS Lett* 2013, 587:1693-702.

[66] Mohammed AF, Abdul-Wahid A, Huang EH, Bolewska-Pedyczak E, Cydzik M, Broad AE, Gariepy J: The *Pseudomonas aeruginosa* exotoxin A translocation domain facilitates the routing of CPP-protein cargos to the cytosol of eukaryotic cells. *J Control Release* 2012, 164:58-64.

[67] Erlwein O, Wels W, Schnierle BS: Chimeric ecotropic MLV envelope proteins that carry EGF receptor-specific ligands and the *Pseudomonas* exotoxin A translocation domain to target gene transfer to human cancer cells. *Virology* 2002, 302:333-41.

[68] Zhang L, Zhao J, Wang T, Yu CJ, Jia LT, Duan YY, Yao LB, Chen SY, Yang AG: Her2-targeting recombinant protein with truncated *Pseudomonas* exotoxin A translocation domain efficiently kills breast cancer cells. *Cancer Biol Ther* 2008, 7:1226-31.

[69] Hetzel C, Bachran C, Fischer R, Fuchs H, Barth S, Stocker M: Small cleavable adapters enhance the specific cytotoxicity of a humanized immunotoxin directed against CD64-positive cells. *J Immunother* 2008, 31:370-6.

[70] Suzuki M, Saxena SK, Boix E, Prill RJ, Vasandani VM, Ladner JE, Sung C, Youle RJ: Engineering receptor-mediated cytotoxicity into human ribonucleases by steric blockade of inhibitor interaction. *Nat Biotechnol* 1999, 17:265-70.

[71] Schiffer S, Hansen HP, Hehmann-Titt G, Huhn M, Fischer R, Barth S, Thepen T: Efficacy of an adapted granzyme B-based anti-CD30 cytolytic fusion protein against PI-9-positive classical Hodgkin lymphoma cells in a murine model. *Blood Cancer J* 2013, 3:e106.

[72] Riccio G, D'Avino C, Raines RT, De Lorenzo C: A novel fully human antitumor immunoRNase resistant to the RNase inhibitor. *Protein Eng Des Sel* 2013, 26:243-8.

[73] Piccoli R, Di Gaetano S, De Lorenzo C, Grauso M, Monaco C, Spalletti-Cernia D, Laccetti P, Cinatl J, Matousek J, D'Alessio G: A dimeric mutant of human pancreatic ribonuclease with selective cytotoxicity toward malignant cells. *Proc Natl Acad Sci USA* 1999, 96:7768-73.

[74] Losasso V, Schiffer S, Barth S, Carloni P: Design of human granzyme B variants resistant to serpin B9. *Proteins* 2012, 80:2514-22.

[75] Leland PA, Staniszewski KE, Kim BM, Raines RT: Endowing human pancreatic ribonuclease with toxicity for cancer cells. *J Biol Chem* 2001, 276:43095-102.

[76] Radaev S, Sun P: Recognition of immunoglobulins by Fcγ receptors. *Mol Immunol* 2002, 38:1073-83.

[77] Nimmerjahn F, Ravetch JV: Fcγ receptors: old friends and new family members. *Immunity* 2006, 24:19-28.

[78] Mancardi DA, Albanesi M, Jonsson F, Iannascoli B, Van Rooijen N, Kang X, England P, Daeron M, Bruhns P: The high-affinity human IgG receptor FcγRI (CD64) promotes IgG-mediated inflammation, anaphylaxis, and antitumor immunotherapy. *Blood* 2013, 121:1563-73.

[79] Guyre CA, Keler T, Swink SL, Vitale LA, Graziano RF, Fanger MW: Receptor modulation by FcγRI-specific fusion proteins is dependent on receptor number and modified by IgG. *J Immunol* 2001, 167:6303-11.

[80] Dupre-Crochet S, Erard M, Nubetae O: ROS production in phagocytes: why, when, and where? *J Leukoc Biol* 2013, 94:657-70.

[81] Harrison PT, Davis W, Norman JC, Hockaday AR, Allen JM: Binding of monomeric immunoglobulin G triggers FcγRI-mediated endocytosis. *J Biol Chem* 1994, 269:24396-402.

[82] Van Vugt MJ, Kleijmeer MJ, Keler T, Zeelenberg I, van Dijk MA, Leusen JHW, Geuze HJ, van de Winkel JGJ: The FcγRIa (CD64) ligand binding chain triggers major histocompatibility complex class II antigen presentation independently of its associated FcR γ-chain. *Blood* 1999, 94:808-17.

[83] Guyre PM, Graziano RF, Vance BA, Morganelli PM, Fanger MW: Monoclonal antibodies that bind to distinct epitopes on FcγRI are able to trigger receptor function. *J Immunol* 1989, 143:1650-5.

[84] Graziano RF, Tempest PR, White P, Keler T, Deo Y, Ghebremariam H, Coleman K, Pfefferkorn LC, Fanger MW, Guyre PM: Construction and characterization of a humanized anti-γ-Ig receptor type I (FcγRI) monoclonal antibody. *J Immunol* 1995, 155:4996-5002.

[85] De Kruif J, Tijmensen M, Goldsein J, Logtenberg T: Recombinant lipid-tagged antibody fragments as functional cell-surface receptors. *Nat Med* 2000, 6:223-7.

[86] Schiffer S, Rosinke R, Jost E, Hehmann-Titt G, Huhn M, Melmer G, Barth S, Thepen T: Targeted *ex vivo* reduction of CD64-positive monocytes in chronic myelomonocytic leukemia and acute myelomonocytic leukemia using human granzyme B-based cytolytic fusion proteins. *Int J Cancer* 2014, 135:1497-508.

[87] Passegue E, Jamieson CH, Ailles LE, Weissman IL: Normal and leukemic hematopoiesis: are leukemias a stem cell disorder or a reacquisition of stem cell characteristics? *Proc Natl Acad Sci USA* 2003, 100 Suppl 1:11842-9.

[88] Yang J, Zhang L, Yu C, Yang XF, Wang H: Monocyte and macrophage differentiation: circulation inflammatory monocyte as biomarker for inflammatory diseases. *Biomark Res* 2014, 2:1.

[89] Zhang F, Liu H, Jiang G, Wang H, Wang X, Wang H, Fang R, Cai S, Du J: Changes in the proteomic profile during the differential polarization status of the human monocyte-derived macrophage THP-1 cell line. *Proteomics* 2015, 15:773-86.

[90] Wermuth PJ, Jimenez SA: The significance of macrophage polarization subtypes for animal models of tissue fibrosis and human fibrotic diseases. *Clin Transl Med* 2015, 4:2.

[91] Jou IM, Lin CF, Tsai KJ, Wei SJ: Macrophage-mediated inflammatory disorders. *Mediat Inflamm* 2013, 2013:316482.

[92] Espinoza-Jimenez A, Peon AN, Terrazas LI: Alternatively activated macrophages in types 1 and 2 diabetes. *Mediat Inflamm* 2012, 2012:815953.

[93] Hristodorov D, Mladenov R, von Felbert V, Huhn M, Fischer R, Barth S, Thepen T: Targeting CD64 mediates elimination of M1 but not M2 macrophages *in vitro* and in cutaneous inflammation in mice and patient biopsies. *MAbs* 2015, 7:853-62.

[94] Van Vuuren AJ, van Roon JA, Walraven V, Stuij I, Harmsen MC, McLaughlin PM, van de Winkel JG, Thepen T: CD64-directed immunotoxin inhibits arthritis in a novel CD64 transgenic rat model. *J Immunol* 2006, 176:5833-8.

[95] Lavin Y, Winter D, Blecher-Gonen R, David E, Keren-Shaul H, Merad M, Jung S, Amit I: Tissue-resident macrophage enhancer landscapes are shaped by the local microenvironment. *Cell* 2014, 159:1312-26.

[96] Hoffmann JJ: Neutrophil CD64: a diagnostic marker for infection and sepsis. *Clin Chem Lab Med* 2009, 47:903-16.

[97] Wright HL, Moots RJ, Bucknall RC, Edwards SW: Neutrophil function in inflammation and inflammatory diseases. *Rheumatology (Oxford)* 2010, 49:1618-31.

[98] Fathi AT, Karp JE: New agents in acute myeloid leukemia: beyond cytarabine and anthracyclines. *Curr Oncol Rep* 2009, 11:346-52.

[99] Scholl C, Gilliland DG, Frohling S: Deregulation of signaling pathways in acute myeloid leukemia. *Semin Oncol* 2008, 35:336-45.

[100] Dohner K, Dohner H: Molecular characterization of acute myeloid leukemia. *Haematologica* 2008, 93:976-82.

[101] Walter RB, Othus M, Burnett AK, Lowenberg B, Kantarjian HM, Ossenkoppele GJ, Hills RK, van Montfort KGM, Ravandi F, Evans A, Pierce SR, Appelbaum FR, Estey EH: Significance of FAB subclassification of "acute myeloid leukemia, NOS" in the 2008 WHO classification: analysis of 5848 newly diagnosed patients. *Blood* 2013, 121:2424-31.

[102] Duchayne E, Demur C, Rubie H, Robert A, Dastugue N: Diagnosis of acute basophilic leukemia. *Leuk Lymphoma* 1999, 32:269-78.

[103] Dunphy CH, Tang W: The value of CD64 expression in distinguishing acute myeloid leukemia with monocytic differentiation from other subtypes of acute myeloid leukemia: a flow cytometric analysis of 64 cases. *Arch Pathol Lab Med* 2007, 131:748-54.

[104] Bacher U, Haferlach T, Schnittger S, Kreipe H, Kroger N: Recent advances in diagnosis, molecular pathology and therapy of chronic myelomonocytic leukaemia. *Br J Haematol* 2011, 153:149-67.

[105] Santos IM, Franzon CM, Koga AH: Laboratory diagnosis of chronic myelomonocytic leukemia and progression to acute leukemia in association with chronic lymphocytic leukemia: morphological features and immunophenotypic profile. *Rev Bras Hematol Hemoter* 2012, 34:242-4.

[106] Jankowska AM, Makishima H, Tiu RV, Szpurka H, Huang Y, Traina F, Visconte V, Sugimoto Y, Prince C, O'Keefe C, Hsi ED, List A, Sekeres MA, Rao A, McDevitt MA, Maciejewski JP: Mutational spectrum analysis of chronic myelomonocytic leukemia includes genes associated with epigenetic regulation: UTX, EZH2, and DNMT3A. *Blood* 2011, 118:3932-41.

[107] Menendez P, del Canizo MC, Orfao A: Immunophenotypic characteristics of PB-mobilised $CD34^+$ hematopoietic progenitor cells. *J Biol Regul Homeost Agents* 2001, 15:53-61.

[108] Strydom DJ, Fett JW, Lobb RR, Alderman EM, Bethune JL, Riordan JF, Vallee BL: Amino acid sequence of human tumor derived angiogenin. *Biochemistry* 1985, 24:5486-94.

[109] Pyatibratov MG, Tolkatchev D, Plamondon J, Xu P, Ni F, Kostyukova AS: Binding of human angiogenin inhibits actin polymerization. *Arch Biochem Biophys* 2010, 495:74-81.

[110] Miyake M, Goodison S, Lawton A, Gomes-Giacoia E, Rosser CJ: Angiogenin promotes tumoral growth and angiogenesis by regulating matrix metallopeptidase-2 expression via the ERK1/2 pathway. *Oncogene* 2015, 34:890-1.

[111] Skorupa A, King MA, Aparicio IM, Dussmann H, Coughlan K, Breen B, Kieran D, Concannon CG, Marin P, Prehn JH: Motoneurons secrete angiogenin to induce RNA cleavage in astroglia. *J Neurosci* 2012, 32:5024-38.

[112] Gao X, Xu Z: Mechanisms of action of angiogenin. *Acta Biochim Biophys Sin (Shanghai)* 2008, 40:619-24.

[113] Kulka M, Fukuishi N, Metcalfe DD: Human mast cells synthesize and release angiogenin, a member of the ribonuclease A (RNase A) superfamily. *J Leukoc Biol* 2009, 86:1217-26.

[114] Liote F, Champy R, Moenner M, Boval-Boizard B, Badet J: Elevated angiogenin levels in synovial fluid from patients with inflammatory arthritis and secretion of angiogenin by cultured synovial fibroblasts. *Clin Exp Immunol* 2003, 132:163-8.

[115] Kishikawa H, Wu D, Hu GF: Targeting angiogenin in therapy of amyotropic lateral sclerosis. *Expert Opin Ther Targets* 2008, 12:1229-42.

[116] Pyatibratov MG, Kostyukova AS: New insights into the role of angiogenin in actin polymerization. *Int Rev Cell Mol Biol* 2012, 295:175-98.

[117] Wiedlocha A: Following angiogenin during angiogenesis: a journey from the cell surface to the nucleolus. *Arch Immunol Ther Exp (Warsz)* 1999, 47:299-305.

[118] Hu G, Xu C, Riordan JF: Human angiogenin is rapidly translocated to the nucleus of human umbilical vein endothelial cells and binds to DNA. *J Cell Biochem* 2000, 76:452-62.

[119] Sheng J, Yu W, Gao X, Xu Z, Hu GF: Angiogenin stimulates ribosomal RNA transcription by epigenetic activation of the ribosomal DNA promoter. *J Cell Physiol* 2014, 229:521-9.

[120] Tsuji T, Sun Y, Kishimoto K, Olson KA, Liu S, Hirukawa S, Hu GF: Angiogenin is translocated to the nucleus of HeLa cells and is involved in ribosomal RNA transcription and cell proliferation. *Cancer Res* 2005, 65:1352-60.

[121] Li S, Hu GF: Angiogenin-mediated rRNA transcription in cancer and neurodegeneration. *Int J Biochem Mol Biol* 2010, 1:26-35.

[122] Czech A, Wende S, Morl M, Pan T, Ignatova Z: Reversible and rapid transfer-RNA deactivation as a mechanism of translational repression in stress. *PLoS Genet* 2013, 9:e1003767.

[123] Emara MM, Ivanov P, Hickman T, Dawra N, Tisdale S, Kedersha N, Hu GF, Anderson P: Angiogenin-induced tRNA-derived stress-induced RNAs promote stress-induced stress granule assembly. *J Biol Chem* 2010, 285:10959-68.

[124] Nawrot B, Sochacka E, Duchler M: tRNA structural and functional changes induced by oxidative stress. *Cell Mol Life Sci* 2011, 68:4023-32.

[125] Saikia M, Krokowski D, Guan BJ, Ivanov P, Parisien M, Hu GF, Anderson P, Pan T, Hatzoglou M: Genome-wide identification and quantitative analysis of cleaved tRNA fragments induced by cellular stress. *J Biol Chem* 2012, 287:42708-25.

[126] Li S, Hu GF: Emerging role of angiogenin in stress response and cell survival under adverse conditions. *J Cell Physiol* 2012, 227:2822-6.

[127] Yamasaki S, Anderson P: Reprogramming mRNA translation during stress. *Curr Opin Cell Biol* 2008, 20:222-6.

[128] Saxena SK, Rybak SM, Davey RT, Jr., Youle RJ, Ackerman EJ: Angiogenin is a cytotoxic, tRNA-specific ribonuclease in the RNase A superfamily. *J Biol Chem* 1992, 267:21982-6.

[129] Hatzi E, Badet J: Expression of receptors for human angiogenin in vascular smooth muscle cells. *Eur J Biochem* 1999, 260:825-32.

[130] Newton DL, Xue Y, Olson KA, Fett JW, Rybak SM: Angiogenin single-chain immunofusions: influence of peptide linkers and spacers between fusion protein domains. *Biochemistry* 1996, 35:545-53.

[131] Yoon JM, Han SH, Kown OB, Kim SH, Park MH, Kim BK: Cloning and cytotoxicity of fusion proteins of EGF and angiogenin. *Life Sci* 1999, 64:1435-45.

[132] Stocker M, Tur MK, Sasse S, Krussmann A, Barth S, Engert A: Secretion of functional anti-CD30-angiogenin immunotoxins into the supernatant of transfected 293T cells. *Protein Expr Purif* 2003, 28:211-9.

[133] Reiners KS, Hansen HP, Krussmann A, Schon G, Csernok E, Gross WL, Engert A, Von Strandmann EP: Selective killing of B cell hybridomas targeting proteinase 3, Wegener's autoantigen. *Immunology* 2004, 112:228-36.

[134] Arndt MA, Krauss J, Vu BK, Newton DL, Rybak SM: A dimeric angiogenin immunofusion protein mediates selective toxicity toward $CD22^{+}$ tumor cells. *J Immunother* 2005, 28:245-51.

[135] Krauss J, Arndt MA, Vu BK, Newton DL, Rybak SM: Targeting malignant B cell lymphoma with a humanized anti-CD22 scFv-angiogenin immunoenzyme. *Br J Haematol* 2005, 128:602-9.

[136] Lee FS, Shapiro R, Vallee BL: Tight-binding inhibition of angiogenin and ribonuclease A by placental ribonuclease inhibitor. *Biochemistry* 1989, 28:225-30.

[137] Lee FS, Vallee BL: Binding of placental ribonuclease inhibitor to the active site of angiogenin. *Biochemistry* 1989, 28:3556-61.

[138] Shapiro R, Vallee BL: Human placental ribonuclease inhibitor abolishes both angiogenic and ribonucleolytic activities of angiogenin. *Proc Natl Acad Sci USA* 1987, 84:2238-41.

[139] Lee FS, Auld DS, Vallee BL: Tryptophan fluorescence as a probe of placental ribonuclease inhibitor binding to angiogenin. *Biochemistry* 1989, 28:219-24.

[140] Lee FS, Vallee BL: Structure and action of mammalian ribonuclease (angiogenin) inhibitor. *Prog Nucleic Acid Res Mol Biol* 1993, 44:1-30.

[141] Leland PA, Raines RT: Cancer chemotherapy - ribonucleases to the rescue. *Chem Biol* 2001, 8:405-13.

[142] Erickson HA, Jund MD, Pennell CA: Cytotoxicity of human RNase-based immunotoxins requires cytosolic access and resistance to ribonuclease inhibition. *Protein Eng Des Sel* 2006, 19:37-45.

[143] Furia A, Moscato M, Cali G, Pizzo E, Confalone E, Amoroso MR, Esposito F, Nitsch L, D'Alessio G: The ribonuclease/angiogenin inhibitor is also present in mitochondria and nuclei. *FEBS Lett* 2011, 585:613-17.

[144] Lomax JE, Bianchetti CM, Chang A, Phillips GN, Jr., Fox BG, Raines RT: Functional evolution of ribonuclease inhibitor: insights from birds and reptiles. *J Mol Biol* 2014, 426:3041-56.

[145] Monti DM, D'Alessio G: Cytosolic RNase inhibitor only affects RNases with intrinsic cytotoxicity. *J Biol Chem* 2004, 279:39195-98.

[146] Pizzo E, Sarcinelli C, Sheng J, Fusco S, Formiggini F, Netti P, Yu W, D'Alessio G, Hu GF: Ribonuclease/angiogenin inhibitor 1 regulates stress-induced subcellular localization of angiogenin to control growth and survival. *J Cell Sci* 2013, 126:4308-19.

[147] Yamasaki S, Ivanov P, Hu GF, Anderson P: Angiogenin cleaves tRNA and promotes stress-induced translational repression. *J Cell Biol* 2009, 185:35-42.

[148] Turcotte RF, Raines RT: Interaction of onconase with the human ribonuclease inhibitor protein. *Biochem Biophys Res Commun* 2008, 377:512-4.

[149] Inoue H, Nojima H, Okayama H: High efficiency transformation of *Escherichia coli* with plasmids. *Gene* 1990, 96:23-8.

[150] Graham FL, Smiley J, Russell WC, Nairn R: Characteristics of a human cell line transformed by DNA from human adenovirus type 5. *J Gen Virol* 1977, 36:59-74.

[151] Gallagher R, Collins S, Trujillo J, McCredie K, Ahearn M, Tsai S, Metzgar R, Aulakh G, Ting R, Ruscetti F, Gallo R: Characterization of the continuous, differentiating myeloid cell line (HL-60) from a patient with acute promyelocytic leukemia. *Blood* 1979, 54:713-33.

[152] Kapp U, Dux A, Schell-Frederick E, Banik N, Hummel M, Mucke S, Fonatsch C, Bullerdiek J, Gottstein C, Engert A, Diehl V, Wolf J: Disseminated growth of Hodgkin's-derived cell lines L-540 and L-540cy in immune-deficient SCID mice. *Ann Oncol* 1994, 5 Suppl 1:121-6.

[153] Mese H, Sasaki A, Alcalde RE, Nakayama S, Matsumura T: Establishment and characterization of cisplatin-resistant human epidermoid carcinoma cell line, A431 cell. *Chemotherapy* 1998, 44:414-20.

[154] Meyers JA, Sanchez D, Elwell LP, Falkow S: Simple agarose gel electrophoretic method for the identification and characterization of plasmid deoxyribonucleic acid. *J Bacteriol* 1976, 127:1529-37.

[155] Sanger F, Nicklen S, Coulson AR: DNA sequencing with chain-terminating inhibitors. *Proc Natl Acad Sci USA* 1977, 74:5463-7.

[156] Laemmli UK: Cleavage of structural proteins during the assembly of the head of bacteriophage T4. *Nature* 1970, 227:680-5.

[157] Burnette WN: "Western blotting": electrophoretic transfer of proteins from sodium dodecyl sulfate-polyacrylamide gels to unmodified nitrocellulose and radiographic detection with antibody and radioiodinated protein A. *Anal Biochem* 1981, 112:195-203.

[158] Hristodorov D: CD64-mediated specific elimination of M1-polarized macrophages - implications for therapeutic intervention in chronic inflammatory diseases. (Doctoral dissertation), RWTH Aachen University, Germany 2013.

[159] Kampmeier F: Site-directed modification of recombinant antibody fragments for *in vivo* fluorescence imaging and targeted drug delivery. (Doctoral dissertation), RWTH Aachen University, Germany 2010.

[160] Huls GA, Heijnen IA, Cuomo ME, Koningsberger JC, Wiegman L, Boel E, van der Vuurst de Vries AR, Loyson SA, Helfrich W, van Berge Henegouwen GP, van Meijer M, de Kruif J, Logtenberg T: A recombinant, fully human monoclonal antibody with antitumor activity constructed from phage-displayed antibody fragments. *Nat Biotechnol* 1999, 17:276-81.

[161] Moroianu J, Riordan JF: Identification of the nucleolar targeting signal of human angiogenin. *Biochem Biophys Res Commun* 1994, 203:1765-72.

[162] Dickson KA, Kang DK, Kwon YS, Kim JC, Leland PA, Kim BM, Chang SI, Raines RT: Ribonuclease inhibitor regulates neovascularization by human angiogenin. *Biochemistry* 2009, 48:3804-6.

[163] Russo N, Shapiro R, Acharya KR, Riordan JF, Vallee BL: Role of glutamine-117 in the ribonucleolytic activity of human angiogenin. *Proc Natl Acad Sci USA* 1994, 91:2920-4.

[164] Chen CZ, Shapiro R: Superadditive and subadditive effects of "hot spot" mutations within the interfaces of placental ribonuclease inhibitor with angiogenin and ribonuclease A. *Biochemistry* 1999, 38:9273-85.

[165] Chen CZ, Shapiro R: Site-specific mutagenesis reveals differences in the structural bases for tight binding of RNase inhibitor to angiogenin and RNase A. *Proc Natl Acad Sci USA* 1997, 94:1761-6.

[166] Leonidas DD, Shapiro R, Subbarao GV, Russo A, Acharya KR: Crystallographic studies on the role of the C-terminal segment of human angiogenin in defining enzymatic potency. *Biochemistry* 2002, 41:2552-62.

[167] Lee FS, Vallee BL: Characterization of ribonucleolytic activity of angiogenin towards tRNA. *Biochem Biophys Res Commun* 1989, 161:121-6.

[168] Ponnambalam S, Baldwin SA: Constitutive protein secretion from the trans-Golgi network to the plasma membrane. *Mol Membr Biol* 2003, 20:129-39.

[169] Notomista E, Mancheno JM, Crescenzi O, Di Donato A, Gavilanes J, D'Alessio G: The role of electrostatic interactions in the antitumor activity of dimeric RNases. *FEBS J* 2006, 273:3687-97.

[170] Shi M, Xie Z, Yu M, Shen B, Guo N: Controlled growth of Chinese hamster ovary cells and high expression of antibody-IL-2 fusion proteins by temperature manipulation. *Biotechnol Lett* 2005, 27:1879-84.

[171] Magalhaes PO, Lopes AM, Mazzola PG, Rangel-Yagui C, Penna TC, Pessoa A, Jr.: Methods of endotoxin removal from biological preparations: a review. *J Pharm Pharm Sci* 2007, 10:388-404.

[172] Hendrzak JA, Wallace PK, Morahan PS: Optimizing the detection of cell surface antigens on elicited or activated mouse peritoneal macrophages. *Cytometry* 1994, 17:349-56.

[173] Shapiro R, Vallee BL: Identification of functional arginines in human angiogenin by site-directed mutagenesis. *Biochemistry* 1992, 31:12477-85.

[174] Leonidas DD, Chavali GB, Jardine AM, Li S, Shapiro R, Acharya KR: Binding of phosphate and pyrophosphate ions at the active site of human angiogenin as revealed by X-ray crystallography. *Protein Sci* 2001, 10:1669-76.

[175] Hou YM: CCA addition to tRNA: implications for tRNA quality control. *IUBMB Life* 2010, 62:251-60.

[176] Megel C, Morelle G, Lalande S, Duchene AM, Small I, Marechal-Drouard L: Surveillance and cleavage of eukaryotic tRNAs. *Int J Mol Sci* 2015, 16:1873-93.

[177] Makarov AA, Ilinskaya ON: Cytotoxic ribonucleases: molecular weapons and their targets. *FEBS Lett* 2003, 540:15-20.

[178] Lee JE, Raines RT: Contribution of active-site residues to the function of onconase, a ribonuclease with antitumoral activity. *Biochemistry* 2003, 42:11443-50.

[179] St Clair DK, Rybak SM, Riordan JF, Vallee BL: Angiogenin abolishes cell-free protein synthesis by specific ribonucleolytic inactivation of ribosomes. *Proc Natl Acad Sci USA* 1987, 84:8330-4.

[180] Leland PA, Schultz LW, Kim BM, Raines RT: Ribonuclease A variants with potent cytotoxic activity. *Proc Natl Acad Sci USA* 1998, 95:10407-12.

[181] Wei H, Bera TK, Wayne AS, Xiang L, Colantonio S, Chertov O, Pastan I: A modified form of diphthamide causes immunotoxin resistance in a lymphoma cell line with a deletion of the WDR85 gene. *J Biol Chem* 2013, 288:12305-12.

[182] Reddy VY, Zhang QY, Weiss SJ: Pericellular mobilization of the tissue-destructive cysteine proteinases, cathepsins B, L, and S, by human monocyte-derived macrophages. *Proc Natl Acad Sci USA* 1995, 92:3849-53.

[183] Hetzel C: Entwicklung, Optimierung und Charakterisierung anti-CD64-basierter Immuntherapeutika. (Doctoral dissertation), RWTH Aachen University, Germany 2009.

[184] Thepen T, van Vuuren AJ, Kiekens RC, Damen CA, Vooijs WC, van De Winkel JG: Resolution of cutaneous inflammation after local elimination of macrophages. *Nat Biotechnol* 2000, 18:48-51.

[185] Guyre PM, Morganelli PM, Miller R: Recombinant immune interferon increases immunoglobulin G Fc receptors on cultured human mononuclear phagocytes. *J Clin Invest* 1983, 72:393-7.

[186] Uciechowski P, Schwarz M, Gessner JE, Schmidt RE, Resch K, Radeke HH: IFNγ induces the high-affinity Fc receptor I for IgG (CD64) on human glomerular mesangial cells. *Eur J Immunol* 1998, 28:2928-35.

[187] Balce DR, Li B, Allan ER, Rybicka JM, Krohn RM, Yates RM: Alternative activation of macrophages by IL-4 enhances the proteolytic capacity of their phagosomes through synergistic mechanisms. *Blood* 2011, 118:4199-208.

[188] Rybicka JM, Balce DR, Khan MF, Krohn RM, Yates RM: NADPH oxidase activity controls phagosomal proteolysis in macrophages through modulation of the lumenal redox environment of phagosomes. *Proc Natl Acad Sci USA* 2010, 107:10496-501.

[189] Casbon AJ, Long ME, Dunn KW, Allen LA, Dinauer MC: Effects of IFNγ on intracellular trafficking and activity of macrophage NADPH oxidase flavocytochrome b558. *J Leukoc Biol* 2012, 92:869-82.

[190] Hsu HY, Wen MH: Lipopolysaccharide-mediated reactive oxygen species and signal transduction in the regulation of interleukin-1 gene expression. *J Biol Chem* 2002, 277:22131-9.

[191] Almeida AC, Rehder J, Severino SD, Martins-Filho J, Newburger PE, Condino-Neto A: The effect of IFNγ and TNF-alpha on the NADPH oxidase system

of human colostrum macrophages, blood monocytes, and THP-1 cells. *J Interferon Cytokine Res* 2005, 25:540-6.

[192] Levy R, Rotrosen D, Nagauker O, Leto TL, Malech HL: Induction of the respiratory burst in HL-60 cells. Correlation of function and protein expression. *J Immunol* 1990, 145:2595-601.

[193] Cui H, Kong Y, Zhang H: Oxidative stress, mitochondrial dysfunction, and aging. *J Signal Transduct* 2012, 2012:646354.

[194] Lee FS, Fox EA, Zhou HM, Strydom DJ, Vallee BL: Primary structure of human placental ribonuclease inhibitor. *Biochemistry* 1988, 27:8545-53.

[195] Haigis MC, Kurten EL, Raines RT: Ribonuclease inhibitor as an intracellular sentry. *Nucleic Acids Res* 2003, 31:1024-32.

[196] Monti DM, Montesano Gesualdi N, Matousek J, Esposito F, D'Alessio G: The cytosolic ribonuclease inhibitor contributes to intracellular redox homeostasis. *FEBS Lett* 2007, 581:930-4.

[197] Blazquez M, Fominaya JM, Hofsteenge J: Oxidation of sulfhydryl groups of ribonuclease inhibitor in epithelial cells is sufficient for its intracellular degradation. *J Biol Chem* 1996, 271:18638-42.

[198] Raina M, Ibba M: tRNAs as regulators of biological processes. *Front Genet* 2014, 5:171.

[199] Saikia M, Jobava R, Parisien M, Putnam A, Krokowski D, Gao XH, Guan BJ, Yuan Y, Jankowsky E, Feng Z, Hu GF, Pusztai-Carey M, Gorla M, Sepuri NB, Pan T, Hatzoglou M: Angiogenin-cleaved tRNA halves interact with cytochrome c, protecting cells from apoptosis during osmotic stress. *Mol Cell Biol* 2014, 34:2450-63.

[200] Kuwabara WM, Zhang L, Schuiki I, Curi R, Volchuk A, Alba-Loureiro TC: NADPH oxidase-dependent production of reactive oxygen species induces endoplasmatic reticulum stress in neutrophil-like HL-60 cells. *PLoS One* 2015, 10:e0116410.

[201] Tsang KY, Chan D, Bateman JF, Cheah KS: *In vivo* cellular adaptation to ER stress: survival strategies with double-edged consequences. *J Cell Sci* 2010, 123:2145-54.

[202] Kharraz Y, Guerra J, Mann CJ, Serrano AL, Munoz-Canoves P: Macrophage plasticity and the role of inflammation in skeletal muscle repair. *Mediat Inflamm* 2013, 2013:491497.

[203] Gao XF, Yang ZW, Li J: Adjunctive therapy with interferon-gamma for the treatment of pulmonary tuberculosis: a systematic review. *Int J Infect Dis* 2011, 15:e594-600.

[204] Conway O'Brien E, Prideaux S, Chevassut T: The epigenetic landscape of acute myeloid leukemia. *Adv Hematol* 2014, 2014:103175.

[205] Li S, Yu W, Hu GF: Angiogenin inhibits nuclear translocation of apoptosis inducing factor in a Bcl-2-dependent manner. *J Cell Physiol* 2012, 227:1639-44.

[206] Li S, Yu W, Kishikawa H, Hu GF: Angiogenin prevents serum withdrawal-induced apoptosis of P19 embryonal carcinoma cells. *FEBS J* 2010, 277:3575-87.

[207] Subramanian V, Feng Y: A new role for angiogenin in neurite growth and pathfinding: implications for amyotrophic lateral sclerosis. *Hum Mol Genet* 2007, 16:1445-53.

[208] Subramanian V, Crabtree B, Acharya KR: Human angiogenin is a neuroprotective factor and amyotrophic lateral sclerosis associated angiogenin variants affect neurite extension/pathfinding and survival of motor neurons. *Hum Mol Genet* 2008, 17:130-49.

[209] Aparicio-Erriu IM, Prehn JH: Molecular mechanisms in amyotrophic lateral sclerosis: the role of angiogenin, a secreted RNase. *Front Neurosci* 2012, 6:167.

[210] Wu D, Yu W, Kishikawa H, Folkerth RD, Iafrate AJ, Shen Y, Xin W, Sims K, Hu GF: Angiogenin loss-of-function mutations in amyotrophic lateral sclerosis. *Ann Neurol* 2007, 62:609-17.

[211] Wei S, Gao X, Du J, Su J, Xu Z: Angiogenin enhances cell migration by regulating stress fiber assembly and focal adhesion dynamics. *PLoS One* 2011, 6:e28797.

[212] Johnson M, Sharma M, Henderson BR: IQGAP1 regulation and roles in cancer. *Cell Signal* 2009, 21:1471-8.

[213] Sbroggio M, Bertero A, Velasco S, Fusella F, De Blasio E, Bahou WF, Silengo L, Turco E, Brancaccio M, Tarone G: ERK1/2 activation in heart is controlled by melusin, focal adhesion kinase and the scaffold protein IQGAP1. *J Cell Sci* 2011, 124:3515-24.

[214] Lu Z, Xu S: ERK1/2 MAP kinases in cell survival and apoptosis. *IUBMB Life* 2006, 58:621-31.

[215] Ascione R, Rowlinson J, Avolio E, Katare R, Meloni M, Spencer HL, Mangialardi G, Norris C, Krankel N, Spinetti G, Emanueli C, Madeddu P: Migration towards SDF-1 selects angiogenin-expressing bone marrow monocytes endowed with cardiac reparative activity in patients with previous myocardial infarction. *Stem Cell Res Ther* 2015, 6:53.

[216] Liu S, Yu D, Xu ZP, Riordan JF, Hu GF: Angiogenin activates ERK1/2 in human umbilical vein endothelial cells. *Biochem Biophys Res Commun* 2001, 287:305-10.

[217] Thompson DM, Parker R: Stressing out over tRNA cleavage. *Cell* 2009, 138:215-9.

[218] Iles KE, Forman HJ: Macrophage signaling and respiratory burst. *Immunol Res* 2002, 26:95-105.

[219] Sadagopan S, Veettil MV, Chakraborty S, Sharma-Walia N, Paudel N, Bottero V, Chandran B: Angiogenin functionally interacts with p53 and regulates p53-mediated apoptosis and cell survival. *Oncogene* 2012, 31:4835-47.

[220] Bronner C, Krifa M, Mousli M: Increasing role of UHRF1 in the reading and inheritance of the epigenetic code as well as in tumorogenesis. *Biochem Pharmacol* 2013, 86:1643-9.

[221] Green DR, Kroemer G: Cytoplasmic functions of the tumour suppressor p53. *Nature* 2009, 458:1127-30.

[222] Chipuk JE, Kuwana T, Bouchier-Hayes L, Droin NM, Newmeyer DD, Schuler M, Green DR: Direct activation of Bax by p53 mediates mitochondrial membrane permeabilization and apoptosis. *Science* 2004, 303:1010-4.

[223] Hetman M, Gozdz A: Role of extracellular signal regulated kinases 1 and 2 in neuronal survival. *Eur J Biochem* 2004, 271:2050-5.

[224] Kieran D, Sebastia J, Greenway MJ, King MA, Connaughton D, Concannon CG, Fenner B, Hardiman O, Prehn JH: Control of motoneuron survival by angiogenin. *J Neurosci* 2008, 28:14056-61.

[225] Thompson DM, Parker R: The RNase Rny1p cleaves tRNAs and promotes cell death during oxidative stress in *Saccharomyces cerevisiae*. *J Cell Biol* 2009, 185:43-50.

[226] Iordanov MS, Ryabinina OP, Wong J, Dinh TH, Newton DL, Rybak SM, Magun BE: Molecular determinants of apoptosis induced by the cytotoxic ribonuclease onconase: evidence for cytotoxic mechanisms different from inhibition of protein synthesis. *Cancer Res* 2000, 60:1983-94.

[227] Cafaro V, Bracale A, Di Maro A, Sorrentino S, D'Alessio G, Di Donato A: New muteins of RNase A with enhanced antitumor action. *FEBS Lett* 1998, 437:149-52.

[228] Sica F, Di Fiore A, Merlino A, Mazzarella L: Structure and stability of the non-covalent swapped dimer of bovine seminal ribonuclease: an enzyme tailored to evade ribonuclease protein inhibitor. *J Biol Chem* 2004, 279:36753-60.

VII Appendix

VII.1 Single-letter code of amino acids

Table 20: Letter code and charges of proteinogenic amino acids at physiological pH

Amino acid	Single-letter-code	Charge of the side chain (pH 7.4)
Alanine	A	Neutral
Arginine	R	Positive
Asparagine	N	Neutral
Aspartic acid	D	Negative
Cysteine	C	Neutral
Glutamic acid	E	Negative
Glutamine	Q	Neutral
Glycine	G	Neutral
Histidine	H	Positive (weak)
Isoleucine	I	Neutral
Leucine	L	Neutral
Lysine	K	Positive
Methionine	M	Neutral
Phenylalanine	F	Neutral
Proline	P	Neutral
Serine	S	Neutral
Threonine	T	Neutral
Tryptophan	W	Neutral
Tyrosine	Y	Neutral
Valine	V	Neutral

VII.2 List of abbreviations

Table 21: List of abbreviations

α	Alpha
β	Beta
γ	Gamma
µl	Microliter
µm	Micrometer
µg	Microgram
AIDA	Advanced image data analyzer
ALS	Amyotrophic lateral sclerosis
AML	Acute myeloid leukemia
amp	Ampicillin
ampR	Ampicillin resistance gene
Ang	Angiogenin
APC	Allophycocyanin
bps	Base pairs
BS	Bovine seminal
BSA	Bovine serum albumin
CD64	Cluster of differentiation receptor 64, FcγRI
CFP	Cytolytic fusion protein

CLS	Capillary leak syndrome
cm	Centimeter
CMML	Chronic myelomonocytic leukemia
CMV	Cytomegalovirus
CPP	Cell penetrating peptide
DEPC	Diethylpyrocarbonate
DMSO	Dimethyl sulfoxide
DNA	Deoxyribonucleic acid
DPBS	Dulbecco's phosphate-buffered saline
EC_{50}	Half maximal effective concentration
E.coli	*Escherichia coli*
EDN	Eosinophil-derived neurotoxin
EDTA	Ethylenediaminetetraacetic acid
eGFP	Enhanced green fluorescent protein
eIF	Eukaryotic initiation factor
EMSA	Electrophoretic mobility shift assay
ERK	Extracellular-signal-regulated kinases
ETA'	Truncated variant of *Pseudomonas aeruginosa* exotoxin A
FAB	French–American–British classification system
FcR	Fc receptor
FCS	Fetal calf serum
FITC	Fluorescein isothiocyanate
FSC-H	Forward scatter
g	Centrifugal force
Gb	Granzyme B
gDNA	Genomic DNA
Gm	Granzyme M
h	Hour
H22	Human CD64-specific, humanized scFv
HEPES	4-(2-hydroxyethyl)-1-piperazineethanesulfonic acid
hMΦ	Human macrophages
hM1Φ	Human classically activated macrophages, pro-inflammatory
hM2Φ	Human alternatively activated macrophages, anti-inflammatory
hnRNA	Heterogeneous nuclear RNA
HPR	Human pancreatic ribonuclease
HRPO	Horseradish peroxidase
IFNγ	Interferon gamma
IgG	Immunoglobulin G
IL	Interleukin
IMAC	Immobilized metal ion affinity chromatography
IRES	Internal ribosome entry site
IT	Immunotoxin
K	Kelvin
K_A	Association constant
K_i	Inhibition constant
kDa	Kilodalton
L	Liter
LB	Lysogeny broth
LPS	Lipopolysaccharide
M	Mole per liter
M22	Human CD64-specific murine monoclonal antibody
MAPK	Mitogen-activated protein kinase

MD	Molecular dynamic
MFI	Mean fluorescence intensity
mg	Milligram
min	Minutes
mL	Milliliter
mM	Millimole per liter
MOPS	3-(N-morpholino)propanesulfonic acid
mRNA	Messenger ribonucleic acid
ng	Nanogram
NLS	Nuclear localization sequence
nm	Nanometer
nM	Nanomole per liter
NTA	Nitrilotriacetic acid
OD	Optical density
o/n	Overnight
PAGE	Polyacrylamide gel electrophoresis
PBS	Phosphate-buffered saline
PBST	Phosphate-buffered saline with Tween 20
PCR	Polymerase chain reaction
PE	Phycoerythrin
pg	Picogram
PI	Propidium iodide
pM	Picomole per liter
pmol	Picomole
PMS	Phenazine methosulfate
rER	Rough endoplasmic reticulum
RISC	RNA-induced silencing complex
RNH1	Eukaryotic ribonuclease inhibitor
ROS	Reactive oxygen species
rpm	Rounds per minute
RPMI	Roswell Park Memorial Institute
rRNA	Ribosomal ribonucleic acid
RT	Room temperature
scFv	Single-chain fragment variable
SD	Standard deviation
SDS	Sodium dodecyl sulfate
SEM	Standard error mean
SOC	Super optimal broth with catabolite repression
SOE	Splicing by overlap extension
SSC-H	Sideward scatter
tiRNA	tRNA-derived stress-induced RNAs
tRNA	Transfer ribonucleic acid
U	Units
UV	Ultraviolet
V	Voltage
VLS	Vascular leak syndrome
WBC	White blood cell
WHO	World Health Organization
XTT	2,3-Bis(2-methoxy-4-nitro-5-sulfophenyl)-5-((phenylamino)carbonyl)-2H-tetrazolium
zeoR	Zeocin^{TM} resistance gene

VII.3 Index of tables

Table 1: Used equipment 12
Table 2: Used reaction kits 13
Table 3: Media compositions 13
Table 4: Buffer compositions 14
Table 5: Other solutions 15
Table 6: Used eukaryotic cell lines 15
Table 7: Antibodies and their application 17
Table 8: Oligonucleotide primer and their application 18
Table 9: Primer combinations and annealing temperatures for mutagenesis PCR 19
Table 10: Workflow for immunodetection of proteins on western blot membranes 24
Table 11: Selected amino acid exchanges for *proof-of-concept* mutagenesis 31
Table 12: *In vitro* cytotoxicity of H22-Ang variants 45
Table 13: Selected mutations to weaken the RNH1-Ang GGRR/QG_{mut} interaction 51
Table 14: EC_{50} values of CFPs obtained in the third evaluation round 56
Table 15: Improvement of cytotoxicity in comparison to H22-Ang wild type 58
Table 16: Clinically relevant patient data 60
Table 17: Determined CD64 frequencies of prepared leukemia cells 62
Table 18: *In vitro* cytotoxicity of H22-Ang $GGRR_{mut}$ and H22-CatAd-Ang $GGRR_{mut}$ 65
Table 19: Properties of H22-Ang variants in comparison to H22-Ang wild type 67
Table 20: Letter code and charges of proteinogenic amino acids at physiological pH 113
Table 21: List of abbreviations 113

VII.4 Index of figures

Figure 1: The development and diversity of hematopoietic immune cells. 4
Figure 2: Assumed cytotoxic activity of an angiogenin-based cytolytic fusion protein 8
Figure 3: Theoretical workflow of mutant generation and evaluation. 10
Figure 4: Schematic overview of the pMS expression vector. 16
Figure 5: Reporter gene expression in transfected HEK293T cells. 32
Figure 6: SDS-PAGE and western blot analysis of purified H22-Ang variants. 33
Figure 7: Cell-specific binding analysis of H22-Ang variants. 34
Figure 8: Representative reduction of cell viability upon exposure to H22-Ang variants. 35
Figure 9: SDS-PAGE and western blot analysis of purified H22-Ang GGRR/QG_{mut}. 37
Figure 10: Ribonucleolytic activity of H22-Ang variants. 38
Figure 11: Substrate cleavage activity of CFPs in the presence of RiboLock™. 39
Figure 12: Inhibition susceptibility of generated cytolytic fusion proteins. 40

Figure 13: Binding activity of H22-Ang variants towards genomic DNA of A431 cells. 41
Figure 14: Morphological comparison of untreated and polarized hM1Φ cells. 42
Figure 15: Binding activity of H22-Ang variants on different cell types. 43
Figure 16: Representative *in vitro* cytotoxicity of CFPs. 44
Figure 17: EC_{50} values of CFPs on stimulated HL-60 cells and human M1 macrophages. 45
Figure 18: Interaction surfaces of RNH1 and human angiogenin. 46
Figure 19: Individual RMSD and RMSF values of simulated RNH1-Ang complexes. 47
Figure 20: Molecular interactions between Ang variants and RNH1 49
Figure 21: SDS-PAGE and western blot analysis of H22-Ang variants. 51
Figure 22: CFP-mediated cleavage of yeast tRNA under varying conditions. 52
Figure 23: CFP-mediated digestion of RNaseAlert® substrate. 53
Figure 24: Inhibition susceptibility of generated H22-Ang variants. 54
Figure 25: Flow cytometry-based binding analysis of CFPs 55
Figure 26: Dose-dependent cytotoxicity of CFPs on different cell types. 57
Figure 27: *In vitro* cytotoxicity of fusion proteins in the third evaluation round. 58
Figure 28: Degradation susceptibility of CFPs in human and mouse serum. 59
Figure 29: Representative determination of CD64 frequency on leukemia cells. 61
Figure 30: Binding analysis of fusion proteins on leukemia cells. 62
Figure 31: CFP efficacies on leukemia cells with CD64 frequencies below 40%. 63
Figure 32: CFP efficacies on leukemia cells with CD64 frequencies of at least 60%. 64
Figure 33: The effect of CatAd on the *in vitro* cytotoxicity of H22-Ang $GGRR_{mut}$ 66
Figure 34: Evaluation of hM1Φ cell polarization. 68
Figure 35: IFNγ-dependent expression of CD14 and CD64 on HL-60 cells. 69
Figure 36: IFNγ modulates the binding activity of H22-Ang towards HL-60 cells. 70
Figure 37: Redox-dependent activity of the RiboLock™ inhibitor. 71
Figure 38: RNH1 contents in stimulated HL-60 cells and hM1Φ cells. 72
Figure 39: IFNγ-mediated effects on the intracellular RNH1 content of HL-60 cells. 73

VII.5 DNA sequence of H22-Ang wild type and primer binding sites

The pMS-L-H22-Ang wild type plasmid DNA sequence (II.1.7, Figure 4) was edited using Clone Manager 9 software. The following section comprises the CFP-encoding reading frame whereas gene annotations are translated into amino acid sequences (grey), respectively. Recognition sites of restriction endonucleases are indicated by discontinuous lines above the DNA sequence. Oligonucleotide sequences (blue) and corresponding labels (black and bold) are illustrated whereas arrows indicate the direction of strand extension (II.1.9, Table 8). Small letters emphasize mismatching bases while complementary bases are written in uppercase.

```
                      NcoI
                    -+-----
          SfiI
    ---------+----

    5'_Sfi_for →
   CGGCCC AGCCGGCC

 965  gacgcggccc agccggccat ggcccaggtg cagctggtgg agagcggtgg aggtgttgtg
      ctgcgccggg tcggccggta ccgggtccac gtcgaccacc tctcgccacc tccacaacac
                        >>.................H22(scFv).................>
                           m  a  q  v  q  l  v  e  s  g  g  g  v  v

1025  caacctggcc ggtccctgcg cctgtcctgc tcctcgtctg gcttcatttt cagtgacaat
      gttggaccgg ccagggacgc ggacaggacg aggagcagac cgaagtaaaa gtcactgtta
      >.............................H22(scFv).............................>
        q  p  g  r  s  l  r  l  s  c  s  s  s  g  f  i  f  s  d  n
1085  tacatgtatt gggtgagaca ggcacctgga aaaggtcttg agtgggttgc aaccattagt
      atgtacataa cccactctgt ccgtggacct tttccagaac tcacccaacg ttggtaatca
      >.............................H22(scFv).............................>
        y  m  y  w  v  r  q  a  p  g  k  g  l  e  w  v  a  t  i  s
1145  gatggtggta gttacaccta ctatccagac agtgtgaagg gaagatttac aatatcgaga
      ctaccaccat caatgtggat gataggtctg tcacacttcc cttctaaatg ttatagctct
      >.............................H22(scFv).............................>
        d  g  g  s  y  t  y  y  p  d  s  v  k  g  r  f  t  i  s  r
1205  gacaacagca agaacacatt gttcctgcaa atggacagcc tgagacccga agacaccggg
      ctgttgtcgt tcttgtgtaa caaggacgtt tacctgtcgg actctgggct tctgtggccc
      >.............................H22(scFv).............................>
        d  n  s  k  n  t  l  f  l  q  m  d  s  l  r  p  e  d  t  g
1265  gtctattttt gtgcaagagg ctactatagg tacgaggggg ctatggacta ctggggccaa
      cagataaaaa cacgttctcc gatgatatcc atgctccccc gatacctgat gaccccggtt
      >.............................H22(scFv).............................>
        v  y  f  c  a  r  g  y  y  r  y  e  g  a  m  d  y  w  g  q

1325  gggaccccgg tcaccgtgag ctcaggaggt ggcggctccg gaggtggagg cagcggaggg
      ccctggggcc agtggcactc gagtcctcca ccgccgaggc ctccacctcc gtcgcctccc
      >.............................H22(scFv).............................>
        g  t  p  v  t  v  s  s  g  g  g  g  s  g  g  g  g  s  g  g

         BamHI
        -+----

1385  ggcggatccg acatccagct gacccagagc ccaagcagcc tgagcgccag cgtgggtgac
      ccgcctaggc tgtaggtcga ctgggtctcg ggttcgtcgg actcgcggtc gcacccactg
      >.............................H22(scFv).............................>
        g  g  s  d  i  q  l  t  q  s  p  s  s  l  s  a  s  v  g  d

1445  agagtgacca tcacctgtaa gtccagtcaa agtgttttat acagttcaaa tcagaagaac
      tctcactggt agtggacatt caggtcagtt tcacaaaata tgtcaagttt agtcttcttg
      >.............................H22(scFv).............................>
        r  v  t  i  t  c  k  s  s  q  s  v  l  y  s  s  n  q  k  n
```

*Kpn*I
-----+

1505 tacttggcct ggtaccagca gaagccaggt aaggctccaa agctgctgat ctactgggca
atgaaccgga ccatggtcgt cttcggtcca ttccgaggtt tcgacgacta gatgacccgt
>.....H22(scFv).....>
y l a w y q q k p g k a p k l l i y w a

*Kpn*I
------+

1565 tccactaggg aatctggtgt gccaagcaga ttcagcggta gcggtagcgg taccgacttc
aggtgatccc ttagaccaca cggttcgtct aagtcgccat cgccatcgcc atggctgaag
>.....H22(scFv).....>
s t r e s g v p s r f s g s g s g t d f

1625 accttcacca tcagcagcct ccagccagag gacatcgcca cctactactg ccatcaatac
tggaagtggt agtcgtcgga ggtcggtctc ctgtagcggt ggatgatgac ggtagttatg
>.....H22(scFv).....>
t f t i s s l q p e d i a t y y c h q y

*Not*I *Xho*I
--+------ -+----

R5A_for →
CGAG

← R5A_rev
GCTC

1685 ctctcctcgt ggacgttcgg ccaagggacc aagctggaga tcaaagcggc cgcactcgag
gagaggagca cctgcaagcc ggttccctgg ttcgacctct agtttcgccg gcgtgagctc
>.....H22(scFv).....>>
l s s w t f g q g t k l e i k

*Xba*I
-+----

Ang-5′-Seq_for →
GG ATAACTCCAG GTACACACAC TTCC

HA_for →
GG ATAACTCCAG GTACACAgcC TTCCTGACCC AGCACTATGA TGC

← HA_rev
CC TATTGAGGTC CATGTGTcgG AAGGACTGGG TCGTGATACT ACG

R5A_for →
TCTAGACAGG ATAACTCCgc GTACACACAC TTCCTGACCC

← R5A_rev
AGATCTGTCC TATTGAGGcg CATGTGTGTG AAGGACTGGG

1745 tctagacagg ataactccag gtacacacac ttcctgaccc agcactatga tgccaaacca
agatctgtcc tattgaggtc catgtgtgtg aaggactggg tcgtgatact acggtttggt
>>.....Angiogenin.....>
q d n s r y t h f l t q h y d a k p

NLS_RA_for →
GC ATCATGAGGA GAgcGGGCCT GACCTCACCC

← NLS_RA_rev
CG TAGTACTCCT CTcgCCCGGA CTGGAGTGGG

R55A_for →
GTGAAAGC ATCATGgcGA GACGGGGCCT GACC

← R55A_rev
CACTTTCG TAGTACcgCT CTGCCCCGGA CTGG

KQ_for →
GCCT GACCTCACCC

← KQ_rev
CGGA CTGGAGTGGG

```
1805  cagggccggg atgacagata ctgtgaaagc atcatgagga gacggggcct gacctcaccc
      gtcccggccc tactgtctat gacactttcg tagtactcct ctgccccgga ctggagtggg
      >.........................Angiogenin.............................>
        q  g  r   d  d  r   y  c  e  s   i  m  r   r  r  g   l  t  s  p
```

KQ_for →
TGCcAAGACA TCAACACATT TATTCATGGC

← KQ_rev
ACGgTTCTGT AGTTGTGTAA ATAAGTACCG

```
1865  tgcaaagaca tcaacacatt tattcatggc aacaagcgca gcatcaaggc catctgtgaa
      acgtttctgt agttgtgtaa ataagtaccg ttgttcgcgt cgtagttccg gtagacactt
      >.........................Angiogenin.............................>
        c  k  d   i  n  t   f  i  h  g   n  k  r   s  i  k   a  i  c  e

1925  aacaagaatg gaaaccctca cagagaaaac ctaagaataa gcaagtcttc tttccaggtc
      ttgttcttac ctttgggagt gtctcttttg gattcttatt cgttcagaag aaaggtccag
      >.........................Angiogenin.............................>
        n  k  n   g  n  p   h  r  e  n   l  r  i   s  k  s   s  f  q  v
```

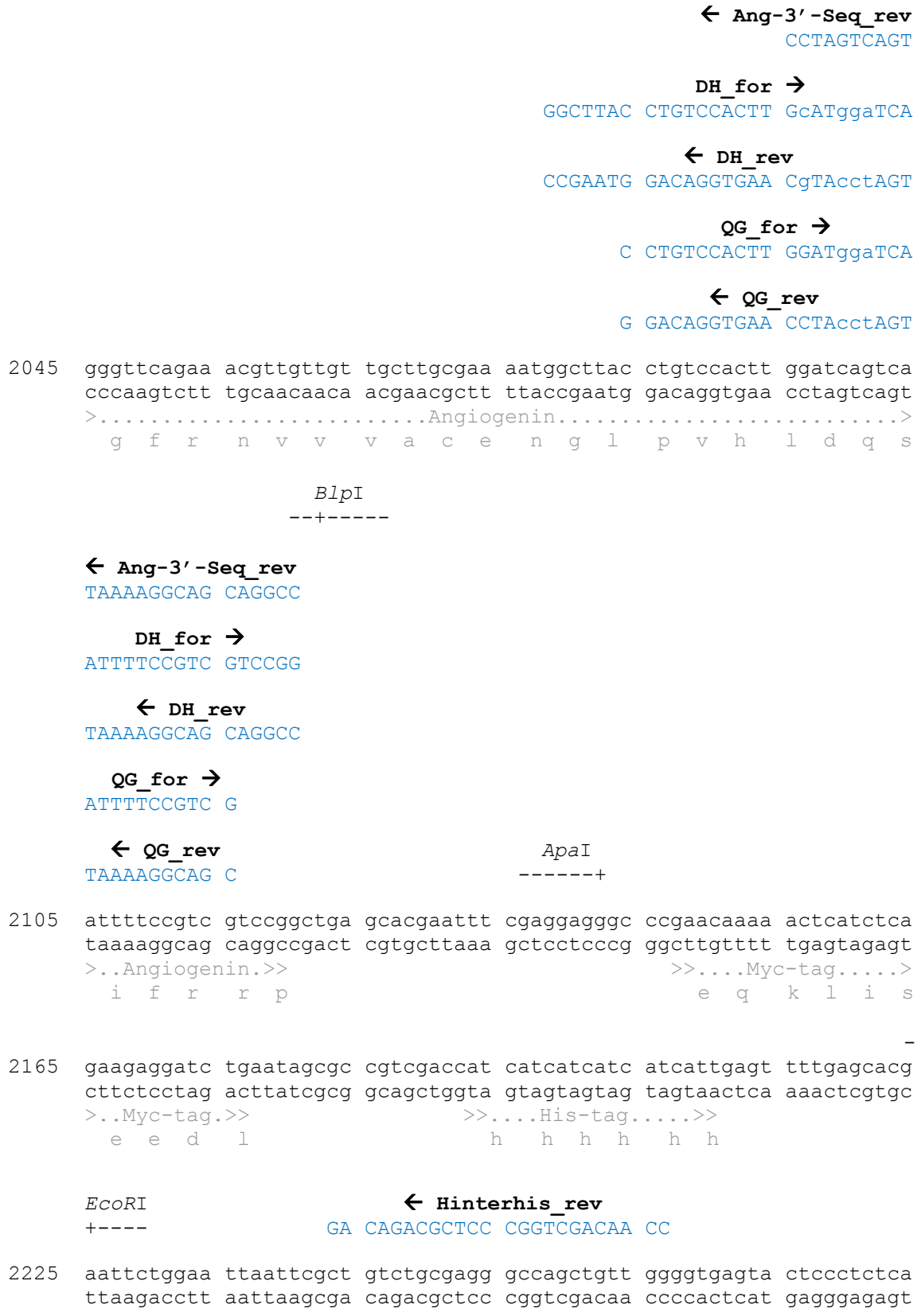
WA_for →
GG AGGTTCCCCC gcGCCTCCAT GCCAG

← WA_rev
CC TCCAAGGGGG cgCGGAGGTA CGGTC

GGRR_for →
CCACTTGCA AGCTACATcG gcGcTCCCCC TGGCCTCCAT GCC

← GGRR_rev
GGTGAACGT TCGATGTAgC cgCgAGGGGG ACCGGAGGTA CGG

```
1985  accacttgca agctacatgg aggttccccc tggcctccat gccagtaccg agccacagcg
      tggtgaacgt tcgatgtacc tccaaggggg accggaggta cggtcatggc tcggtgtcgc
      >.........................Angiogenin.............................>
        t  t  c   k  l  h   g  g  s  p   w  p  p   c  q  y   r  a  t  a
```


← Ang-3′-Seq_rev
CCTAGTCAGT
DH_for →
GGCTTAC CTGTCCACTT GcATggaTCA
← DH_rev
CCGAATG GACAGGTGAA CgTAcctAGT
QG_for →
C CTGTCCACTT GGATggaTCA
← QG_rev
G GACAGGTGAA CCTAcctAGT
2045 gggttcagaa acgttgttgt tgcttgcgaa aatggcttac ctgtccactt ggatcagtca
cccaagtctt tgcaacaaca acgaacgctt ttaccgaatg gacaggtgaa cctagtcagt
>.....Angiogenin.....>
g f r n v v v a c e n g l p v h l d q s
BlpI
--+-----
← Ang-3′-Seq_rev
TAAAAGGCAG CAGGCC
DH_for →
ATTTTCCGTC GTCCGG
← DH_rev
TAAAAGGCAG CAGGCC
QG_for →
ATTTTCCGTC G
← QG_rev
TAAAAGGCAG C
ApaI
------+
2105 attttccgtc gtccggctga gcacgaattt cgaggagggc ccgaacaaaa actcatctca
taaaaggcag caggccgact cgtgcttaaa gctcctcccg ggcttgtttt tgagtagagt
>..Angiogenin.>> >>....Myc-tag.....>
i f r r p e q k l i s
-
2165 gaagaggatc tgaatagcgc cgtcgaccat catcatcatc atcattgagt tttgagcacg
cttctcctag acttatcgcg gcagctggta gtagtagtag tagtaactca aaactcgtgc
>..Myc-tag.>> >>....His-tag.....>>
e e d l h h h h h h
EcoRI
+----
← Hinterhis_rev
GA CAGACGCTCC CGGTCGACAA CC
2225 aattctggaa ttaattcgct gtctgcgagg gccagctgtt ggggtgagta ctccctctca
ttaagacctt aattaagcga cagacgctcc cggtcgacaa ccccactcat gagggagagt

VII.6 Acknowledgements

I would like to express my sincere thanks to the people that supported my dissertation either in a scientific or a personal manner.

First of all, I would like to thank Prof. Dr. Rainer Fischer who gave me the opportunity to work in the Fraunhofer IME, who helpfully advised me and who did the first examination of this thesis. Furthermore, I thank Prof. Dr. Dr. Stefan Barth for being readily available for discussions and his experienced suggestions. My thanks also go to Prof. Dr. Paolo Carloni and Prof. Dr. Johannes Bohrmann for being the second and third examiners, respectively.

In particular, I would like to address a special thank to my day-to-day supervisor Dr. Thomas Nachreiner. During the last years, he continuously supported me by constructive discussions, corrections and written comments, the closer examination of my hypotheses and by promoting my personal and professional growth.

Furthermore, I am very grateful to Prof. Dr. Tim H. Brümmendorf and Dr. Edgar Jost, who kindly provided the patient material and to Dr. Xiaojing Cong for carrying out the MD simulation studies. The collaboration was always pleasant and inspiring for me. I would also like to thank my master students Melanie Neß, Tim Vierbuchen and Hanna Braun for their efforts and the great teamwork.

Finally, I wish to thank our technicians Anh-Tuan Pham and Kai Fuhrmann for their helping hand and the people from my office and the entire PPD group for relaxing coffee breaks, productive discussions and the nice working atmosphere.

Apart from the scientific aspect, an exceptional “thank you” is reserved for my parents, my grandparents, my brother and especially my girlfriend. They always trusted in me, provided me with support and encouraged me whenever I lost patience.

VII.7 Curriculum Vitae

Personal details

Name	Cremer, Christian
Date of birth	June 13th, 1985
Place of birth	Düren-Birkesdorf
Citizenship	German



School Career

1996 - 2004	Grammar school, Kreuzau Degree: Abitur (Grade: 2.7)
1991 - 1995	Elementary school, Hürtgenwald-Vossenack

Professional Career

2012 - 2016	Doctoral studies at the Helmholtz-Institute of Applied Medical Engineering, University Hospital Aachen
2005 - 2011	Biology studies at the RWTH Aachen University Main subjects: General and Molecular Biotechnology, Microbiology, Molecular Biology, Molecular Medicine Degree: Diploma (Grade 1.2) Title of the thesis: *Herstellung neuartiger Immuntherapeutika zum Targeting autoreaktiver B-Lymphozyten*

Additional skills

Training course	FELASA B certificate